

Department of Physics and Astronomy

University of Heidelberg

Master thesis

in Physics

submitted by

Florian Volker Nicolai

born in Karlsruhe

2017

**Design and construction
of a fiber-coupled
tapered amplifier system**

This Master thesis has been carried out by Florian Volker Nicolai

at the

Kirchhoff-Institute for Physics

under the supervision of

Prof. Dr. Markus K. Oberthaler

Design and construction of a fiber-coupled tapered amplifier system

High power lasers play an important role in atomic physics, where laser cooling is required. One possibility to achieve high laser powers with a single-mode diode laser is to combine them with a tapered amplifier (TA). This thesis deals with the design and construction of a fiber-coupled TA system which allows stable adjustment of the collimation lenses. Two different designs were tested, one simple and compact design which allows the position of the collimation lenses to be adjusted along the optical axis and one more complex design which allows the position of the collimation lenses to be adjusted in all three directions. It was found to be crucial for fiber coupling optimization that the position of the collimation lenses can be controlled in all three spatial degrees of freedom. With the latter design and a $\lambda = 808 \text{ nm}$ TA diode, it was possible to achieve a single-mode fiber coupling efficiency of 50 % and a total power of 800 mW after the single-mode fiber for a seed beam power of 30 mW. Furthermore, a robust and cost-effective stand-alone TA unit is proposed and a list with all necessary information to build up such a stand-alone unit is given.

Entwurf und Aufbau eines fasergekoppelten Trapezverstärkersystems

Hochleistungslaser spielen eine wichtige Rolle in der Atomphysik, wo Laserkühlung betrieben wird. Eine Möglichkeit, hohe Laserleistungen mit einem Einmodendiodenlaser zu erreichen, besteht darin, diese mit einem Trapezverstärker (TA) zu kombinieren. Diese Arbeit beschäftigt sich mit dem Entwurf und Aufbau eines fasergekoppelten TA-Systems, welches eine stabile Einstellung der Kollimationslinsen ermöglicht. Zwei verschiedene Bauarten wurden getestet; eine einfache und stabile Bauart, bei der die Position der Kollimationslinsen entlang der optischen Achse verändert werden kann und eine komplexere Bauart, bei der die Position der Kollimationslinsen in allen drei Raumrichtungen verändert werden kann. Für optimiertes Faserkoppeln erwies es sich als entscheidend, dass die Position der Kollimationslinsen in allen drei Raumrichtungen kontrolliert werden kann. Mit letztgenanntem Design und einer $\lambda = 808 \text{ nm}$ TA-Diode war es möglich, eine Faserkuppeeffizienz von 50 % für eine Einmodenfaser zu erreichen, sowie eine Gesamtausgangsleistung von 800 mW nach der Einmodenfaser bei einer Leistung des Seed-Strahls von 30 mW. Weiterhin wurden Pläne für ein stabiles, kostengünstiges, eigenständiges TA-Modul vorgeschlagen und eine Liste mit allen dazu benötigten Informationen zusammengestellt.

Contents

1	Introduction	1
2	Basic features of a tapered amplifier	3
2.1	Structure of a tapered amplifier	3
2.2	Taper angle and waveguide	4
2.3	Amplified spontaneous emission (ASE)	5
2.4	Filamentation	7
3	Setup of a tapered amplifier system	8
3.1	Handling of the TA diode	8
3.2	Protection circuit	9
3.3	Lenses of the TA setup	11
3.3.1	q-parameter and ABCD law	11
3.3.2	Calculation of the focal length for the cylindrical lens	13
3.4	Experimental setup	17
4	Tapered amplifier designs	22
4.1	TA design with lensholder tubes	22
4.1.1	Components of the design	22
4.1.2	Attempts to control the position of the chip	26
4.1.3	Coupling the output beam into an optical fiber	29
4.1.4	Conclusion on this design	30
4.2	TA design with cage system	31
4.2.1	Components of the design	31
4.2.2	Conclusion on this design	35
4.3	Stand-alone TA unit	36
5	TA diode characteristics	42
5.1	Output power characteristics of a TA chip	42
5.2	Fiber coupling efficiency and mode profiles	44
5.3	Conclusion	51
6	Summary and outlook	52

I	Appendix	54
A	Lists	55
B	Components of the protection circuit	60
C	Drawings of lens holder tube design	61
D	Drawings of cage system copper parts	71
E	Drawings of aluminum block	81
F	Components and prices of a stand-alone TA unit	88
G	Bibliography	92

1 Introduction

In modern technology lasers play an important role. In everyday life, they appear for example in bar code scanners, laser pointers or telecommunication networks. In medicine there is an own field that deals with medical applications of lasers, so-called laser medicine. This includes for example the treatment of tumors with photodynamic therapy or the correction of refractive errors by laser eye surgery [1].

In experimental atomic physics lasers are the essential tool to induce electronic transitions and thus provide the possibility to investigate electronic energy levels and to control atoms via laser cooling and trapping.

Among the different kinds of lasers, it are diode lasers that have the best conversion efficiency from electrical power to laser light [2]. Moreover, diode lasers are cost effective, compact and, in combination with an external grating, generate tunable laser light with narrow linewidth [3]. This makes them well suited for many applications in atomic and molecular physics. However, when high beam quality is required, that means if the emitted laser light shall only be in one spatial mode, the transverse dimension of the laser diode's output aperture has to be of the order of the emitted wavelength [4]. This narrow output aperture in turn limits the total emitted power to several tens of milliwatts. Output powers of some hundred milliwatts would damage the output facet of the laser diode due to the high optical intensity occurring at the output aperture.

To overcome this power limitation one can make use of tapered amplifiers (TAs). The output aperture of TAs is wide in one direction, typically 200 μm . This increases the threshold power for permanent damage at the output facet. A tunable, well defined laser beam of several milliwatts from a diode laser can then be amplified by a TA up to several watts. The amplified laser beam mainly maintains the spectral properties of the injected beam. A TA can also amplify multiple frequencies simultaneously [5]. Thus a combination of diode laser and tapered amplifier can be useful if the power of the diode laser alone is not sufficient. Due to the tapered structure of a TA, its output beam has an improved spatial mode compared to other amplifier types, such as broad-area striped amplifiers. An examples for the use of TAs is the realization of optical tweezers to trap and investigate biological samples [6].

In atomic physics TAs play an important role for laser cooling and trapping. Especially if it is about large capture regions, the total power of the laser beam has to be high in order to provide sufficiently high intensities. This is for example the case in the ArTTA experiment that measures the relative abundance of the radioactive ^{39}Ar isotope in order to date water samples. There, a total amount of five TAs is used to slow down and capture Argon atoms. The TA is one of the working horses

of this experiment.

Complete TA systems are commercially available for upwards of 20.000 € per unit. On the other hand the core of a TA system, the TA diode, is also commercially available and all necessary components to set up a TA system on ones own are in total several thousand Euros cheaper. This makes it worthwhile to built up a TA system by oneself. This work deals with the design and construction of a TA system operating at 812 nm, the closed $1s_5 \rightarrow 2p_9$ cooling transition¹ of Argon needed for the ArTTA experiment.

¹Paschen notation used.

2 Basic features of a tapered amplifier

The purpose of a tapered amplifier (TA) is to amplify the power of an incoming laser beam, the so-called seed beam, from several milliwatts to the order of watts. The operation principle of a TA is very similar to that of a semiconductor laser diode. In this chapter some basic features about tapered amplifiers will be introduced.

2.1 Structure of a tapered amplifier

A sketch of the structure of a typical TA diode is shown in fig. 2.1: The core of the amplifier is an active layer (red) which is embedded in waveguiding layers (light grey) having a higher refractive index than the cladding layers (green). This waveguide structure confines the optical mode in vertical direction. The active region often consists of one or several quantum wells. On top of the structure there is an electrical contact pad (brown) which consists of two parts: A straight, narrow (ca. $3\ \mu\text{m}$) ridge waveguide and a taper with a relatively large output aperture (ca. $200\ \mu\text{m}$) [7, 8, 9]. When a seed beam enters the TA at the side of the ridge waveguide, the ridge waveguide acts as a spatial mode filter due to its small dimensions, leaving only a single mode beam at its end [8]. By traveling through the tapered section of the TA, the beam gets most of its power amplification and exits the TA-diode at the other side. Input and output facets are both antireflection coated. Also shown in fig. 2.1 are the cavity-spoiling grooves near the input facet that are etched into the material. They support the mode filtering of the ridge waveguide and suppress unwanted modes by deflecting backward traveling photons away from the amplifying region.

TAs are usually gain guided in the tapered part, this means that the optical confinement is due to the shape of the electrical contact: Only the area under the tapered contact is electrically pumped and thus optical amplification occurs only in this area, whereas there is no electrical pumping outside that region and optical losses are high. The lateral optical confinement in the ridge waveguide section can be either due to gain guiding as well or due to a special index structure [9, 10]. The opening angle of the taper is usually near the Gaussian diffraction angle of the beam at the end of the waveguide [11]. In order to be amplified by a TA, the incoming beam can be of low power, it just has to have a high power density at the input aperture of the TA [9].

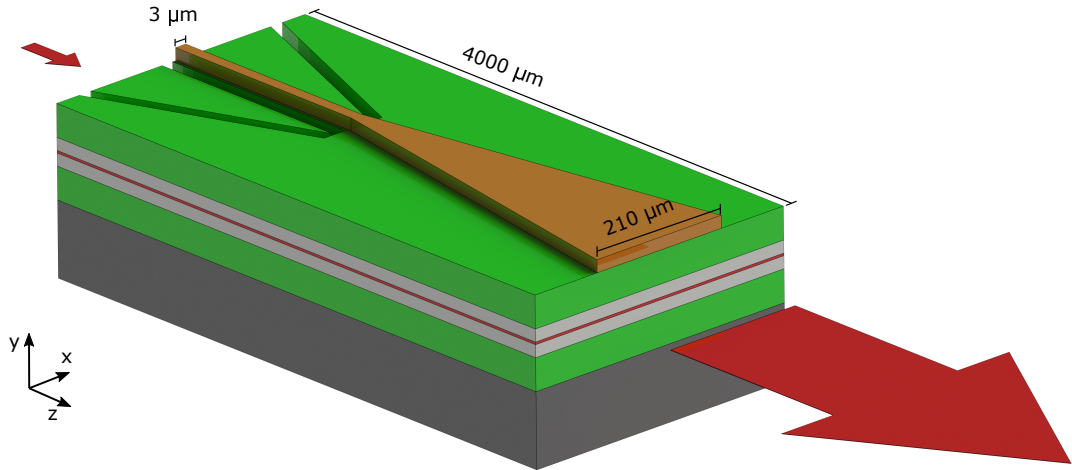


Figure 2.1: Sketch of the structure of a tapered amplifier diode (not to scale) with active layer (red), waveguiding layers (light grey), cladding (green), electrical contact pad (brown) and bulk (dark grey). Cavity spoiling grooves are etched next to the ridge waveguide section. The dimensions are for the TA chip used in this work (EYP-TPA-0808-02000-4006-CMT04-0000 by eagleyard photonics).

2.2 Taper angle and waveguide

The description of the physics that happens inside the active medium of a semiconductor laser amplifier can be very complex. The complexity arises from the many-body interactions between phonons, electrons in the conduction band and holes in the valence band as well as from the interplay between the optical light field and the charge carriers. Phenomenological rate equations are not sufficient for the description of the physics happening in a TA as they do not account for non-linear effects (such as self-focusing and filamentation) [12]. Nevertheless it is possible to describe the complex dynamics and interplay of the electron and hole distributions and the optical light field with so-called Maxwell-Bloch theory. The Maxwell-Bloch theory is a semiclassical theory, i.e. it describes the charge carrier distribution quantum mechanically whereas the light field is mainly treated in a classical manner. The theory is able to consider both: Physical processes occurring on a microscopic level (such as carrier-carrier scattering) as well as macroscopic device properties (e.g. waveguide structure or laser geometry) [12]. The theory includes the space and momentum dependence of the charge carrier distributions and describes the spectral and spatial dynamics of the light field inside the TA diode. It is well suited to describe various semiconductor laser and amplifier systems [12]. More information on Maxwell-Bloch theory can be found in [12, 13].

In [10, 14] numerical simulations have been carried out on the basis of Maxwell-Bloch theory. These simulations investigate the role of the waveguide length and

the opening angle of the taper. From these simulations one can infer that it is important that the waveguide has at least a length of several 100 μm in order to achieve a good beam quality. The waveguide has to be sufficiently long to efficiently mode select the incoming beam [15]. A good mode selection smoothes out the intensity distribution of the propagating light field in the tapered region of the amplifier and thus provides a good quality of the outgoing beam [10]. On the other hand a longer waveguide provides a sufficient preamplification of the injected beam so that the intensity of the beam at the end of the waveguide is big enough to saturate the stimulated emission in the tapered section and thus provide high output powers [14]. According to the simulations presented in [10, 14, 15], the opening angle of the taper should be close to the diffraction angle that a Gaussian beam which exits the waveguide has. If the taper angle corresponds to the Gaussian diffraction angle, the injected beam can keep its Gaussian shape while propagating in the tapered section. Furthermore, there is a good overlap of the active region with the propagating beam [14] (cf. fig. 2.2). If the opening angle of the tapered section is smaller than the Gaussian diffraction angle, the intensity of the light field at the output facet has no longer a Gaussian profile but is laterally cut and looks more like a top hat function. A tapered angle significantly smaller than the Gaussian diffraction angle also favors filamentation [8] (cf. sec. 2.4). If on the other hand the opening angle of the taper is larger than the Gaussian diffraction angle, the tapered region is not fully covered any more by the injected light field at the lateral edges and contributions of amplified spontaneous emission to the output beam increase. The profile of the output beam is then enlarged in lateral direction [14]. In both cases, too small or too large, the quality of the output beam is reduced if the taper angle deviates significantly (i.e. $\sim 1^\circ$) from the Gaussian diffraction angle.

The anti-reflection-coating of the output facet also plays an important role for the quality of the output beam. A bad anti-reflection coating ($R \approx 10^{-2}$) leads to reflected backwards propagating light fields. The interplay of the backwards propagating wave with the charge carriers then can result in multimode lasing behavior and the formation of filaments (c.f. sec. 2.4) [10, 14]. For good beam quality, the anti-reflection coating should be at least $R \approx 10^{-4}$ [14].

It should be noted that the length of the waveguide, the taper angle and the anti-reflection coating are properties of the TA diode which are all set by the diode manufacturer. A user who buys an off-the-shelf TA diode cannot change these properties.

2.3 Amplified spontaneous emission (ASE)

In order to sufficiently amplify the injected seed beam, the carrier inversion inside the active area has to be high. But this high inversion leads also to an increased amount of spontaneous emission occurring inside the active region. Inside the amplifier, not only the injected beam but also the spontaneous emission is amplified. This leads to so-called amplified spontaneous emission (ASE). Thus the total power

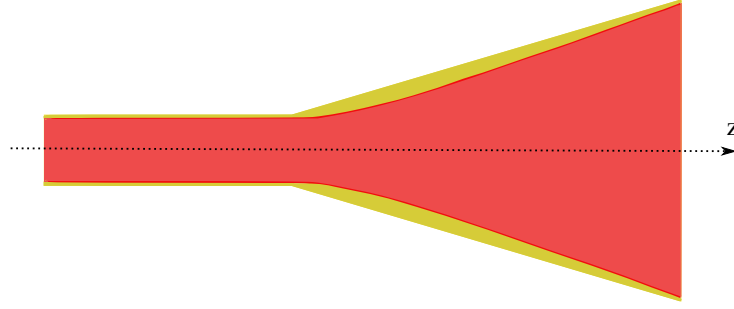


Figure 2.2: Sketch of a TA with a taper angle close to the Gaussian diffraction angle. The light field (red) is not cut by the taper edges and covers almost the whole active area (yellow).

coming out of a seeded tapered amplifier has two contributions: The power from the amplified signal and the power originating from ASE. The wavelength spectrum of the amplified signal corresponds to the wavelength spectrum of the injected beam because the injected beam is amplified via stimulated emission. On the other hand spontaneous emission takes place over the whole bandwidth of the semiconductor active material and thus the spectrum of ASE is much broader than the spectrum of the amplified seed beam [11, 14]. The broad ASE background is illustrated in fig. 2.3.

If one increases the power of the seed beam, the output power of the amplified signal beam rises whereas the contribution of ASE to the output power decreases [11, 14]. This is due to gain competition between the amplified seed beam and ASE. Increasing input power of the seed beam reduces the gain of ASE via the following mechanism: A strong seed beam leads to a strong reduction in inversion in the spectral region of the input beam. This spectral "hole" is refilled by the injection current and by already present charge carriers from other spectral regions via carrier-carrier and carrier-phonon scattering processes. As a consequence of this "hole filling", there is less inversion left for spontaneous emission processes and the gain for ASE is reduced. The ASE is not only reduced in the spectral region of the input beam but over the whole spectral bandwidth of the tapered amplifier [11, 14]. However, at a certain input power of the injected beam (usually some milliwatts), the amplifier is saturated and both the ratio of amplified seed beam and ASE and the total output power cannot be further increased [11, 14]. As already has been mentioned above, the contribution of ASE to the output beam is increased if the taper angle of the amplifier is significantly larger than the Gaussian diffraction angle because there is no gain competition in the outer edges of the tapered region [14].

Even if ASE in general is a parasitic effect of which one wants to get rid of, it can be quite useful in some cases. For example the emitted light by ASE at the input side of an unseeded tapered amplifier makes it much more easy to align a seed laser in order to seed the TA.

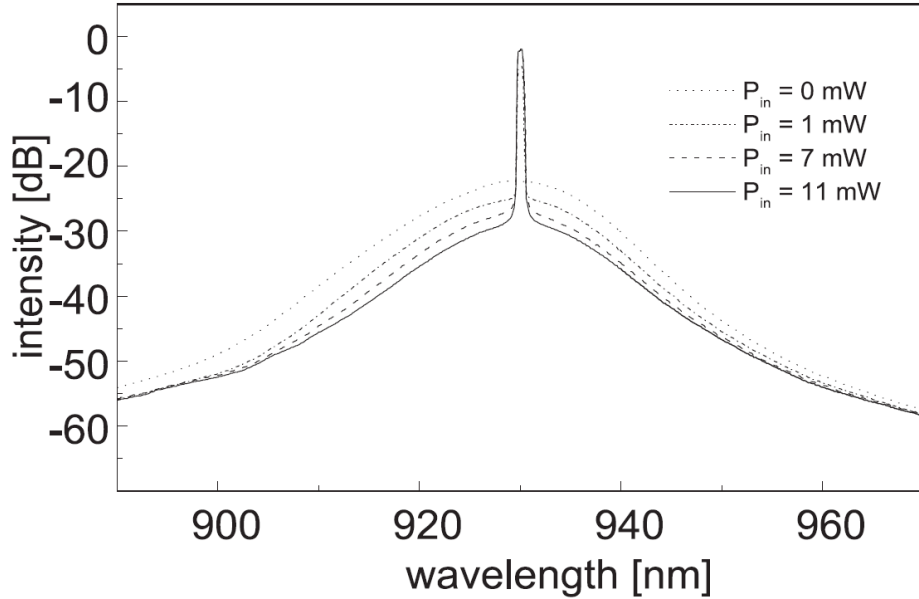


Figure 2.3: Measured spectrum of a 925 nm TA at different seed powers. One can see the broad ASE background and also how the power of ASE reduces with increasing seed beam power P_{in} . The picture is taken from [11].

2.4 Filamentation

One of the main reasons for poor quality of the output beam of TAs is filamentation [8]. Filamentation is a non-linear process that originates from the interplay between optical intensity and refractive index inside the semiconductor medium. This interplay leads to self-focussing of the optical field [9]. In regions of high optical intensities the charge carrier density is reduced due to stimulated emission. This reduction in charge carrier density in turn leads to an increased refractive index in these regions [7, 9, 14, 16]. The locally increased refractive index finally leads to focusing of the propagating light field towards regions with high optical intensity. The described self-focusing mechanism can be detrimental because it can deteriorate the amplification profile of the seed beam. This may happen for example by amplification of small perturbations inside the semiconductor medium (caused by current or temperature fluctuations) [8] or by amplification of spontaneous emission, especially near the taper edges [8, 17]. Filaments caused by self-focused backwards propagating waves can also severely degrade the profile of the output beam if the anti-reflection-coating of the output facet is bad ($\geq 10^{-2}$) [10, 14]. It should be noted that filamentation is strongly reduced by the tapered geometry of TAs compared to, for example, broad-area striped amplifiers.

3 Setup of a tapered amplifier system

In this chapter the most important considerations for setting up a tapered amplifier (TA) system are presented. In particular, one has to handle the TA diode carefully and protect it against wrong electrical handling. Additionally, the highly divergent and astigmatic output beam of the amplifier has to be reshaped in order to make proper use of it. The chapter concludes with a description of the optical path from a seed laser to the output optical isolator of the TA.

3.1 Handling of the TA diode

In fig. 3.1 a mounted TA chip as delivered by TA manufacturers is shown. The particular type of mount in fig. 3.1 is a so-called C-mount. The semiconductor diode is mounted on a heat spreader which connects it thermally and electrically to a metal block. The metal block serves both as heat sink and anode. Additionally there is a clearance hole in the metal block to screw the block to other components. Several parallel bond wires connect the cathode with the semiconductor chip.

The TA diode is very delicate with respect to mechanical stress, one of the most important rules while handling the TA device is thus not to touch the semiconductor part of the device or the bond wires, otherwise it can lead to scratches at the facets of the semiconductor crystal or the thin bond wires can rip. Fig. 3.2 shows top views of two TA diodes, an old diode with bent wires and a new one whose bond wires are all almost parallel to each other. The diode with the bent wires shows a bad performance, since the mode of its output beam has a poor quality that manifests in reduced fiber coupling efficiency and its maximum output power of 1.1 W is far below the specified maximum output power of 2 W. Even if the pure bending of the bond wires is probably not responsible for the performance loss, it is a strong indication that the chip was mechanically damaged (it could have been dropped, touched with tweezers etc.). One way to relatively safely handle a TA device is to use a pair of tweezers and touch the device only at the metal block.

It is not only mechanical stress that one has to be cautious with, there are also a variety of other things that might damage the TA permanently [4]: dust that is accumulated at the end facets of the TA chip can be permanently burnt into the facets by the high output power of the TA. There might occur transient peak voltages that could damage the chip. For this reason a user who handles a TA chip should be electrically grounded. Another source of danger for the chip is to seed the TA while the TA current is turned off. In [4] it is reported that a seed beam with a power larger than 15 mW is already enough to immediately permanently damage an undriven TA chip. On the other hand, the TA chip should not be driven with

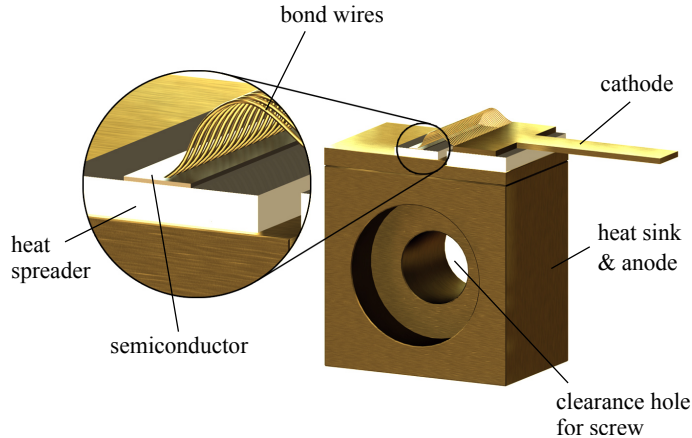


Figure 3.1: TA chip on metal C-mount. The semiconductor diode is electrically connected with a wing shaped cathode via several bond wires. The metal block serves both as heat sink and anode. The picture is taken from [18].

high currents over a longer period of time (\sim hours) without a seed laser [4]. If the TA is seeded, a high fraction of the electrical input power is converted to optical power, whereas the conversion from electrical to optical power drops significantly if the TA is unseeded, where there is only ASE. Thus most of the electrical input power dissipates as heat in the chip. If the TA is driven at high currents for several hours without seed, the TA chip might thermally degrade [4].

3.2 Protection circuit

The TA chip is sensitive to electrical transients. Therefore it is favorable to have a protection circuit between the current controller and the contacts of the chip to protect the TA. The protection circuit should be as close to the TA diode as possible to avoid long cables that might couple to radio frequencies (RF). The protection circuit is inspired by [18], but slightly modified. A sketch of the protection circuit is shown in fig. 3.3. The components from left to right and their functions are listed in the following paragraph.

A rectifier diode, which is reversed biased in normal operation, protects the TA chip against wrong polarity. A ferrite bead blocks frequencies higher than 100 MHz. The resistor together with the capacitors builds a low pass filter. Ferrite bead and low pass filter are important because in the ArTTA-experiment, where the TA shall be used later, frequencies of ca. 50 MHz to 200 MHz are present that shall not be coupled into the TA chip (these frequencies come mainly from acousto-optic modulators and a plasma generating RF-coil [18]). Furthermore, ferrite bead and low pass filter complement one another: The ferrite bead blocks high parasitic frequencies in a range that the low pass filter cannot suppress efficiently any more. A transient

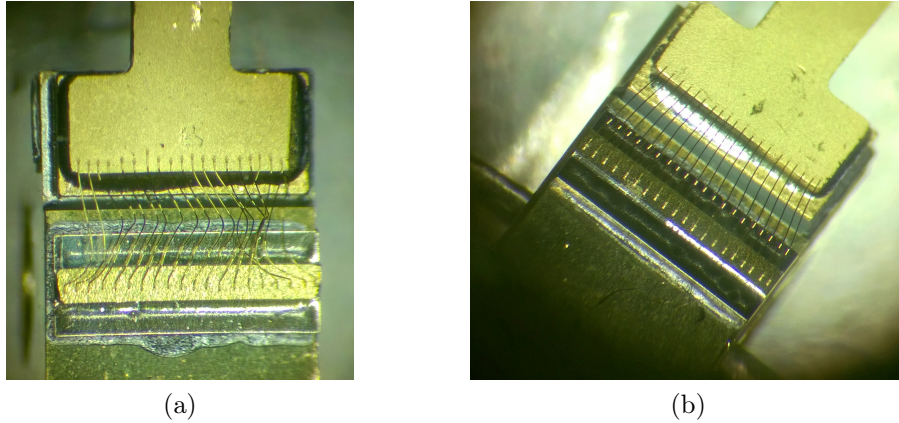


Figure 3.2: Top view on TA chips and bond wires. a) Bond wires of an old chip with bad performance. The bond wires are bent, a clear hint that the chip might have been mechanically damaged. b) Bond wires of a new chip. The wires are all parallel to each other.

voltage suppressor (TVS) diode protects the TA chip against sudden voltage peaks that might arise for example if an electrically charged user gets in electrical contact with the chip. The components of the protection circuit are listed in appendix B. In [18] three diodes in series were used instead of the TVS diode. With this configuration it happened that we observed a sudden drop in the TA output power after having run the TA a certain time (ca. 30 min). The reason was that the threshold voltage of the three diodes in series decreased and instead of the usual small current suddenly all the current went over the diodes in series instead of the TA chip. The decrease in threshold voltage might have arisen due to temperature changes of the diodes.

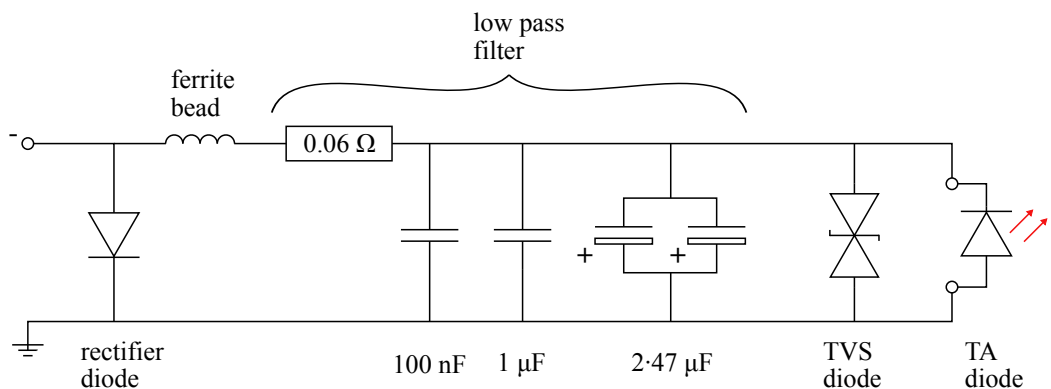


Figure 3.3: Protection circuit for the TA diode with rectifier diode, low pass filter and TVS diode.

3.3 Lenses of the TA setup

In order to generate high output power with the TA and couple it into an optical fiber, some optics in front and right after the TA chip is required. There is an aspheric lens just in front of the input facet of the diode to focus the seed beam onto the small input aperture of the amplifier diode. The output beam of the TA diode is both strongly divergent and asymmetric which means that the beam divergences in the horizontal and vertical direction are very different. In our case, the fast diverging axis corresponds to the vertical axis and the slow diverging axis to the horizontal axis. Furthermore, the output beam shows astigmatism, i.e. the focal point of the fast diverging (vertical) axis is located at the facet of the chip, whereas the focal point of the slow diverging (horizontal) axis lies somewhere inside the chip. It is desirable to couple the output beam into a fiber. In order to achieve high coupling efficiencies the beam should be radially symmetric, i.e. its characteristics in horizontal and vertical direction should be the same. Two lenses are used to reshape the output beam, an aspheric and a cylindrical lens.

In this section both the optimal focal length of the cylindrical lens and its distance from the aspheric lens are estimated with the ABCD law for Gaussian beams. Due to the spatial filtering process in the ridge waveguide section of the TA (cf. sec. 2.1) the horizontal and vertical component of the TA output beam are assumed to behave like Gaussian beams. They are treated independently and thus have different waists and waist locations. For the results of the calculations it is assumed that the aspherical lens has a focal length of 4.51 mm, like it is the case for Thorlabs C230TME-B lenses. This focal length for the aspheric lens was chosen because on the one hand it is small enough to prevent the output beam from opening too much, on the other hand its working distance is large enough to ensure that the lens can be moved close enough to the TA chip without bumping against the TA chip's housing (cf. sec. 4.2.1). A sketch of the lens configuration is shown in fig. 3.4.

3.3.1 q-parameter and ABCD law

The formulas used in this part are all taken from [19] where also additional information about Gaussian beams can be found.

A Gaussian beam is described by several parameters, such as wavelength or waist location. By knowing the size of the beam waist W_0 , i.e. the smallest radius of the beam, and the wavelength of the light λ , one can infer the beam width $W(z)$ at a given distance z from the beam waist

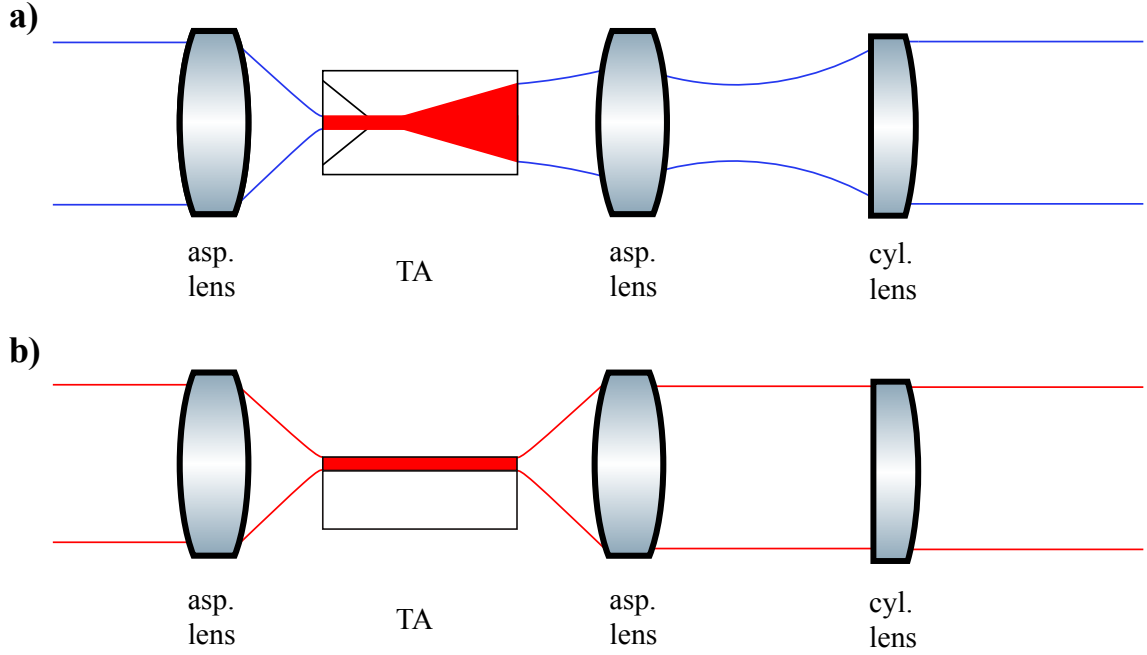


Figure 3.4: Sketch of the beam shape and lens configuration to form the beams before and after the TA chip for a) horizontal (blue) and b) vertical (red) direction. Note that the cylindrical lens is oriented with its curved surface towards the collimated beam to reduce aberrations.

$$W(z) = W_0 \sqrt{1 + \left(\frac{z}{z_0}\right)^2} \quad (3.1)$$

$$z_0 = \frac{\pi W_0^2}{\lambda} \quad (3.2)$$

$$\theta_0 = \frac{W_0}{z_0} = \frac{\lambda}{\pi W_0} \quad (3.3)$$

Here z_0 denotes the Rayleigh range, i.e. the distance z_0 from the beam waist at which the beam radius $W(z_0)$ becomes $W(z_0) = \sqrt{2} \cdot W_0$, and θ_0 is the divergence angle.

A sketch of a Gaussian beam with the corresponding parameters is shown in fig. 3.5. Another possibility to characterize a Gaussian beam is to use the so called q-parameter, a complex number defined via

$$q(z) = z + iz_0 \quad (3.4)$$

The q-parameter is related to the beam width and the radius of curvature of the

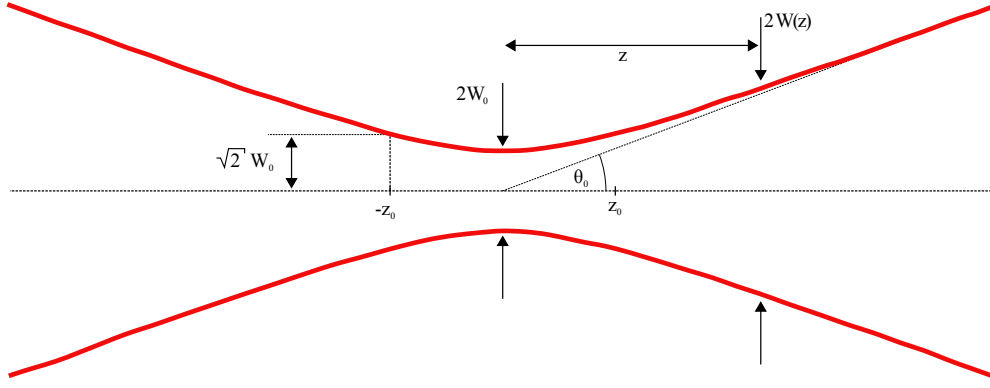


Figure 3.5: Sketch of a Gaussian beam with important parameters. The red lines represent the beam width, i.e. the intensity at the red lines at any transverse plane is $1/e^2$ compared to the intensity on the beam axis.

wavefronts $R(z)$ via

$$\frac{1}{q(z)} = \frac{1}{R(z)} - i \frac{\lambda}{\pi W^2(z)} \quad . \quad (3.5)$$

In paraxial approximation one can use matrices to describe the effect of an optical system on a Gaussian beam. This procedure is similar to ray optics, the same matrices to describe an optical system are used and a combination of optical elements can be also be described by multiplication of the corresponding matrices. The difference is that in ray optics the matrices relate the ray height and angle (with respect to the optical axis) of the input and output rays, whereas in Gaussian beam optics the matrices relate the q-parameters of the input and output beams. Let an optical system be described by a matrix M

$$M = \begin{pmatrix} A & B \\ C & D \end{pmatrix} \quad .$$

The output q-parameter q_2 is related to the input q-parameter q_1 via the so called ABCD law

$$q_2 = \frac{Aq_1 + B}{Cq_1 + D} \quad . \quad (3.6)$$

Note that the q-parameter is a complex number. To get q_2 from q_1 , one does not multiply q_1 with the matrix M , but relates q_2 to q_1 via the individual components of M in the manner given by the ABCD law. In paraxial approximation the ABCD law is sufficient to describe the effect of an optical system on a Gaussian beam.

3.3.2 Calculation of the focal length for the cylindrical lens

To shape the output beam of the TA we use a simple combination of an aspheric and cylindrical lens. The aspheric lens we use is a Thorlabs C230TME-B with a focal length $f_{asp} = 4.51$ mm. The goal is to produce a beam with the same q-parameters

in both the vertical and horizontal direction. Therefore the ABCD-matrices for both directions are calculated. We need [19]

$$\text{propagation in free space: } M_{prop}(d) = \begin{pmatrix} 1 & d \\ 0 & 1 \end{pmatrix}, \quad (3.7)$$

$$\text{transmission through a thin lens: } M_{lens}(f) = \begin{pmatrix} 1 & 0 \\ -\frac{1}{f} & 1 \end{pmatrix}. \quad (3.8)$$

Here f and d denote the focal length of the thin lens and the distance covered in free space, respectively. Thus the transfer matrix for the vertical component of the Gaussian beam is

$$\begin{aligned} M_{ver} &= M_{prop}(d) \cdot M_{lens}(f_{asp}) \cdot M_{prop}(f_{asp}) \\ &= \begin{pmatrix} 1 & d \\ 0 & 1 \end{pmatrix} \cdot \begin{pmatrix} 1 & 0 \\ -\frac{1}{f_{asp}} & 1 \end{pmatrix} \cdot \begin{pmatrix} 1 & f_{asp} \\ 0 & 1 \end{pmatrix} \\ &= \begin{pmatrix} 1 - \frac{d}{f_{asp}} & f_{asp} \\ -\frac{1}{f_{asp}} & 0 \end{pmatrix}. \end{aligned} \quad (3.9)$$

This describes the propagation of the vertical component from the output facet of the chip until it exits the cylindrical lens. d denotes the distance between the principal planes of the cylindrical and aspheric lenses. It is assumed that the distance between output facet and aspheric lens corresponds to the geometrical focal length of the aspheric lens. Furthermore, to simplify calculations, the effect of the cylindrical lens on the vertical beam component is neglected, as it is hardly affected by the cylindrical lens¹.

From now on f_{cyl} shall denote the focal length of the cylindrical lens. The transfer matrix for the horizontal component is the one for the vertical component multiplied by the matrix for the cylindrical lens

$$M_{hor} = M_{lens}(f_{cyl}) \cdot M_{ver} = \begin{pmatrix} 1 - \frac{d}{f_{asp}} & f_{asp} \\ -\frac{1}{f_{cyl}} - \frac{1}{f_{asp}} + \frac{d}{f_{cyl} \cdot f_{asp}} & -\frac{f_{asp}}{f_{cyl}} \end{pmatrix}. \quad (3.10)$$

Eq. (3.10) describes the propagation of the horizontal component from the output facet of the chip until it exits the cylindrical lens.

We now need to know the input q-parameters $q_{1,ver}$ and $q_{1,hor}$ of the vertical and horizontal component of the beam. For the vertical component it is $q_{1,ver} = iz_0$ as the beam waist is located at the output facet of the chip². One can estimate z_0 via

¹For the vertical beam component, the cylindrical lens can be seen as a thin glass plate. To be precise, a glass plate causes a beam displacement if the beam does not incide perpendicular to the plate. However, in the calculations it is assumed that the beam does incide perpendicular on the cylindrical lens.

²The vertical confinement of the beam inside the TA chip is achieved by the epitaxial layer structure, cf. fig. 2.1. The vertical structure of the TA diode stays nearly constant over the whole chip. Thus the beam can only expand in vertical direction after it has left the semiconductor

the divergence angle that is specified in the manufacturer's datasheet³

$$z_0 = \frac{\lambda}{\pi\theta_0^2} \quad . \quad (3.11)$$

With $\theta_{0,ver} = 14^\circ$ and $\lambda = 812 \text{ nm}$ we get

$$z_{0,ver} = 4.33 \times 10^{-3} \text{ mm}$$

and thus

$$q_{2,ver} = \frac{\left(1 - \frac{d}{f_{asp}}\right)iz_{0,ver} + f_{asp}}{-\frac{1}{f_{asp}}iz_{0,ver}} = \underbrace{\left(d - f_{asp}\right)}_{:=z_{2,ver}} + i \underbrace{\frac{f_{asp}^2}{z_{0,ver}}}_{:=z_{0,2,ver}} \quad . \quad (3.12)$$

This result means that after the transition through the aspheric lens the new beam waist of the vertical component is located at $d = f_{asp}$ behind the aspheric lens. At first sight this might be a little bit surprising because one might expect the beam waist to be exactly at the location of the lens. A look on the new Rayleigh length $z_{0,2,ver} \approx 4700 \text{ mm}$ reveals that this is much larger than the distance between new beam waist and aspheric lens. If one additionally takes a look on the new radius of curvature R of the wavefronts

$$\begin{aligned} \frac{1}{q_{2,ver}(d)} &= \frac{1}{\left(d - f_{asp}\right) + i \frac{f_{asp}^2}{z_{0,ver}}} = \frac{d - f_{asp}}{\underbrace{\left(d - f_{asp}\right)^2 + \frac{f_{asp}^4}{z_{0,ver}^2}}_{R(d)^{-1}}} - i \frac{\frac{f_{asp}^2}{z_{0,ver}}}{\left(d - f_{asp}\right)^2 + \frac{f_{asp}^4}{z_{0,ver}^2}} \\ \Rightarrow R(d) &= \frac{\left(d - f_{asp}\right)^2 + \frac{f_{asp}^4}{z_{0,ver}^2}}{d - f_{asp}} \stackrel{d=0}{=} \underset{\text{at asp. lens}}{-f_{asp}} \left(1 + \left(\frac{f_{asp}}{z_{0,ver}}\right)^2\right) \quad , \end{aligned}$$

one sees that the absolute value of R is extremely large (as $f_{asp} \gg z_{0,ver}$) and its sign is negative. That means that the wavefronts are almost plane and converging. Thus the distance between the new beam waist and the lens is extremely small compared to the "diverging dimensions" of the beam. The reason why in the calculation the beam waist is not exactly at the position of the lens is because it was assumed that the distance between the aspheric lens and the TA chip corresponds to the *geometrical* focal length. However, in Gaussian optics this distance has to be a little bit smaller in order to set the new beam waist exactly at the position of the aspheric lens [19].

The horizontal component of the beam has its beam waist somewhere inside the chip, thus its input q-parameter is $q_{1,hor} = z_{hor} + iz_{0,hor}$ and its output q-parameter

material. This causes the beam waist in vertical direction to lie at the chip's output facet.

³We use a chip by eagleyard photonics with centerwavelength 808 nm and 2 W output power, EYP-TPA-0808-02000-4006-CMT04-0000. The datasheet can be downloaded at <http://www.eagleyard.com/products/tapered-amplifiers/>

is (with the matrix coefficients taken from M_{hor} , see eq. (3.10))

$$\begin{aligned}
q_{2,hor} &= \frac{(1 - \frac{d}{f_{asp}})(z_{hor} + iz_{0,hor}) + f_{asp}}{(-\frac{1}{f_{cyl}} - \frac{1}{f_{asp}} + \frac{d}{f_{cyl} \cdot f_{asp}})(z_{hor} + iz_{0,hor}) - \frac{f_{asp}}{f_{cyl}}} = \dots = \\
&= \left[\left[\left(-\frac{1}{f_{cyl}} - \frac{1}{f_{asp}} + \frac{d}{f_{cyl} \cdot f_{asp}} \right) z_{hor} - \frac{f_{asp}}{f_{cyl}} \right]^2 \right. \\
&\quad \left. + z_{0,hor}^2 \left(-\frac{1}{f_{cyl}} - \frac{1}{f_{asp}} + \frac{d}{f_{cyl} \cdot f_{asp}} \right)^2 \right]^{-1} \times \\
&\left[\left(\left(1 - \frac{d}{f_{asp}} \right) z_{hor} + f_{asp} \right) \left(\left(-\frac{1}{f_{cyl}} - \frac{1}{f_{asp}} + \frac{d}{f_{cyl} \cdot f_{asp}} \right) z_{hor} - \frac{f_{asp}}{f_{cyl}} \right) \right. \\
&\quad \left. + z_{0,hor}^2 \left(1 - \frac{d}{f_{asp}} \right) \left(-\frac{1}{f_{cyl}} - \frac{1}{f_{asp}} + \frac{d}{f_{cyl} \cdot f_{asp}} \right) \right. \\
&\quad \left. + iz_{0,hor} \right] . \tag{3.13}
\end{aligned}$$

Now the input q-parameter of the horizontal component $q_{1,hor}$ has to be known. $z_{0,hor}$ can again be calculated using the divergence angle (see eq. (3.11)). With $\theta_{0,hor} = 7^\circ$ one gets

$$z_{0,hor} = 1.73 \times 10^{-2} \text{ mm} .$$

To estimate z_{hor} (i.e. how far the beam waist of the horizontal component is away from the exit facet of the chip) we make the assumption that the beam fully covers the output aperture (cf. sec. 2.2) that is $210 \mu\text{m}$ wide according to the datasheet. From this, with the knowledge of $z_{0,hor}$ and eqs. (3.2) and (3.3) one gets

$$z = z_0 \sqrt{\left(\frac{\pi \theta_0 W(z)}{\lambda} \right)^2 - 1} \tag{3.14}$$

and therefore

$$z_{hor} = 859 \mu\text{m} .$$

This value is not the actual position of the beam waist inside the TA chip (because of the higher refractive index of the semiconductor material), but one can use it to carry out the calculations with the ABCD formalism ⁴.

The goal is now to choose the focal length of the cylindrical lens and the distance between the cylindrical and the aspheric lens such that the q-parameters of the

⁴This is consistent because the propagation matrix $M_{prop}(f_{asp})$ that was used to calculate M_{hor} deals with propagation in air. Also the backcalculation of the input q-parameter $q_{1,hor}$ is done with the divergence angle in air $\theta_{0,hor}$. Thus it is okay to disregard the refraction index of the semiconductor material in the formalism, as the details of the propagation inside the TA chip do not matter in the formalism, the only quantity that counts is $q_{1,hor}$ that is calculated from quantities measured in air.

horizontal and the vertical component are equal:

$$q_{2,hor} = q_{2,ver} \quad , \quad (3.15)$$

which is equivalent to

$$\text{Re}(q_{2,hor}) = \text{Re}(q_{2,ver}) \quad (3.16)$$

and

$$\text{Im}(q_{2,hor}) = \text{Im}(q_{2,ver}) \quad . \quad (3.17)$$

Eqs. (3.16) and (3.17) were solved numerically (with $f_{asp} = 4.51$ mm). The result for the focal length of the cylindrical lens f_{cyl} and the distance between the principal planes of the aspheric and the cylindrical lens d are

$$f_{cyl} = 47.4 \text{ mm}$$

$$d = 75.5 \text{ mm} \quad .$$

Fig. 3.6 shows the calculated beam radii for the horizontal and vertical component for the above values of f_{cyl} , d and f_{asp} . It is important to note that the above calculation can only give an estimation of the right focal length of the cylindrical lens as we made the assumption that the beam emerging from the TA diode is purely single-mode and behaves perfectly Gaussian in each component. Furthermore, lens manufacturers offer lenses only with certain focal lengths, so the best lens combination has to be found experimentally.

Fig. 3.7a and 3.7b show calculated beam radii for a $f_{cyl} = 40.0$ mm and a $f_{cyl} = 50.0$ mm cylindrical lens, respectively. These focal lengths are available off-the-shelf. For the simulations in fig. 3.7a and 3.7b, the distance of the cylindrical lenses from the horizontal beam waist is set to the focal length of the cylindrical lenses. This makes sense from a geometrical point of view and is also confirmed in fig. 3.6, where the deviation between focal length and distance between horizontal beam waist and cylindrical lens is less than 0.3%.

3.4 Experimental setup

The setup that we used to seed the TA and to shape its output beam is shown in fig. 3.8. As a seed laser an external cavity diode laser (ECDL) in Littrow configuration with a wavelength of 812 nm was used⁵. After the seed laser a Faraday optical isolator is placed to avoid backreflections that might create an additional external cavity and thus influence the spectrum of the ECDL. After the optical isolator a $\frac{\lambda}{2}$ -waveplate is placed to turn the polarization of the seed beam in order to maximize the transmission through the anamorphic prism pair. The anamorphic prism pair reshapes the seed beam from elliptical to spherical. The output power of the TA

⁵The TA diode we use is officially specified for $\lambda = 808$ nm, but it has a certain wavelength range where it can be used, so it also operates fine at $\lambda = 812$ nm.

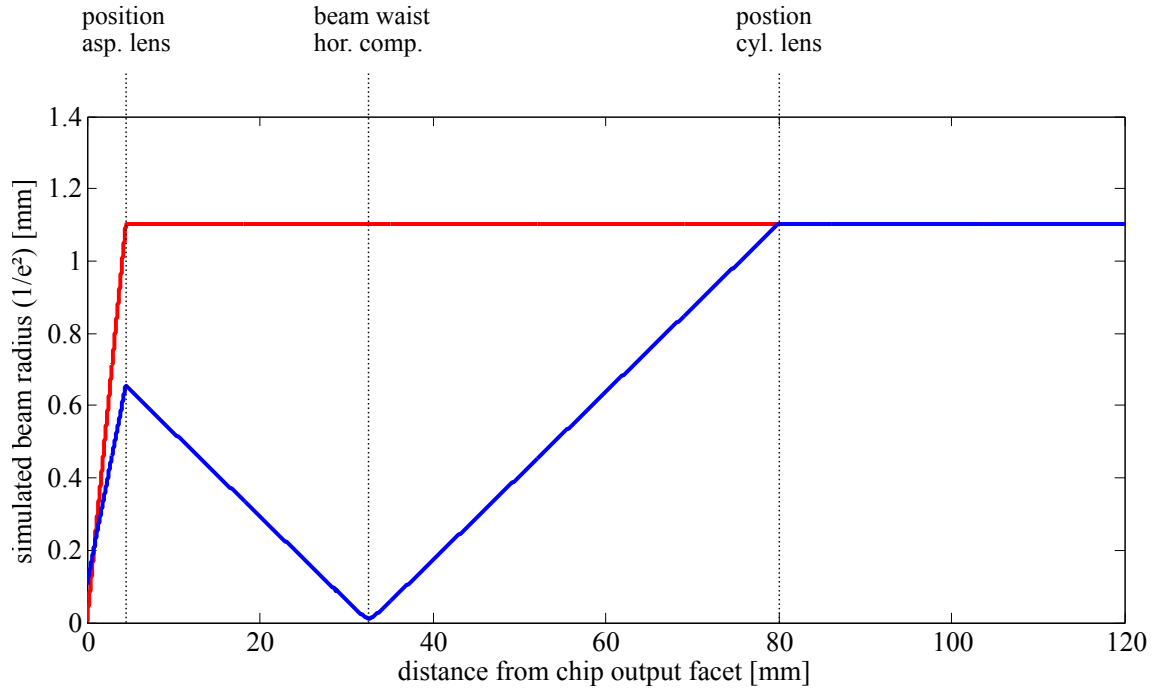
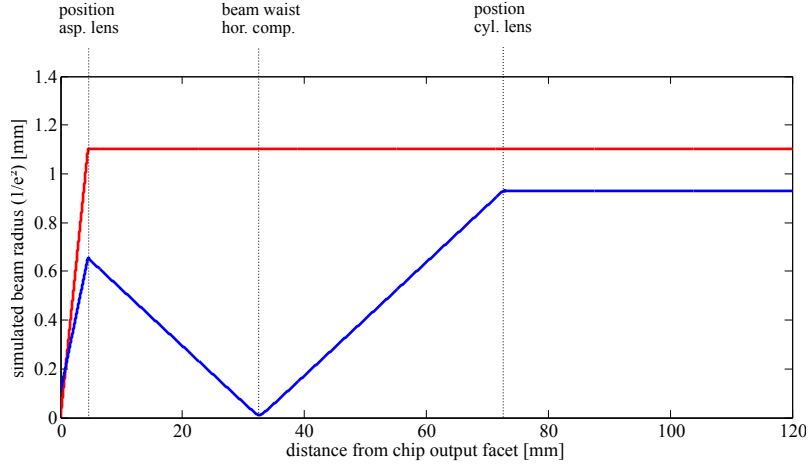


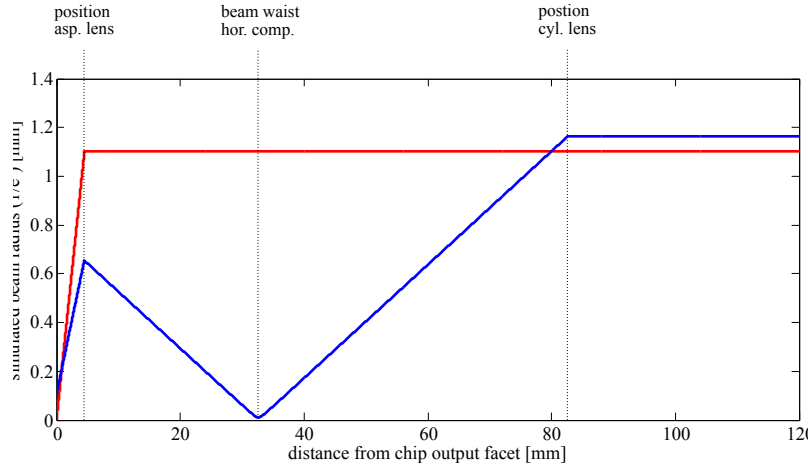
Figure 3.6: Simulation of the evolution of the vertical (red) and horizontal (blue) beam radii of the output beam for a $f_{cyl} = 47.4$ mm cylindrical lens. The origin of the x-axis lies at the output facet of the TA diode. The aspheric lens is placed at 4.5 mm, the cylindrical lens at 80.0 mm after the output facet. This corresponds to a perfect configuration where both beam components have the same radii and are both collimated after the cylindrical lens.

is dependent on the polarization of the seed beam (cf. sec. 5.1), that is why right before the aspheric lens there is another $\frac{\lambda}{2}$ -waveplate. The aspheric lens before the TA focuses the seed beam to the narrow (ca. $3 \mu\text{m}$) input aperture of the TA diode, the two lenses following the TA diode reshape the highly diverging and astigmatic output beam (cf. sec. 3.3). After the cylindrical lens there is another optical isolator as one wants to avoid reflected laser light entering the output facet of TA diode. This may cause damage to the diode [4] or degenerate the quality of its output beam⁶. Mirrors M2 and M3 align the seed beam and direct it to the input aperture. The seeding procedure works as follows: One operates the TA at a current of about 1 A. This causes ASE. Then one adjusts the aspheric lens Asp1 such that the back-

⁶An estimation of how large the attenuation of the isolator should be can be made as follows: Later in this work we measured a 200-times seed beam amplification. According to the TA chip's datasheet, the power at the input facet should not exceed 50 mW. With an amplification of 200, this corresponds to a reflected beam that enters the output aperture of $50 \text{ mW}/200 = 0.25 \text{ mW}$, which is $1/8000$ of the maximum output power of 2 W. Thus the optical isolator should have at least a 8000-times attenuation which corresponds to $\sim 40 \text{ dB}$. However, to be definitely on the safe side, a 60 dB optical isolator was used in this work.



(a) $f_{cyl} = 40.0$ mm, the aspheric lens is placed at 4.5 mm, the cylindrical lens at 72.7 mm after the output facet. The beam components have different radii after the cylindrical lens. The beam is wider in vertical direction, the ratio of the radii is 1:1.18. The divergence angle in horizontal direction is $(1.59 \times 10^{-2})^\circ$, in vertical direction $(1.34 \times 10^{-2})^\circ$.



(b) $f_{cyl} = 50.0$ mm, the aspheric lens is placed at 4.5 mm, the cylindrical lens at 82.7 mm after the output facet. The beam components have different radii after the cylindrical lens. The beam is wider in horizontal direction, the ratio of the radii is 1:1.06. The divergence angle in horizontal direction is $(1.27 \times 10^{-2})^\circ$, in vertical direction $(1.34 \times 10^{-2})^\circ$.

Figure 3.7: Simulation of the evolution of the vertical (red) and horizontal (blue) beam radii of the output beam for different cylindrical lenses. The origin of the x-axis lies at the output facet of the TA diode.

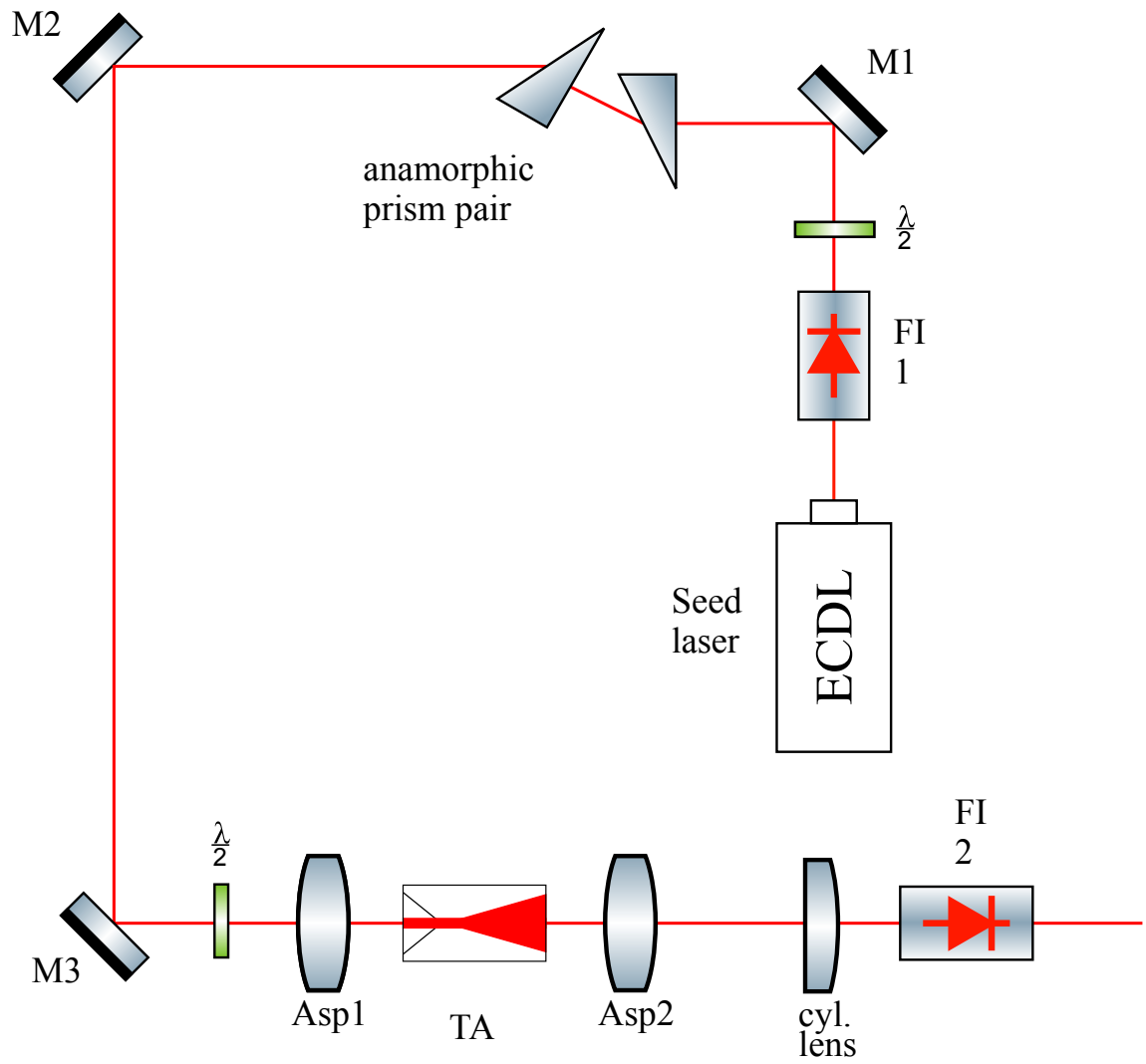


Figure 3.8: Optical path of the setup. Abbreviations used are M: mirror, FI: Faraday isolator, Asp: aspheric lens.

ward propagating ASE is focused at a long distance (e.g. at optical isolator FI1). Now one aligns mirror M3 such that the beam from the ASE and the beam from the seed laser overlap at the output side of FI1 (this can be checked e.g. by placing a lens cleaning tissue there as a "screen" at which one can see both beams). After overlapping the beams at FI1 one overlaps the beams before Asp1 by adjusting mirror M2. The beam overlapping procedure is repeated iteratively until both beams overlap at FI1 and Asp1 at the same time, i.e. they overlap over the whole optical path before the TA. If the seed beam is roughly aligned in the described manner, one can do the fine adjustment of M2, M3 and Asp1 by maximizing the output power of the TA.

4 Tapered amplifier designs

In ch. 3 general considerations about the setup of a tapered amplifier (TA) were presented. One of the biggest challenges in the realization of a TA system is to have precise control of the adjustment of the aspheric lenses and the cylindrical lens as well as mechanical stability of the assembly. This chapter deals with two different TA designs. One design uses a lens holder tube with a fine thread to house the aspheric lens, the other uses commercially available translation mounts to house the aspheric lenses. Furthermore, a fiber-coupled stand-alone TA unit is proposed where all necessary components to seed the TA and to couple its output beam into a fiber are mounted on a single aluminum block.

4.1 TA design with lensholder tubes

The TA design presented in this section is proposed in [4]. The main reason why we tried out this design was its simplicity and thus its low cost. Besides good performance of that design is reported in [4].

4.1.1 Components of the design

This design uses a copper block to mount the TA chip, see fig. 4.1. The TA chip is placed in a slot in that copper block, cf. **2**) in fig. 4.1, and is locked with a M2 screw, cf. **8**) in fig. 4.1.

We additionally placed a sheet of indium foil between the wall of the slot and the C-mount of the chip to increase the electrical and thermal contact between copper block and chip¹. This is important because during operation the chip produces a considerable amount of heat. Additionally, the copper block is electrically connected with the anode of the current controller. At the end of the anode cable there is an eyelet that is connected to the copper block via the set screw, of the lens holder assembly, cf. **3**). Thus the copper block serves three purposes: Housing, anode and heat sink for the TA chip. The cathode of the chip is connected to the current controller via a small copper pin. This copper pin has a slit in its middle for the wing shaped cathode of the TA chip, see fig. 4.2. A M2 headless screw is used to fix the TA chip wing cathode with the copper pin. The copper pin is surrounded by a heat shrink tube to ensure electrical isolation between the copper pin cathode and the copper block anode. The isolated copper pin cathode is lead through a drilled

¹Indium is more malleable than copper and therefore better adjusts to mechanical flatness imperfections.

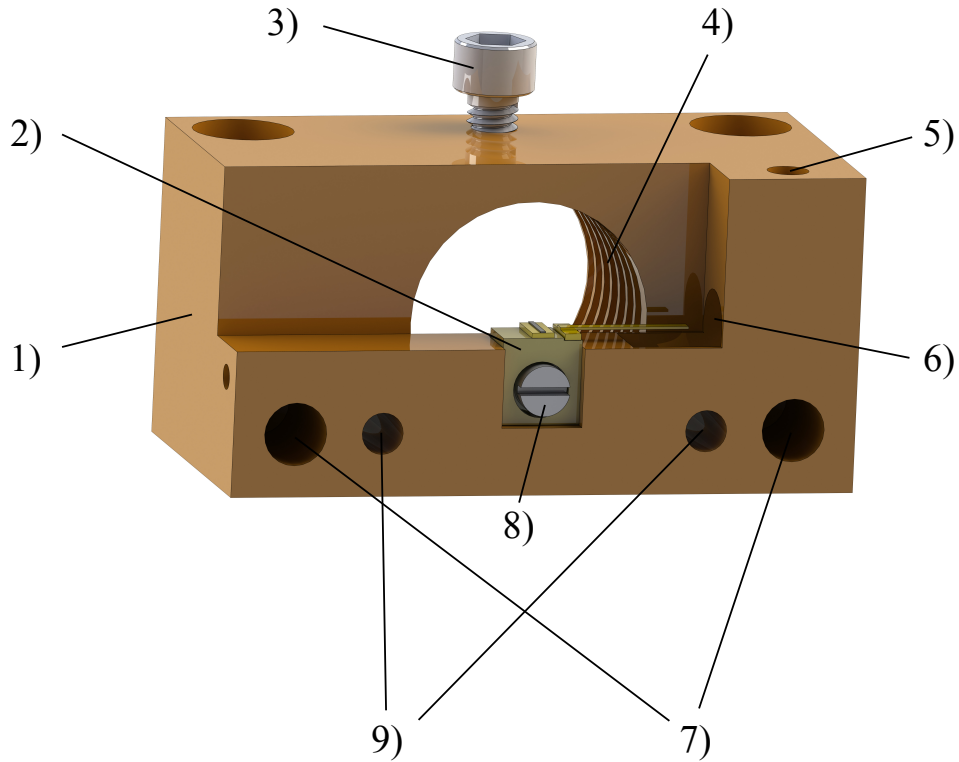


Figure 4.1: Copper mount for TA diode. **1)** copper block, **2)** TA chip housed in slot, **3)** set screw for lens holder assembly and contact for anode, **4)** coarse internal thread for lens holder assembly, **5)** M4 threaded hole for set screw of guiding tunnel, **6)** guiding tunnel for copper pin cathode, **7)** clearance holes for centering rods, **8)** M2 screw, **9)** M4 threaded holes.

hole in the copper block, cf. **6)**. This drilled hole serves as guidance for the cathode pin and improves mechanical stability.

At this point our design differs from the original design in [4]. When we first tried the original design without the guidance, it happened several times that during alignment of the aspheric lenses the cables leading from the protection circuit to the copper pin were touched accidentally. Each time this happened the lenses and mirrors had to be readjusted because even a slight mechanical contact with the cables connected with the TA chip changed its position. This position change was only slight but big enough that one had to realign the optics. With the guidance tunnel and a locking screw, cf. **5)**, the cables that came from the protection circuit and the cathode wing of the TA chip were mechanically decoupled and this problem did not occur further.

The hole in the back behind the TA chip in fig. 4.1 has a coarse thread inside, cf. **4)**, for the lens holder, cf. fig. 4.3. Additionally, there are four holes at the bottom of the copper block. Two of them are threaded, cf. **9)**, and two of them are clearance holes for centering rods (cf. **7)** in fig. 4.1 and fig. 4.3).

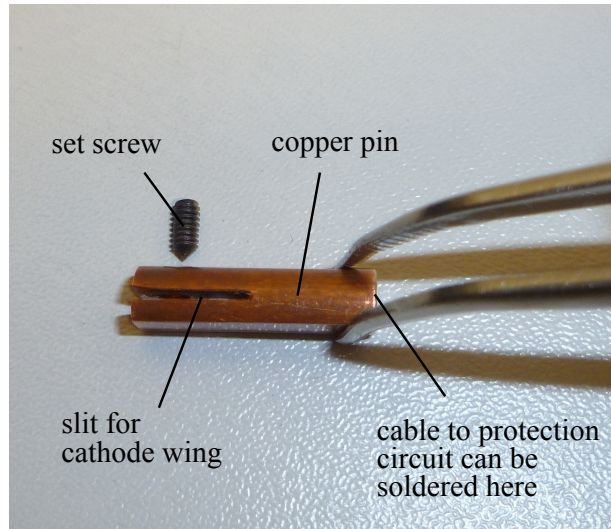


Figure 4.2: Copper pin for the connection of the TA diode with the cathode. Not shown in the picture is the heat shrink tube for electrical isolation.

Fig. 4.3 shows the whole copper block with lens holders and baseplate. The TA chip is mounted in a recess at one of the copper blocks and is fixed by a M2 screw. The aspheric lenses, cf. **e**) in fig. 4.3, that focus the seed beam and shape the output beam of the TA, respectively, are housed in two lens holder assemblies. These lens holder assemblies consist of two parts: An outer brass tube with a coarse external thread, cf. **f**) in fig. 4.3, and an internal fine thread. The inner tube, cf. **a**) in fig. 4.3, is made of stainless steel and has an external fine thread that mates with the internal fine thread of the outer brass tube. The fine thread has a pitch of 0.35 mm per turn. Additionally, the inner lens holder has an internal thread for the aspheric lens (we used a Thorlabs C230TME-B lens with $f = 4.51$ mm).

We decided for the combination of brass and stainless steel to have the inner tube to be made of a harder material than the outer tube. This has the advantage that the risk of damaging the relatively sensitive fine thread is reduced. One mechanism of damaging could be for example that a tiny chip gets onto the fine thread and eats into the thread while screwing the two tubes together. If the two tubes were made of the same material the risk of shavings eating into the threads would be increased whereas with the use of different materials one notices it easier if there is a chip seized between the threads and one then can remove the chip before screwing the tubes together.

The lens holder assemblies are screwed into copper parts with corresponding inner threads, cf. **d**). To ensure the correct relative position between the two copper parts with the lens holders there are two clearance holes in each copper part, cf. **7**) in fig. 4.1. Centering rods are inserted into the clearance holes and connect the two copper parts, cf. **h**). Additional to the centering rods there are two M4 screws that connect the two copper parts, cf. **g**). The two copper parts are screwed on a copper

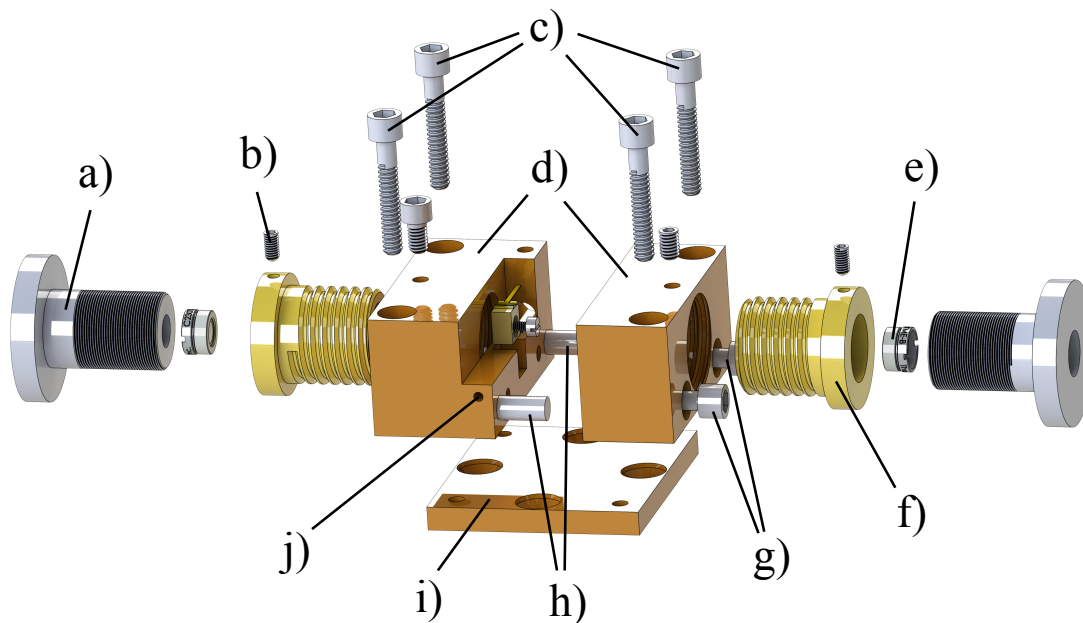


Figure 4.3: Copper mount with lens holder assemblies. **a)** inner lens holder tube, **b)** set screws for inner lens holder tube, **c)** M4 screws for connecting copper parts with baseplate, **d)** copper parts, the left one is in detail shown in fig. 4.1, **e)** aspheric lens, **f)** outer lens holder tube, **g)** M4 screws to connect the two copper parts, **h)** centering rods, **i)** copper baseplate, **j)** hole to place a thermistor.

What is not shown in the picture is that the grips of the inner lens tubes are knurled.

baseplate with another four M4 screws, cf. **c**). Beside the four threaded holes for the connecting M4 screws there are another four M4 countersunk holes in the baseplate for plastic screws that later connect the whole assembly with an aluminum base block (plastic screws are not shown in fig. 4.3).

The TA chip should only be placed in the slot of the copper block *after* the two copper parts have been assembled. This has two reasons: First, heat paste is used to improve the thermal contact between the copper parts and it should not accidentally smear on the TA chip. Second, there is not much play between the clearance holes and the centering rods of the two copper blocks, therefore some force might be necessary to put the two parts together. It can happen that the two parts slightly seize and after trying to press them together even stronger, they suddenly release and slam together. It is safer for the TA diode to not feel the shock of this slam.

Additionally, there are set screws for the outer and inner lens holder tubes, cf. **b**), as well as for the cathode pin (set screw of the cathode pin not shown in fig. 4.3). The small hole at the side of the copper part with the TA chip is to house a thermistor that gives feedback for temperature control, cf. **j**).

The whole assembly that is described in fig. 4.3 is mounted on a aluminum block (fig. 4.4). Between the aluminum base and the copper baseplate a Peltier element is used which provides proper temperature control of the copper parts and the TA diode, cf. **IV**) in fig. 4.4. The aluminum block serves as a heat sink. While working with the whole setup we set the temperature slightly below room temperature. This is cool enough to provide sufficient cooling of the TA diode but still not so cold that condensation on the copper parts or the TA chip occurs. The aluminum block is screwed on the optical table by four M6 screws, cf. **II**) in fig. 4.4. Additionally, there are two sub-D9 size pockets at the lower part of the aluminum block, cf. **VI**). These are for the connection with the current and temperature controller. Two tunnels inside the aluminum block lead cables from the sub-D9 plug connected with the temperature controller to the Peltier element and a thermistor on the one side and from the plug connected with the current controller to the protection circuit on the other side, cf. **V**). The pockets for the controller plugs are placed at the entrance side of the TA (seed side) so the connectors from the controllers are no obstacle to the cylindrical lens after the aluminum block.

Technical drawings of the components in this section can be found in appendix C.

4.1.2 Attempts to control the position of the chip

The design described in the previous subsection allows to adjust the position of the aspheric lenses only in longitudinal direction along the optical axis. There is no possibility to change the lens positions in transverse direction perpendicular to the optical axis. Therefore it is crucial for the performance of the whole design that the TA diode is placed exactly on the optical axis. Despite conscientious planning of the position and dimensions of the slot in the copper block, we had problems to achieve correct alignment of the position of the TA diode. Deviations of the position of the TA diode from the optical axis manifested in a slanting output beam, cf. fig. 4.8.

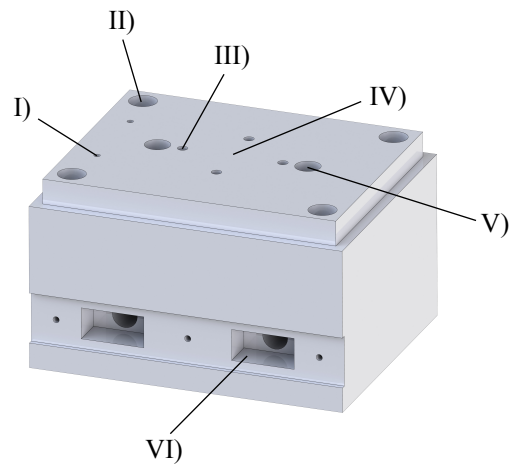


Figure 4.4: Aluminum base of the TA design. **I)** M3 threaded holes to mount the protection circuit, **II)** M6 clearance holes to put the TA setup on an optical table, **III)** M4 threaded holes for connection with copper baseplate (cf. fig. 4.3), **IV)** position of Peltier element, **V)** tunnels for cables, **VI)** Sub-D9 sized pockets.

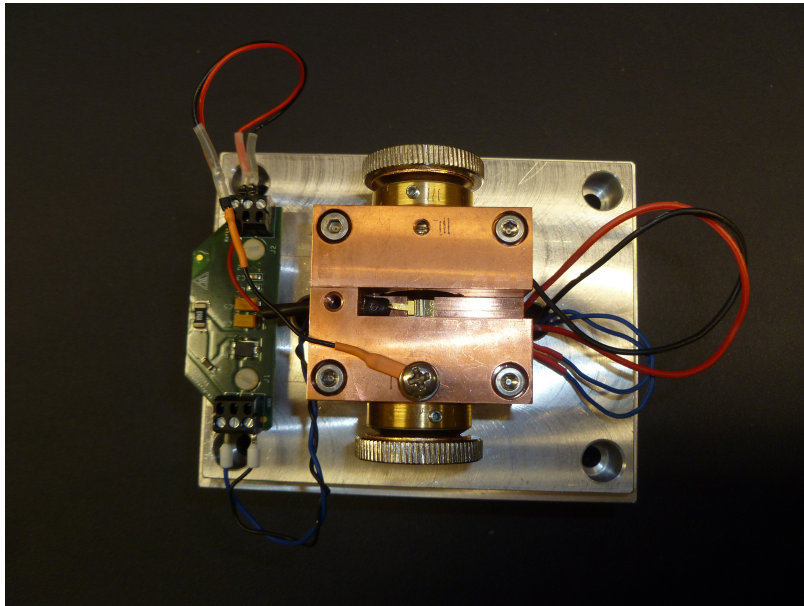


Figure 4.5: Top view on the whole TA setup.

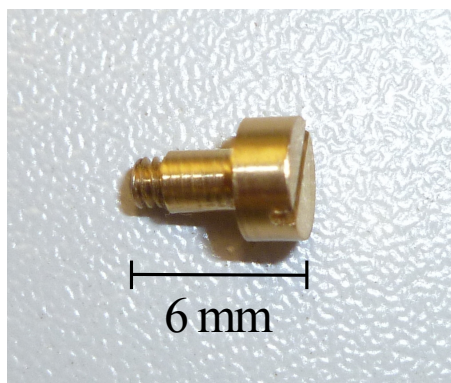


Figure 4.6: Special screw with M2 thread at its tip. The cylinder in the middle part is to define the TA chip's position.

We tried to exactly define the TA diode's position in two different ways.

The first attempt was to define the position only via the position of the threaded hole in the slot of the copper block. Defining the chip's position in that way is a bit challenging because the clearance hole of the C-mount is 2.3 mm, whereas the external diameter of a M2 screw is only 2.0 mm. Thus there is a play of 0.3 mm. A deviation of 0.3 mm from the optical axis is already enough to produce a slanting output beam. Therefore a special screw was fabricated, cf. fig. 4.6. This screw has a M2 thread on its tip and a cylinder in its middle part with a diameter of 2.25 mm that snugly fits into the clearance hole of the C-mount. Unfortunately the problem of the slanting output beam could not be solved even with this special screw. Furthermore, with this screw it was much more difficult to screw the TA diode to the copper block as it was harder to lead the screw through the clearance hole of the C-mount of the chip with that little play. While connecting the TA chip with the copper block one had to be even more cautious than usual to not slip off with the screwdriver and damage the TA diode.

The other method of trying to define the chip's position was to align the chip at the "floor" and the "wall" of the slot in the copper block. For this reason the measures and distances of that slot have to be very precise. But this method did not provide the desired result either.

It was not possible for us to produce an output beam that lies on the optical axis, instead the output beam was always slanting. We tried out several copper blocks and had this problem with each of them. However, the direction of the output beam was different for the different copper blocks. Furthermore it has to be considered that also the C-mounts of the TA chips have tolerances, so even if the aligning procedures described in this section had worked out for one chip, it could well have been that exchanging the TA chip would again give a slanting output beam. This is a big drawback when one wants to produce several TAs of this design as the direction of the output beam would not be well defined. Especially obliqueness of the output beam in vertical direction can cause severe problems with the optical isolator (cf. fig. 3.8) because parts of a vertically slanting beam might be cut by the apertures

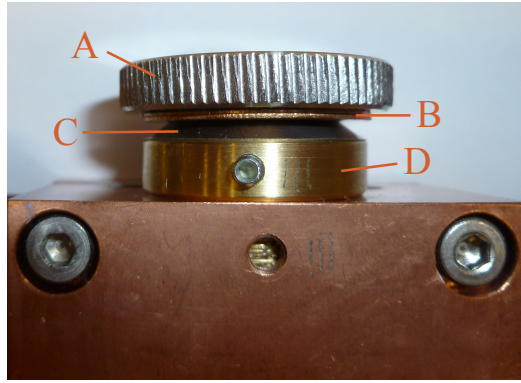


Figure 4.7: Inner (A) and outer (D) lens holder tube together with a combination of Belleville (C) and plain (B) washers to increase the tightness of the fine thread.

of the isolator. It should be noted that in [4] no such problems were reported.

4.1.3 Coupling the output beam into an optical fiber

In order to couple the output beam into an optical fiber the block with the least slanting output beam was used (cf. sec. 4.1.2). It turned out that in the original design in [4], the inner tube of the lens holder assembly (the one that actually houses the aspheric lens) has too much play for stable adjustment of the aspheric lens. There are set screws for the inner tubes (cf. in fig. 4.3), but these are used only if the final position of the aspheric lens is reached. The set screws are loose during the adjustment process. In order to accurately adjust the aspheric lenses, it is therefore desirable that the fine threads of the inner tube are a little bit tighter. Two possibilities were considered to increase the tightness of the fine threads. One way would be the use of another material combination for the lens holder assembly. Conceivable would be for example stainless steel for the inner tube and hard plastic for the outer tube to increase the friction between the two tubes. If the outer tube would be made of plastic, it would not necessarily need to be connected with the copper block via a coarse thread, but could also just be pressed in. The play of the fine thread could then also be adjusted by how tight the set screw is tightened, cf. **3**) in fig. 4.1.

The other possibility that we finally decided for was to decrease the play of the lens holder assembly with a combination of plain washers and Belleville washers that increased the tightness of the fine thread by pressing the threads of the inner and outer tube against each other, cf. fig. 4.7. The Belleville washers we used have only a small range where they work effectively (ca. 1 mm). Therefore one must already roughly know the optimal position of the aspheric lens to place the right number of plain washers between the grips of the inner and outer tube. Thus the fiber coupling procedure can be done iteratively: first, without the Belleville washer in use, adjust the aspheric lens into the approximately right position, then check the space

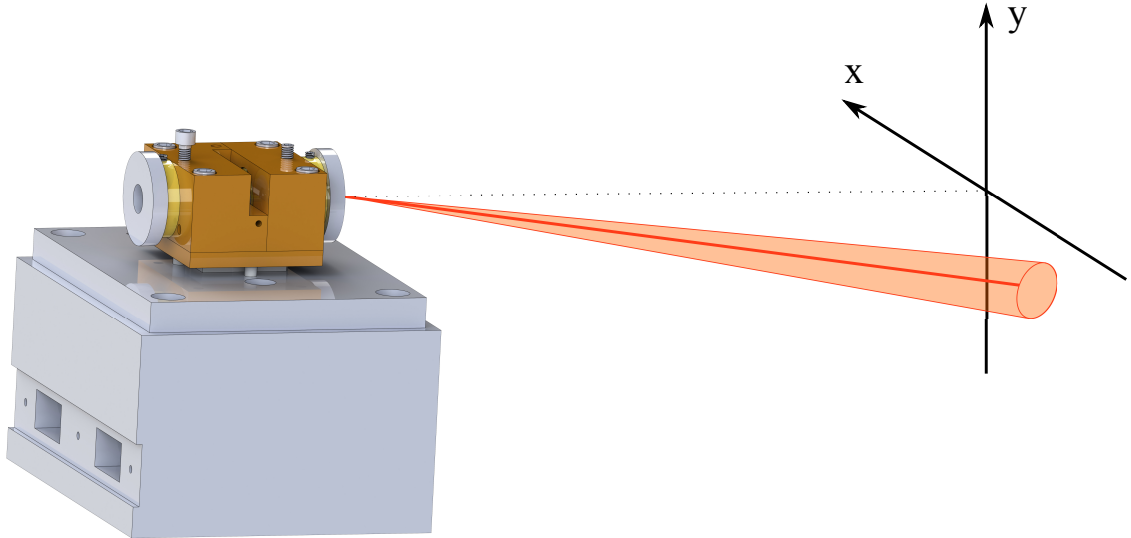


Figure 4.8: Sketch of the slanting output beam. The cone shows the change in position when the aspheric lens is moved.

between inner and outer tube of the lens assembly and how many plain washers will be needed to fill up this space. Then unscrew the inner lens tube, insert the right amount of plain washers and the Belleville washer, screw the inner lens tube in again and now do the fine adjustment of the aspheric lens with the tightened thread. Another problem which occurred during the fiber coupling process was that the position of the output beam changed noticeably when the aspheric lens was moved along the optical axis (see fig. 4.8). This position change was so strong that the optical isolator had to be readjusted several times during the fiber coupling procedure. Most likely the aspheric lens was the cause of these position changes of the output beam: Probably the lens was slightly misaligned in the lens holder tube and thus wobbled when turned back and forth.

4.1.4 Conclusion on this design

The TA design presented in this chapter was proposed in [4]. The big advantage of this design is its simplicity. All optomechanics needed can be built in the workshop of our institute and thus the costs of this design are low. Good performance of this design was reported in [4]. We modified the original design presented in [4]. A guidance drilled hole for the copper pin cathode was added to mechanically decouple the cables from the protection circuit and the cathode wing of the TA diode. With this guidance drilled hole it is not necessary any longer to realign lenses and mirrors after having accidentally touched the cathode wires. We also used a combination of plain and Belleville washers to increase the tightness of the fine thread of the lens holders in order to adjust the lens position more accurately. However, we did not

find a way to control the position of the output beam and, even worse, the output beam changed its position when the aspheric lens at the output side was moved along the optical axis. This made it inefficient and cumbersome to couple the beam into an optical fiber. It thus would be desirable to have a design that allows control of the lens position not only in longitudinal direction, but also in transverse direction and that prevents the lens from wobbling while being shifted back and forth.

4.2 TA design with cage system

In sec. 4.1 it was found to be crucial for efficient fiber coupling that the position of the aspheric lens can be well controlled. The control needs to be both in the direction along the optical axis and in the plane perpendicular to it. In this section a design based on a cage system is presented that allows for this control.

4.2.1 Components of the design

To give precise control of the position of the aspheric lenses, a cage system was applied. Fig. 4.9 shows the components of this cage system design. The TA chip is mounted on a copper block, cf. **3)** and **10)** in fig. 4.9, respectively. This mounting copper block is placed on a copper baseplate, cf. **9)** in fig. 4.9. Mounting block and baseplate are connected via two M4 countersunk metal bolts, cf. **8)** in fig. 4.9. We used copper as material due to its good thermal and electrical conductance. In the baseplate there are another four counterbored holes for M4 plastic screws, cf. **7)**. Cage rods are led through corresponding clearance holes in the mounting copper block, cf. **6)**. A translation mount that houses an aspheric lens is placed on each side of the TA diode on the cage rods, cf. **1)** and **11)**. The translation mount is a Thorlabs CXYZ05/M device. With this translation mount one can adjust the position of the aspheric lens along the optical axis and perpendicular to it. The adjustment accuracy in z-direction is 500 μm per turn and 254 μm in both x- and y-direction (this corresponds to 50.8 and 100.0 turns per inch, respectively). The total travel range is 3 mm in each direction. During translation in z-direction the aspheric lens does not rotate. This prevents wobbling of the lens as it was observed in sec. 4.1.3. In this work a Thorlabs C230TME-B lens ($f = 4.51 \text{ mm}$) was used as aspheric lens. An adapter between the SM05 internal thread of the translation mount and the M9 \times 0.5 external thread of the aspheric lens is also needed, cf. **5)**. The cage rods were chosen to be rather short and only hold the translation mounts for the aspheric lenses. The reason for the shortness of the cage system is that this reduces the lever of the cage rods. This in turn decreases the risk of bending of the rods and the risk that components aligned along the cage rods seize. In [18] a TA design was proposed with a longer cage system that also includes a cylindrical lens and a mirror. In that design jamming of the components held by the cage rods as well as bending of the rods was observed.

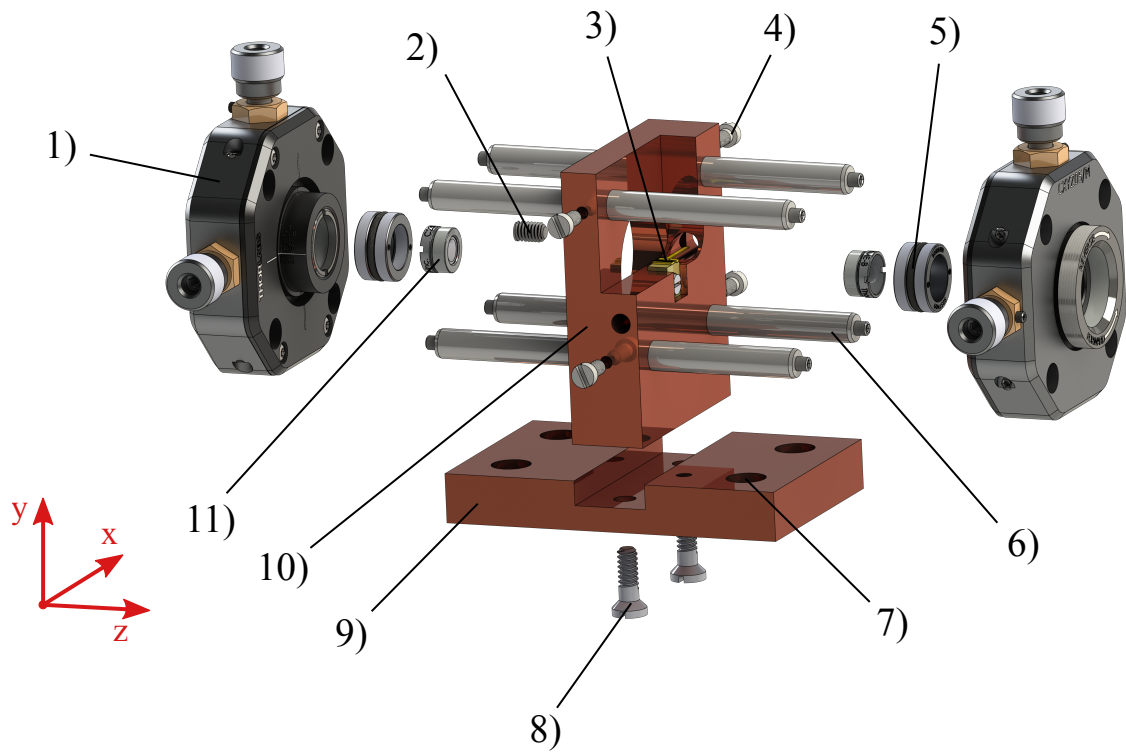


Figure 4.9: Components of the cage system. **1)** Translation mount, **2)** headless M4 plastic set screw for cathode pin guiding, **3)** TA chip, **4)** M3 plastic set screws for cage rods, **5)** adapter for threads of lens and translation mount, **6)** cage rods, **7)** counterbored holes for plastic screws, **8)** M4 countersunk screws, **9)** copper baseplate, **10)** mounting copper block, **11)** aspheric lens.

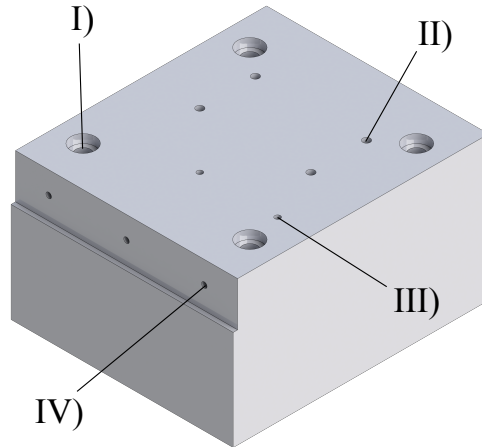


Figure 4.10: Aluminum socket to mount the cage system. **I)** Four M6 counterbored holes to screw the aluminum block to an optical table, **II)** four M4 threaded holes to connect with the cage system via plastic screws, **III)** two M3 threaded holes to place the protection circuit, **IV)** three M3 threaded holes to place a metal plate that holds the plugs for the temperature and current controllers.

Four M4 plastic screws mount the whole assembly on an aluminum socket. Between the aluminum socket and the copper baseplate a Peltier element is placed that provides temperature regulation (cf. sec. 4.1.1). Fig. 4.10 shows the aluminum socket.

In this work a lot of considerations were put into the design of the copper mount (cf. fig. 4.11) of the TA chip, therefore it is described here in more detail.

The TA chip is placed in a slot in the middle of the copper block, cf. **b)** in fig. 4.11. The dimensions of the slot are chosen such that the TA diode should lie, according to the chip's data sheet, right on the optical axis if the C-mount of the chip abuts against one of the side walls and the bottom of the slot, cf. **k)** in fig. 4.11. The C-mount of the chip snugly fits inside the slot, there is a maximum play of 0.15 mm. Between the C-mount of the TA diode and the back wall of the slot, cf. **h)** in fig. 4.11, a sheet of indium foil is placed to increase the electrical and thermal contact between TA chip and copper block. The TA chip is fixed with a M2 screw to the copper mount. The slot is ca. 1.5 mm deeper than the depth of the C-mount of the TA chip. This has the advantage that the TA chip is protected against accidental collision with the aspheric lens. With the slot being deeper than the C-mount of the chip one can at the most bump the edges of the slot with the lens mount but not the TA chip itself. The slot is not too deep either so that the aspheric lens still can be moved close enough to the chip to shape the output beam properly.

The opening behind the TA chip, cf. **g)**, is to give space for the seed side translation mount to move the seed focusing aspheric lens close enough to the TA diode. Here a compromise had to be found: On the one hand the back wall of the slot, cf. **h)**, should be thick to improve heat conduction away from the TA chip and mechanical stability of the threaded hole. On the other hand a thin back wall provides a

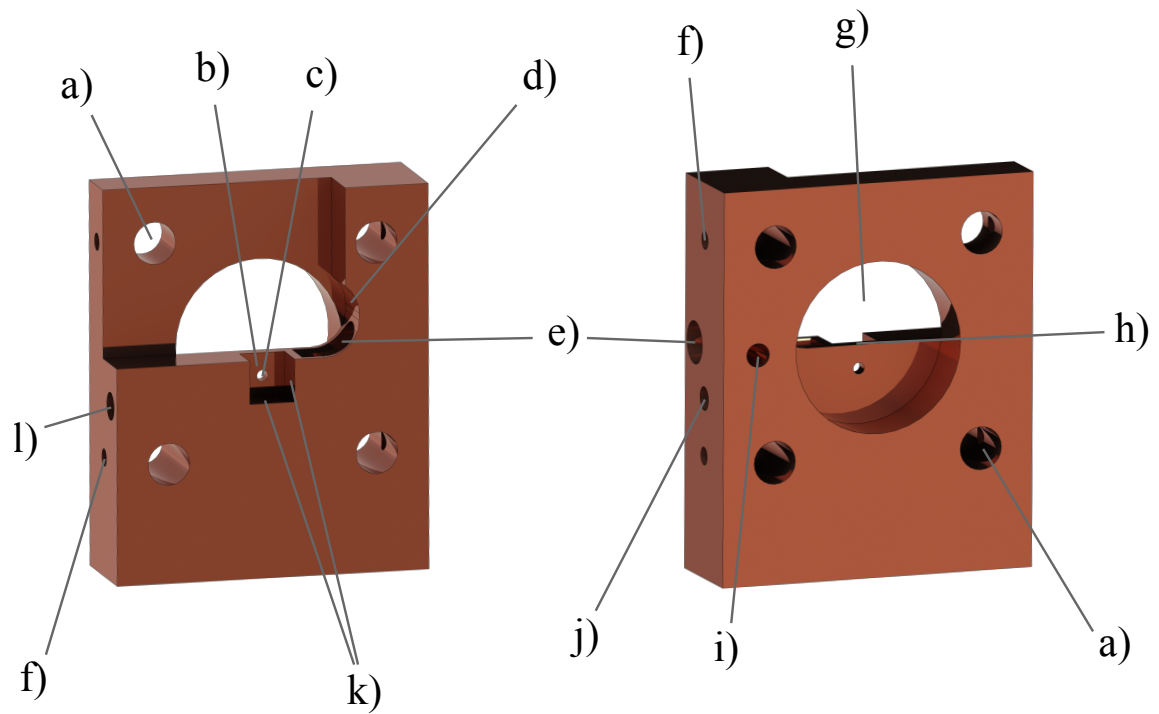


Figure 4.11: Front and back side of the copper housing of the TA chip. **a)** clearance holes for cage rods, **b)** slot to place the TA chip, **c)** M2 threaded hole, **d)** recess, **e)** guiding tunnel for cathode connection pin, **f)** M3 threaded holes for set screws, **g)** opening for translation mount, **h)** back wall of slot for TA chip, **i)** M4 threaded hole for set screw, **j)** M4 threaded hole to connect with anode cable, **k)** planes that define the TA chip's position, **l)** hole to place thermistor.

larger range for the aspheric lens and allows the aspheric lens to get closer to the TA diode. With the finally chosen thickness of the back wall of 1.9 mm, one gets sufficient mechanical stability and heat conduction and the aspheric lens can still be moved close enough to the TA chip.

The drilled hole next to the TA chip, cf. **e)**, is a guidance for the cathode connecting copper pin (cf. sec. 4.1.1 and fig. 4.2). A M4 plastic set screw additionally fixes the isolated copper pin, cf. **2)** in fig. 4.9. The plastic set screw is a headless one that allows the translation mount on the seed side to move close enough to the TA diode. The recess at the cathode guiding tunnel, cf. **d)** in fig. 4.11, serves two purposes. First, it facilitates the positioning of the TA chip into the slot. Second, it reduces the risk of an electrical short caused by contact between the headless set screw of the cathode copper pin (cf. fig. 4.2) and the copper block. Without the recess such electrical shorts actually did occur.

The M4 threaded hole at the side of the copper block is for connection with the eyelet of the anode cable, cf. **j)**, such that the whole copper block serves as anode for the TA chip. The drilling at the other side of the copper block is to house a thermistor close to the TA chip, cf. **l)**. We glued the thermistor into this hole with 2-component epoxy resin adhesive. To increase the thermal conductivity of the epoxy resin adhesive, it was mixed with zinc oxide.

Four clearance holes hold the rods for the cage system, cf. **a)**. M4 plastic set screws are used to additionally fix their position, cf. **4)** in fig. 4.9. We chose for plastics set screws and not for metal set screws to avoid scratching the cage rods with the set screws. Scratched rods have increased risk to seize and damage the clearance holes. With this cage system design the problems mentioned in sec. 4.1 concerning the direction of the output beam did not occur any longer. With this design it is also easier to place the chip into the slot compared to the design described in sec. 4.1. However, while coupling the output beam into a fiber, hysteresic behavior of the translation mount holding the aspheric lens was observed, i.e. turning the position adjusters of the translator in one direction a certain number of turns and then turning it back into the other direction the same number of turns did not result in the exactly same position of the lens². Nevertheless, good accuracy of the lens position could be achieved if the lens was only moved in one direction.

Fig. 4.12 shows the realized cage system. Detailed drawings of the mounting copper block, the copper baseplate and the aluminum socket can be found in appendix D.

4.2.2 Conclusion on this design

In this section a design for a TA setup was presented that allows convenient and stable positioning of the aspheric lenses. This design consists of a cage system and commercially available translation mounts for the aspheric lenses. Furthermore, the presented design facilitates mounting of the TA diode compared to the design presented in sec. 4.1.

²Hysteresic behavior was also observed for the other design described in sec. 4.1.

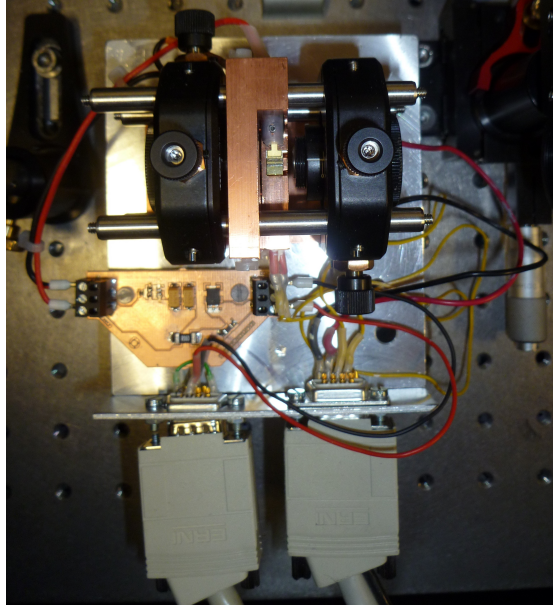


Figure 4.12: TA setup with cage system. Also shown on the picture are the protection circuit as well as the connections of the current and temperature controller.

4.3 Stand-alone TA unit

For the TA setups which are presented in sec. 4.1 and 4.2, most of the components like mirrors or cylindrical lens were mounted on an optical table. The purpose of a TA is to amplify an input laser beam of some tens of milliwatts and give an output beam with a power of some hundreds of milliwatts to some watts. For the setup of an experiment it can be convenient to divide the experiment into different modules. Thus it is desirable to have a stand-alone TA unit that is connected to the rest of the experiment only by two optical fibers, one input fiber for the seed beam and one output fiber for the amplified beam. Such a stand-alone fiber-coupled unit could look like the one shown in fig. 4.13.

In fig. 4.13 all necessary components are mounted on an aluminum block. The cylindrical lens is mounted in a z-axis translation mount, in this case a Thorlabs SM1ZP/M device that allows for a total travel of 2.0 mm in z-direction with an accuracy of 50 μm per revolution of the actuator knob (that corresponds to 508 turns per inch). Translation mount of the cylindrical lens and optical isolator are both post mounted. This allows for adjustment of their positions in x- and y-direction as well as a tilt in y-direction. The fiber couplers of the seed beam and output beam are composed of several off-the-shelf components and are housed in a kinematic ro-

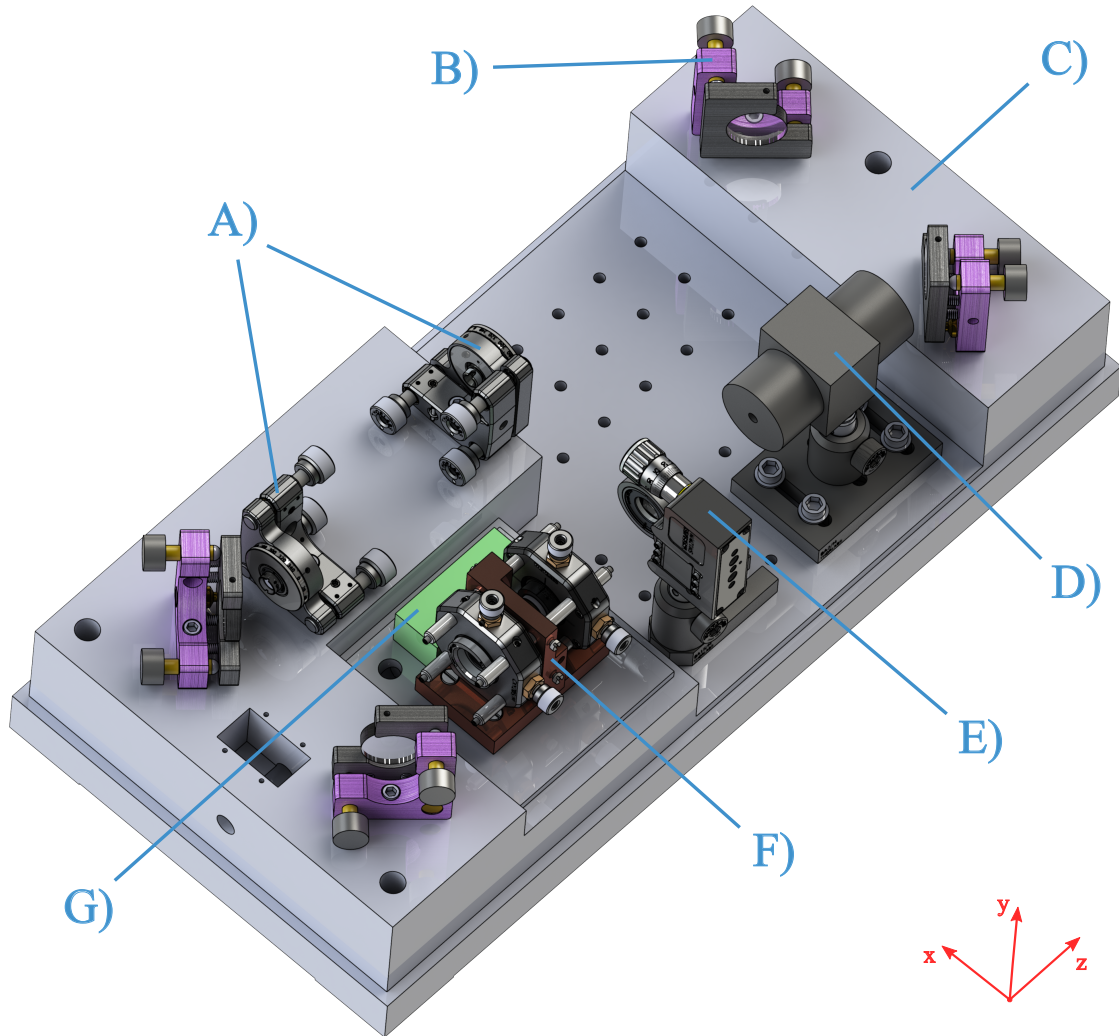


Figure 4.13: Stand-alone fiber-coupled TA unit with **A)** fiber couplers, **B)** mirrors, **C)** mounting aluminum block, **D)** optical isolator, **E)** z-axis translation mount that houses the cylindrical lens, **F)** cage system with TA diode and aspheric lenses, **G)** electrical protection circuit. The fibers themselves are not shown in the picture.

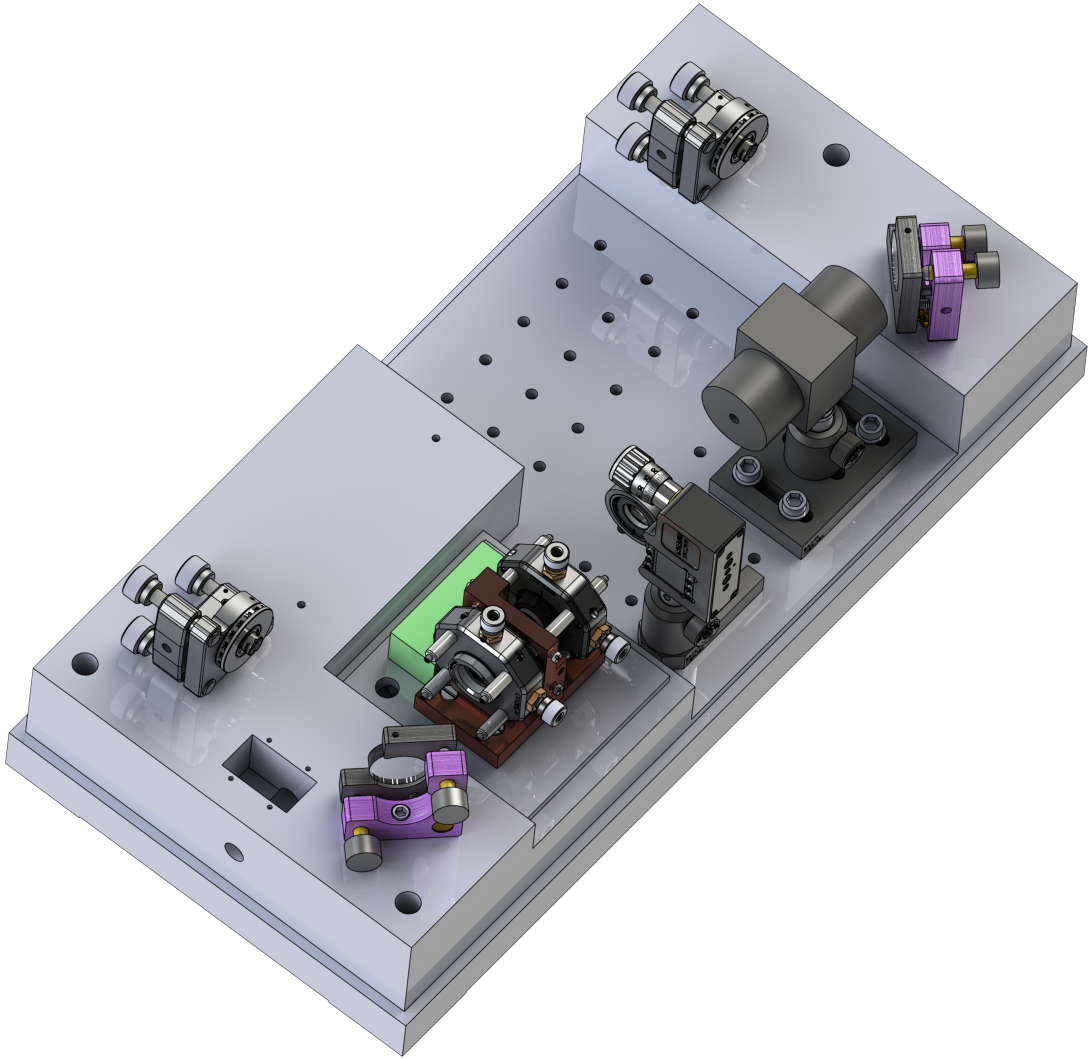


Figure 4.14: Configuration of the stand-alone fiber-coupled TA unit with alternative position of the fiber couplers.

tation mount³. The kinematic rotation mount of the seed beam fiber coupler allows to adjust the polarization direction of the seed beam to maximize the TA output power (cf. sec. 5.1). For the coupler of the output beam, the rotation mount allows to align the slow axis of a polarization maintaining fiber with the polarization of the output beam, such that no $\frac{\lambda}{2}$ -waveplate is needed for polarization maintaining fiber coupling.

In front of the output beam fiber coupler there is space to place additional optics if necessary. Grooves in the aluminum block around the cage system and at the edge of the whole aluminum block are intended to put protective housings around the cage system and the whole aluminum block, respectively. These housings can protect against dust that could be burnt onto the TA chip's output facet or onto the surfaces of the optics at the output side of the TA diode. On the other hand, the protective housings prevent accidental touching and resulting misalignment of the optomechanics. Once the optics on the aluminum block is properly aligned, the block can be covered with the protective housings and left is a stand-alone box with an optical fiber leading in, an optical fiber leading out and two cables leading in for current and temperature control. In the configuration shown in fig. 4.13 the fibers leave this box along the long side of the block. By removing the mirror close to the fiber coupler on each the input and output side of the TA diode and placing the fiber couplers at the position where the two mirrors used to be, the fibers will leave the TA module perpendicular to its long side⁴ (cf. fig. 4.14 and **4**) in fig. 4.15). However, then no additional optics can be placed in front of the output coupler. Such a fiber-coupled stand-alone TA unit has the advantage that it can be placed anywhere in the lab where there is space for it. A picture of the bare aluminum block is shown in fig. 4.15. Detailed technical drawings of this aluminum block can be found in appendix E.

If one wants to have the seed or output beam of the TA not to be fiber-coupled, but to be free space, the height of the aluminum block is chosen such that the optical axis lies 100 mm above the optical table, a distance that is typically used also for other free space optics.

The components of a stand-alone TA system as shown in fig. 4.13 cost in total ca. 9.000 € without VAT (ca. 11.000 € with VAT). That is about half the price of a commercially available system and one can save more than 10.000 € per TA unit by building it oneself. A detailed list of companies and prices for all the components required to built up such a stand-alone fiber-coupled TA unit is given in appendix F.

In the scope of this work, however, such a fiber-coupled stand-alone TA unit was not actually built up. Nevertheless, the results that will be presented in ch. 5 are very

³The components of the fiber couplers are an aspheric lens with $f = 11.0$ mm (Thorlabs C220TMD-B), a fiber adapter plate to plug in the fiber (Thorlabs SM05FCA) and an adapter (Thorlabs S05TM09) to screw the aspheric lens into a kinematic rotation mount (Thorlabs KS05RS).

⁴One can remove the mirror and still has all necessary degrees of freedom for fiber coupling because the kinematic rotation mount compensates the loss of two degrees of freedom.

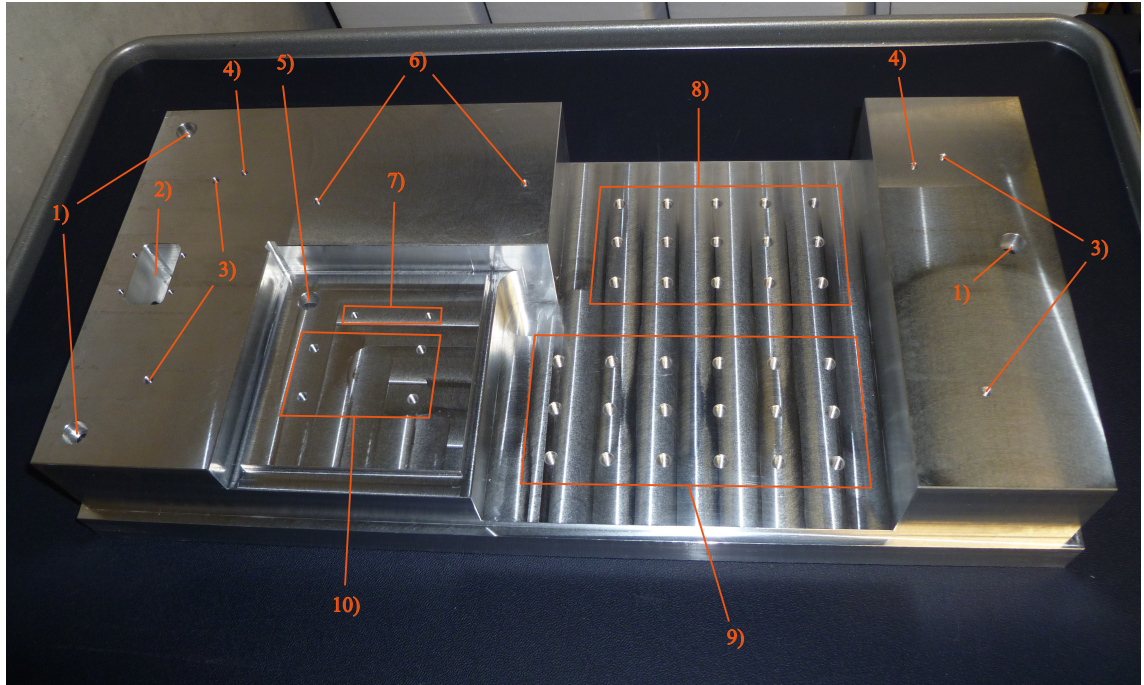


Figure 4.15: Picture of the bare aluminum block to mount all components that are necessary for a fiber coupled TA setup. **1)** Three M6 counterbored holes to connect the block with an optical table, **2)** recess to place two sub-D9 connectors for current and temperature controller. The cables can be led from the recess through a tunnel to an opening near the cage system (cf. **5**). **3)** Four M4 threaded holes to place mirrors, **4)** two M4 threaded holes for alternative position of the fiber couplers, **5)** exit of cable tunnel for current and temperature control, **6)** two M4 threaded holes to place fiber couplers, **7)** two M3 threaded holes to place protection circuit, **8)** 25 mm×25 mm array of M6 threaded holes to place additional optics if needed, **9)** 25 mm×25 mm array of M6 threaded holes to place cylindrical lens and optical isolator, **10)** four M4 threaded holes to place cage system.

promising. The stand-alone fiber-coupled TA unit has the same degrees of freedom in the adjustment of the optomechanics as the setup which is used to achieve the results presented in ch. 5 and we are very confident that the fiber-coupled stand-alone TA unit proposed in this chapter will have the desired performance and will deliver about 800 mW power after the single-mode fiber (cf. ch. 5). Furthermore, the aluminum block shown in fig. 4.15 is only a first prototype. After having actually set up the whole system, one will see how much space between the different components is actually required and in later iterations the aluminum block can maybe be dimensioned more compactly.

5 TA diode characteristics

With the cage system design presented in sec. 4.2, measurements on the output characteristics of a TA diode and on fiber coupling efficiency were carried out. We carried out these measurements with the cage system design because of its better control of the aspheric lenses compared to the design with the lens holder tubes. The TA chips that were used in this chapter operate around a wavelength of $\lambda = 808 \text{ nm}$ and yield a maximum output power of 2 W. They are produced by eagleyard photonics, type EYP-TPA-0808-02000-4006-CMT04-0000.

5.1 Output power characteristics of a TA chip

Fig. 5.1a shows the output power of a 808 nm, 2 W TA chip as a function of TA driving current for different powers of the seed laser. One sees from the graph that for TA currents larger than 1000 mA the output power increases linearly with driving current. The slope in the linear part for this particular TA diode is ca. $900 \frac{\text{mW}}{\text{A}}$. The figure also shows that the dependence of the TA output power on the power of the seed laser is small. This is confirmed by fig. 5.1b where the output power of the TA is plotted against various seed powers for different TA currents. In this graph the curves for each TA current are almost flat and no general tendency of the curves can be seen. This behavior is a consequence of saturation effects: If the power of the seed laser is high enough, the stimulated emission completely reduces the population inversion that is built up by the injection current. Further increasing the seed power then does not increase the output power because the upper energy level of the charge carriers is already completely depleted. However, for seed powers lower than the minimal seed power in fig. 5.1b, the TA output power is clearly dependent on the seed power, because then saturation of the stimulated emission is not yet reached [4, 11, 18]. In fig. 5.1a and fig. 5.1b the power was measured directly after the aspheric lens. For the measurements of fig. 5.1a and 5.1b, the seed beam was readjusted at each seed beam power. It was found that adjusting the seed beam at only one seed beam power and then taking measurements for other seed beam powers without readjusting the seed beam, leads to a decrease in output power of about 5%. The dependence of output power on the polarization of the seed beam is shown in fig. 5.1c and 5.1d for different TA currents and seed beam powers of 25 mW and 10 mW, respectively. In these figures, 0° corresponds to maximal output power. Fig. 5.1c and 5.1d reveal that the dependence of output power on seed polarization is small near the optimum angle. At these seed beam powers, a deviation of $\pm 30^\circ$ from the optimum polarization angle changes the output power maximally 5%. However, at these seed beam powers the TA is already saturated.

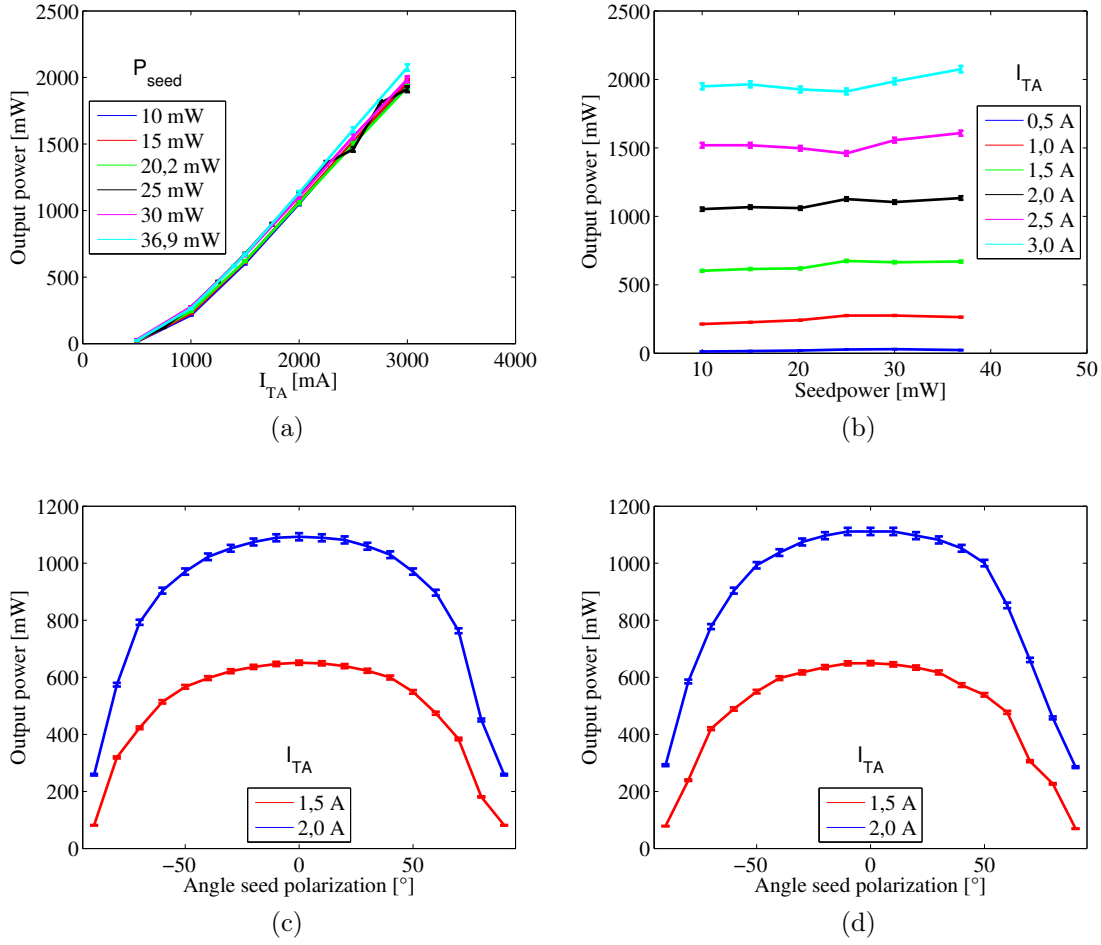


Figure 5.1: a) TA output power as a function of TA driving current for different powers of the seed laser. b) Same data as in a), but this time plotted as output power versus seed power at different TA currents. The range in seed power was chosen according to the recommendations by the manufacturer. The measurements in a) and b) are done after the aspheric lens. c) TA output power as a function of seed polarization angle for $I_{TA} = 1.5$ A and $I_{TA} = 2.0$ A, respectively, at a seed beam power of $P_{seed} = 25$ mW. d) TA output power as a function of seed polarization angle for $I_{TA} = 1.5$ A and $I_{TA} = 2.0$ A, respectively, at a seed beam power of $P_{seed} = 10$ mW. The measurements in c) and d) are done after the optical isolator. The angle shown in c) and d) is the actual seed polarization angle, not the angle of the $\frac{\lambda}{2}$ -waveplate. The errorbars arise from the attenuator of the powermeter and slight power fluctuations. The lines are to guide the eye.

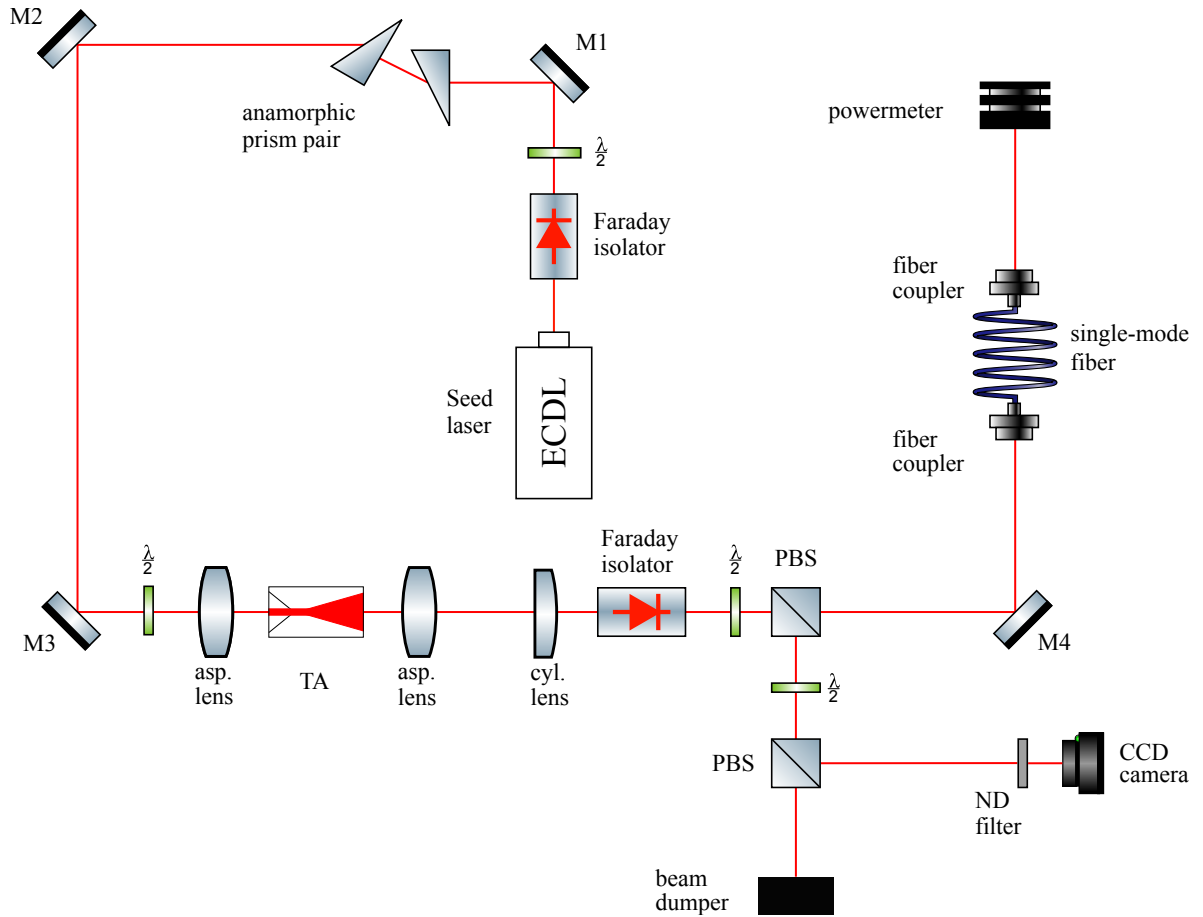


Figure 5.2: Optical path to couple the TA output beam into a fiber and simultaneously watch its mode profile on a CCD-camera. Right before the fiber coupler, another $\frac{\lambda}{2}$ -waveplate can be placed for polarization maintaining fiber coupling. Cf. also sec. 3.4.

For lower seed powers an increased dependence is expected.

5.2 Fiber coupling efficiency and mode profiles

It is desirable to couple the TA output beam into an optical single-mode fiber in order to make convenient use of the high optical powers generated by a TA. Furthermore, the single-mode fiber acts as a mode filter and only one single mode is left after the fiber. In this work, fiber coupling efficiency for both low and high powers was measured. Also mode profiles of the best coupling efficiencies were recorded with a CCD camera¹.

The experimental setup is an extension of the setup presented in sec. 3.4 and is

¹The specific camera we used here is a AVT Guppy F-044B NIR.

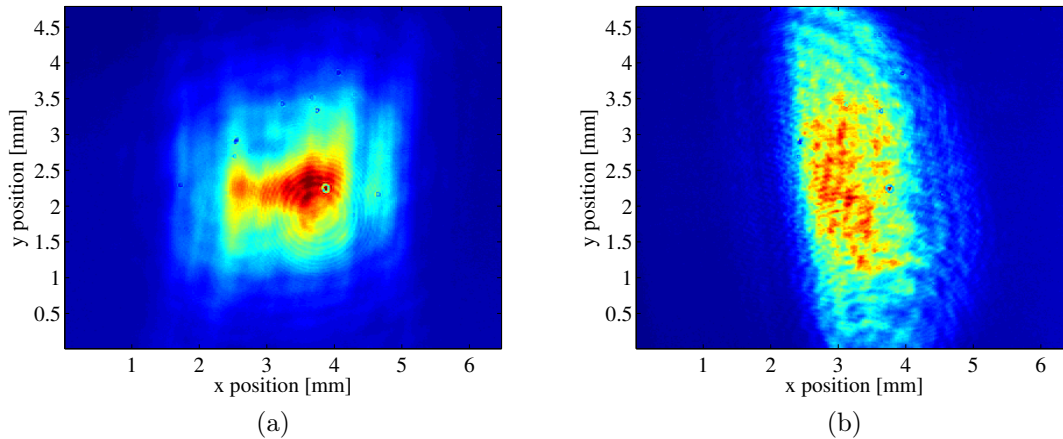


Figure 5.3: Mode profiles at fiber coupler at $I_{TA} = 1000$ mA. a) 54% coupling efficiency with a $f_{cyl} = 40$ mm cylindrical lens. The concentric interference pattern is caused by one of the elements of the analyzing optics. b) 32% coupling efficiency with a $f_{cyl} = 50$ mm cylindrical lens.

shown in fig. 5.2. After the optical isolator the beam passes a $\frac{\lambda}{2}$ -waveplate and a polarizing beamsplitter. One component of the split beam is coupled into a single-mode fiber whereas the other part passes another $\frac{\lambda}{2}$ -waveplate and beamsplitter. One part of the so again split beam travels through a neutral density filter and is recorded by a CCD camera. Thus the recorded mode profile corresponds to the mode profile at the fiber coupler. The combination of $\frac{\lambda}{2}$ -waveplates, beamsplitters and neutral density filter is necessary to attenuate the high power output beam sufficiently so that it can be recorded by the CCD camera. Without this combination the CCD camera would be immediately saturated, even at low TA currents.

In sec. 3.3.2 it was estimated that the focal length of the cylindrical lens should be $f_{cyl} = 47.4$ mm if an aspheric lens with a focal length of $f_{asp} = 4.51$ mm is used (as it is the case in this work). Off-the-shelf cylindrical lenses having focal lengths that are closest to our estimation are Thorlabs LJ1402L1-B and Thorlabs LJ1695RM-B with focal lengths of $f_{cyl} = 40.0$ mm and $f_{cyl} = 50$ mm, respectively.

Fig. 5.3a shows a mode profile that gave a coupling efficiency of 54% at low output powers ($I_{TA} = 1000$ mA), which was the highest coupling efficiency we could achieve². Here a $f_{cyl} = 40$ mm cylindrical lens was used. The mode is smeared out in horizontal direction but the majority of its intensity is concentrated at the right side. This can be seen from the deep red spot on the right side of the mode in fig. 5.3a. We also used an adjustable iris to cut off the left-side parts of the mode and confirmed that it was indeed the deep red spot that contains the majority of the light which is coupled into the fiber. What cannot be seen from fig. 5.3a is that

²The lens of the fiber coupler for this coupling efficiency had a focal length of 11.0 mm.

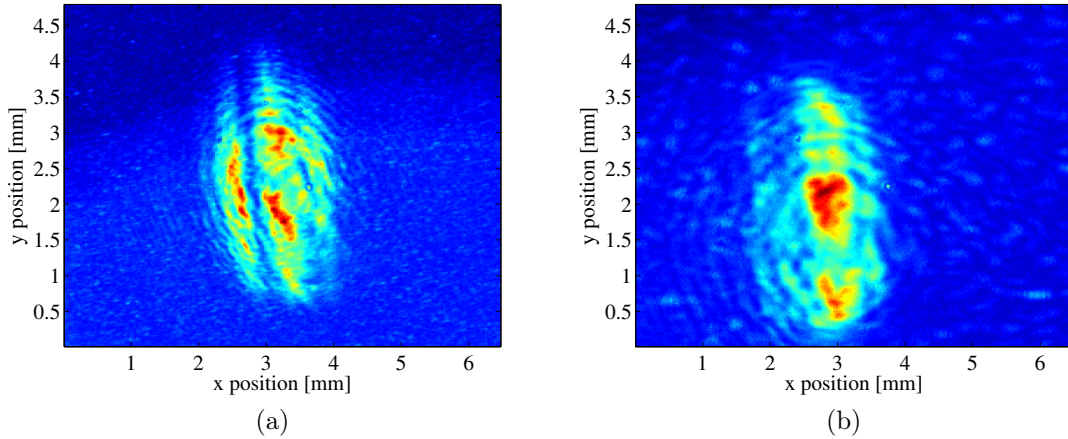


Figure 5.4: Mode profiles of high coupling efficiencies at high TA currents. a) 35% coupling efficiency at $I_{TA} = 2500$ mA. Serial-no. of this chip: EA-06811. b) 50% coupling efficiency at $I_{TA} = 2800$ mA. Serial-no. of this chip: EA-06820.

In both a) and b) a cylindrical lens with $f_{cyl} = 40$ mm was used. The concentric interference pattern most likely comes from the aspheric lens.

this mode has a focus both in vertical and horizontal direction in front of the fiber coupler.

In fig. 5.3b the mode with highest coupling efficiency at low power ($I_{TA} = 1000$ mA) for the $f_{cyl} = 50$ mm lens is shown. The highest coupling efficiency that was achieved with that lens was 32%. One immediately sees that the mode in fig. 5.3a is much more smoother than the one in fig. 5.3b. The mode in fig. 5.3b is spread in vertical direction. Furthermore, no spot with increased energy density can be observed. Thus it is not surprising that this mode has a worse coupling efficiency than the one shown in fig. 5.3a.

Modes with high fiber coupling efficiency at high TA output powers ($I_{TA} \geq 2500$ mA) are shown in fig. 5.4. Due to the bad coupling efficiency at low powers for the $f_{cyl} = 50$ mm cylindrical lens, we only investigated the high power behavior for the $f_{cyl} = 40$ mm cylindrical lens. The modes with high coupling efficiency at high power look completely different than the ones at low powers (cf. fig. 5.3a). One cannot adjust the lenses for high coupling efficiency at low power and then just increase the TA current and hope for a constant high coupling efficiency at high power. The reason is that the refractive index of the gain medium changes with TA current. This in turn causes a change in astigmatism, i.e. how far the beam waist of the horizontal beam component is inside the TA diode, cf. sec. 3.3.2 [4]. Thus for fiber coupling the lenses should be adjusted at the current at which the TA later is actually operated.

The modes in fig. 5.4 are smeared out in vertical direction. With the mode shown

in fig. 5.4a a coupling efficiency of 35 % was achieved at a TA current of 2500 mA. There are three regions of high intensity. Two at $x \approx 3.3$ mm above and below the center and one stripe like region left to the center at $x \approx 2.6$ mm. A remarkable feature of this mode profile is the stripe of low intensity at $x \approx 2.8$ mm that cuts the mode into two regions. With the particular TA chip used in fig. 5.4a we could not achieve more than 36 % coupling efficiency which was not satisfactory. That is why we exchanged the TA chip for another chip of the same type. A mode profile for this newly put in TA chip is showed in fig. 5.4b. With this chip a coupling efficiency of 50 % could be achieved. This exceeds coupling efficiencies reported in [4, 18] and can compete with the efficiency reported in [20]. Both TA chips we used have been unopened in the original packaging from the manufacturer before we carried out the presented measurements with them. It is also reported in [3] that the fiber coupling efficiency varies between individual TA chips of the same type.

The mode in fig. 5.4b looks similar to the one shown in fig. 5.4a. However, there is no stripe of low intensity visible that splits up the mode. Furthermore, there is clearly a spot with high energy density visible in the center of the mode. After removing the combination of beamsplitter and $\frac{\lambda}{2}$ -waveplate necessary to analyze the mode profile with the CCD camera, we got a power of 800 mW after the single-mode fiber at a TA current of $I_{TA} = 3000$ mA. A $\frac{\lambda}{2}$ -waveplate was placed right before the fiber coupler for polarization maintaining coupling. A M12 fiber coupler by Schäfter+Kirchhoff with a focal length of $f = 12$ mm was used. The power of the seed laser was 30 mW. The voltage of the piezo element of the ECDL seed laser was chosen to give a wavelength of 811.754 nm which corresponds to the closed $1s_5 \rightarrow 2p_9$ cooling transition of Argon³. A picture of the whole fiber coupling setup is shown in fig. 5.5.

The stripe pattern observed in fig. 5.4a could also be observed otherwise. For the same chip as in fig. 5.4a the output beam was made as round as possible at a large distance of several meters away from the $f_{cyl} = 40$ mm cylindrical lens. With this lens configuration, at a distance several decimeters away from the cylindrical lens, the mode looked like the one shown in fig. 5.6a. There is one broad vertical stripe of high intensity in the middle and a vertical stripe of medium intensity right to the main stripe. Left to the main stripe, a region of very low intensity can be seen. The stripe structure gets more pronounced at higher TA currents (cf. fig. 5.6b). In fig. 5.6a and 5.6b the seed beam is centered on the TA's entrance aperture. If the seed beam is moved in horizontal direction, the stripe of high intensity also moves in horizontal direction whereas the side stripes do not change their position. If the seed beam is decentered further horizontally, only two stripes remain, see fig. 5.6c. These two stripes disappear almost simultaneously if the seed beam's position is changed further in horizontal direction. The TA is then unseeded. A corresponding behavior is not observed for a seed beam off-center in vertical direction. There the mode just gets darker and then disappears completely.

³ $1s_5$ and $2p_9$ are in Paschen notation.

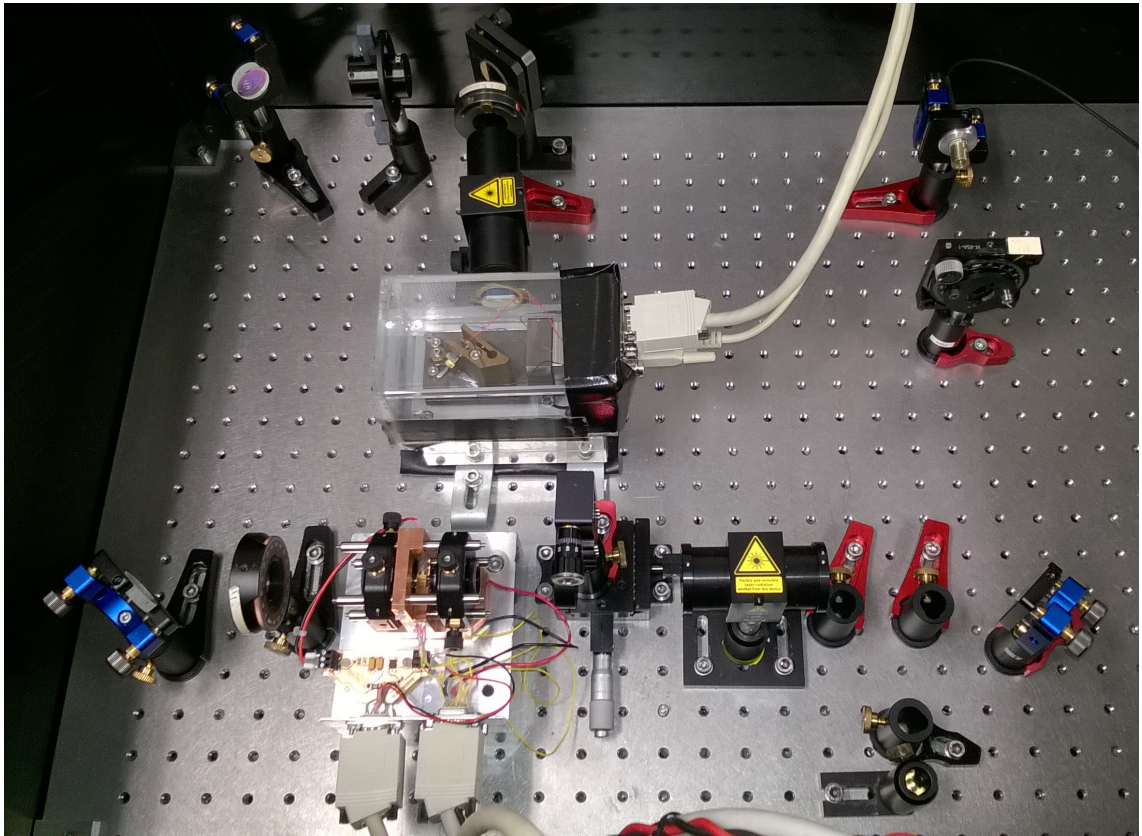


Figure 5.5: Top view on the fiber coupling setup (see also fig. 5.2). The optics to analyze the beam profile on a CCD-camera is removed to achieve maximum power after the optical fiber. The $\frac{\lambda}{2}$ -waveplate in front of the fiber coupler is used for polarization maintaining coupling.

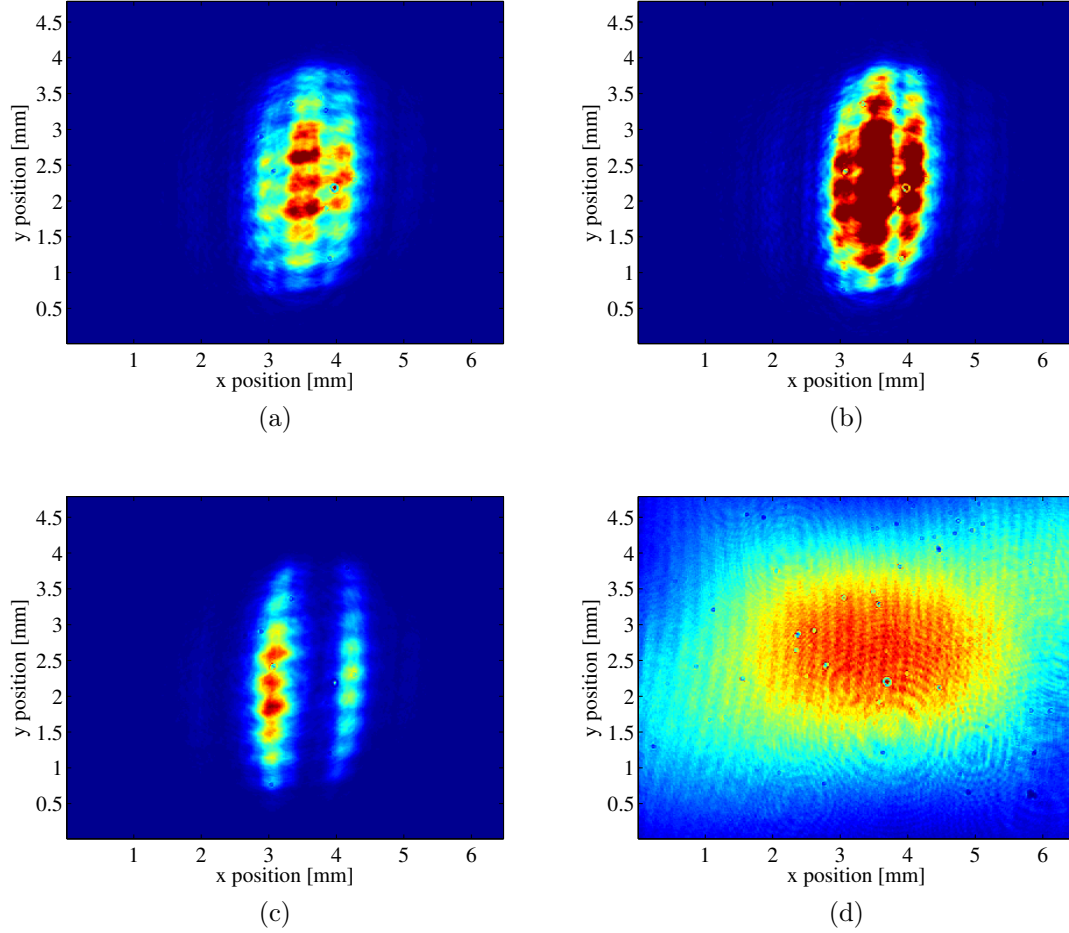


Figure 5.6: Mode profiles for TA chip with serial-no. EA-06811. a) Mode recorded ca. 0.3 m after the cylindrical lens. Seed beam is centered on the input aperture. $I_{TA} = 1400$ mA. b) Mode recorded ca. 0.3 m after the cylindrical lens. Seed beam is centered on the input aperture. $I_{TA} = 2000$ mA. c) Mode recorded ca. 0.3 m after the cylindrical lens. Seed beam is off-center in horizontal direction. $I_{TA} = 1400$ mA. d) Reference picture of the mode at a distance of ca. 7.9 m after the cylindrical lens, same lens configuration as in a), b) and c). $I_{TA} = 1400$ mA. The vertical stripes are caused by interferences at the CCD-camera.

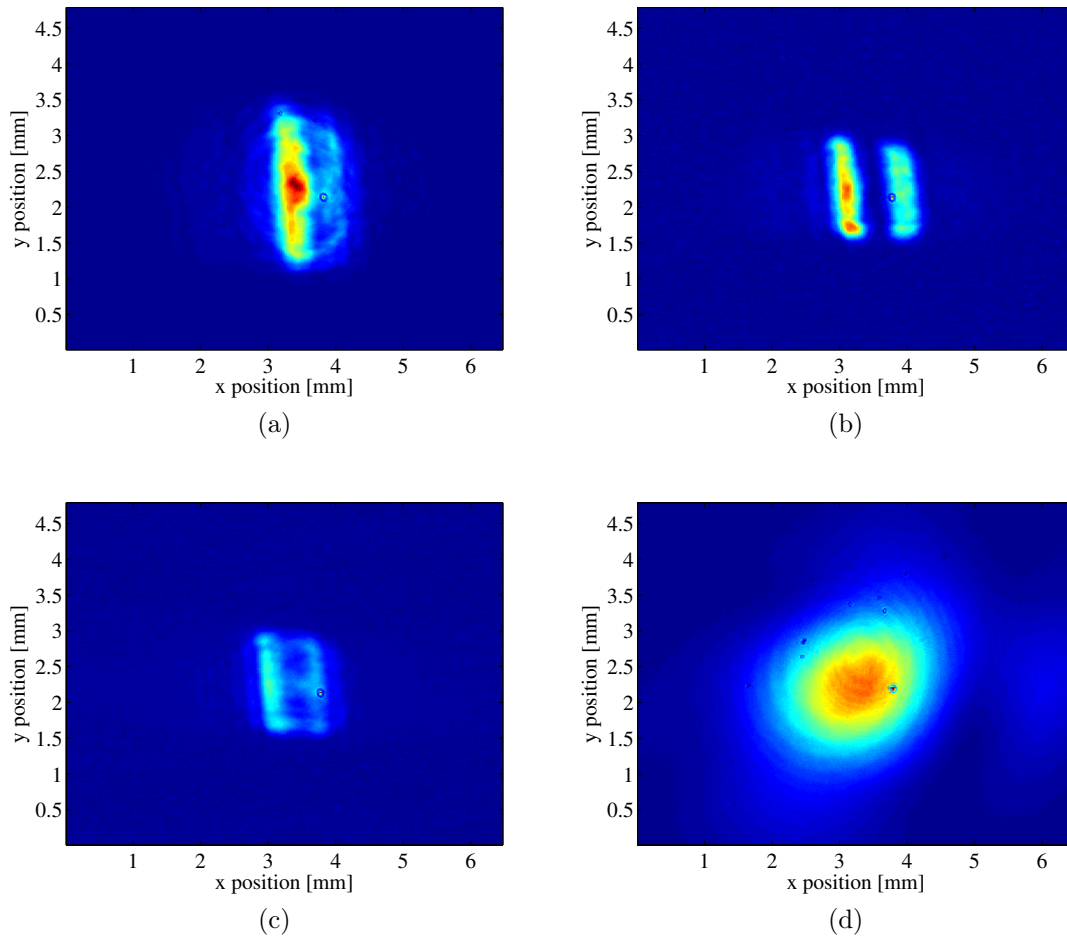


Figure 5.7: Mode profiles for TA chip with serial-no. EA-06820, $I_{TA} = 1500$ mA a) Mode recorded ca. 0.4 m after the cylindrical lens. b) Mode recorded ca. 0.4 m after the cylindrical lens, seed beam is off-center in horizontal direction. Output power corresponds to 56% compared to a centered seed beam. c) Mode recorded ca. 0.4 m after the cylindrical lens, seed beam is off-center in horizontal direction. Output power corresponds to 18% compared to a centered seed beam. d) Reference picture of the mode at a distance of ca. 3.6 m after the cylindrical lens, same lens configuration as in a), b) and c). Even if this mode might suggest that it is very well suited for fiber coupling as it looks nice and Gaussian, it only shows the intensity distribution at one particular plane and contains no information about the wavefront curvature.

After exchanging the TA chip, a similar procedure like the one previously described was carried out: The output beam was made as round as possible at a distance of several meters and the mode was recorded several decimeters away from the cylindrical lens. There one could see a mode profile like the one shown in fig. 5.7a. One single vertical stripe of high intensity can be seen. One might see a side stripe right to the main stripe, but this side stripe is extremely weak. This coincides with the results found in fig. 5.4a and 5.4b. However, also with this TA chip two side stripes arose in the mode as soon as the seed beam got off-center in horizontal direction, see fig. 5.7b and 5.7c. These stripes might possibly arise from waveguiding effects at the taper edges, but their exact origin was not further investigated in the scope of this work.

5.3 Conclusion

With the cage system design presented in sec. 4.2 it was possible to achieve a coupling efficiency of 50% at a TA current of 3000 mA. With that we achieved an output power of 800 mW after a single-mode optical fiber for a 2 W TA diode. The combination of lenses used for high power fiber coupling was an aspheric lens with $f_{asp} = 4.51$ mm and a cylindrical lens with $f_{cyl} = 40.0$ mm. There are also indications that several TA chips of the same type have different performance concerning the beam quality and fiber coupling efficiency of the output beam, even if they are freshly unpacked.

6 Summary and outlook

This work dealt with the design and setup of a fiber-coupled TA system. Practical guidelines in handling a TA chip were given and an electrical protection circuit to protect the TA diode against wrong electrical handling and unwanted coupling to RF noise was presented. To couple the TAs output beam into an optical fiber, a combination of aspheric and cylindrical lens was applied. A method to estimate the focal length of the cylindrical lens and its distance from the aspheric lens was presented. This method was based on the ABCD law for Gaussian beams.

Two designs for a TA setup were tested. The first design uses a simple and compact combination of an inner and outer threaded tube to mount and position the aspheric lens. However, in this work it turned out that fiber coupling with this design is cumbersome and inefficient. The positions of the aspheric lenses cannot be controlled in the plane perpendicular to the optical axis. This results in a lack of control of the angle at which the output beam exits the TA setup. We tried out several blocks of this design type and had a slanting output beam with each of them, albeit the degree of obliqueness was different for each block. Moreover, the output beam changed its position if the output aspheric lens was moved along the optical axis. This change in position most likely came from a misalignment of the aspheric lens in the lensholder tube and thus the aspheric lens wobbled when moved back and forth. The change in the output beam's position made it necessary to readjust the optical isolator several times during the fiber coupling procedure, which was time-consuming.

The second design uses a cage system and commercially available translation mounts to house the aspheric lenses. With these translation mounts it is possible to control the position of the aspheric lens both along the optical axis and in the plane perpendicular to it. Thus also the inclination of the output beam can be precisely controlled. With this design, the problem of a slanting output beam did not occur further. We achieved a single-mode fiber coupling efficiency of 54% for $I_{TA} = 1000$ mA and a coupling efficiency of 50% for $I_{TA} = 3000$ mA. The maximum output power that we achieved after a single-mode fiber was 800 mW for a seed beam power of 30 mW. Furthermore, there are indications that different TA chips of the same type have different quality concerning the mode of their output beams and thus differ in maximum fiber coupling efficiency, even if they are freshly unpacked.

Based on this cage system, a robust stand-alone TA unit is proposed. This stand-alone TA unit has an input fiber for the seed beam and an output fiber for the TA output beam. All necessary components to align the seed beam and to couple the TA output beam into a fiber are mounted on a robust aluminum block. A list of all

necessary components to built up such a stand-alone TA unit and the corresponding manufacturers is given in appendix F. The total costs of such a self-built TA system is about 11.000 € (VAT included). This is about half the price of a commercially available TA system.

A robust stand-alone TA unit would facilitate one's everyday lab life. In the ArTTA experiment, for example, TAs are used for a MOT and longitudinal slowing and transversal collimation of an Argon beam. Dating with ArTTA is based on a stable reference count rate and fluctuations of laser power directly lead to uncertainties of the Argon concentration. In worst case, the whole measurement has to be discarded if the laser power fluctuations are too high. The experiment thus relies on stable operation of the TAs, in particular if one considers that the TA should provide a stable output power after the fiber without need for realignment over a long time. Furthermore, with its input and output fiber a robust stand-alone TA unit could be conveniently placed nearly independently from the other parts of the experiment. This in turn provides space on the optical table for other components of the experiment.

TAs are used for example in MOTs with high capture regions to provide a sufficiently high light intensity. Even if this thesis dealt with a $\lambda = 808$ nm TA diode, the design presented in this work can also be used for chips with other wavelengths, as the dimensions of the C-mounts of other types of chips are similar or even exactly the same as for the $\lambda = 808$ nm chip. Solely the choice of cylindrical lens might have to be reconsidered for TA chips with different wavelengths. Bearing in mind how many high power lasers are used in atomic physics experiments and that each self-built TA costs ~ 10.000 € less than a commercially available TA system, the proposed stand-alone fiber-coupled TA unit might also considerably relieve experiment planning from an economic point of view.

Part I

Appendix

A Lists

List of Figures

2.1	Sketch of the structure of a tapered amplifier diode (not to scale) with active layer (red), waveguiding layers (light grey), cladding (green), electrical contact pad (brown) and bulk (dark grey). Cavity spoiling grooves are etched next to the ridge waveguide section. The dimensions are for the TA chip used in this work (EYP-TPA-0808-02000-4006-CMT04-0000 by eagleyard photonics).	4
2.2	Sketch of a TA with a taper angle close to the Gaussian diffraction angle. The light field (red) is not cut by the taper edges and covers almost the whole active area (yellow).	6
2.3	Measured spectrum of a 925 nm TA at different seed powers. One can see the broad ASE background and also how the power of ASE reduces with increasing seed beam power P_{in} . The picture is taken from [11].	7
3.1	TA chip on metal C-mount. The semiconductor diode is electrically connected with a wing shaped cathode via several bond wires. The metal block serves both as heat sink and anode. The picture is taken from [18].	9
3.2	Top view on TA chips and bond wires. a) Bond wires of an old chip with bad performance. The bond wires are bent, a clear hint that the chip might have been mechanically damaged. b) Bond wires of a new chip. The wires are all parallel to each other.	10
3.3	Protection circuit for the TA diode with rectifier diode, low pass filter and TVS diode.	10
3.4	Sketch of the beam shape and lens configuration to form the beams before and after the TA chip for a) horizontal (blue) and b) vertical (red) direction. Note that the cylindrical lens is oriented with its curved surface towards the collimated beam to reduce aberrations. . .	12

3.5	Sketch of a Gaussian beam with important parameters. The red lines represent the beam width, i.e. the intensity at the red lines at any transverse plane is $1/e^2$ compared to the intensity on the beam axis.	13
3.6	Simulation of the evolution of the vertical (red) and horizontal (blue) beam radii of the output beam for a $f_{cyl} = 47.4$ mm cylindrical lens. The origin of the x-axis lies at the output facet of the TA diode. The aspheric lens is placed at 4.5 mm, the cylindrical lens at 80.0 mm after the output facet. This corresponds to a perfect configuration where both beam components have the same radii and are both collimated after the cylindrical lens.	18
3.7	Simulation of the evolution of the vertical (red) and horizontal (blue) beam radii of the output beam for different cylindrical lenses. The origin of the x-axis lies at the output facet of the TA diode.	19
3.8	Optical path of the setup. Abbreviations used are M: mirror, FI: Faraday isolator, Asp: aspheric lens.	20
4.1	Copper mount for TA diode. 1) copper block, 2) TA chip housed in slot, 3) set screw for lens holder assembly and contact for anode, 4) coarse internal thread for lens holder assembly, 5) M4 threaded hole for set screw of guiding tunnel, 6) guiding tunnel for copper pin cathode, 7) clearance holes for centering rods, 8) M2 screw, 9) M4 threaded holes.	23
4.2	Copper pin for the connection of the TA diode with the cathode. Not shown in the picture is the heat shrink tube for electrical isolation.	24
4.3	Copper mount with lens holder assemblies. a) inner lens holder tube, b) set screws for inner lens holder tube, c) M4 screws for connecting copper parts with baseplate, d) copper parts, the left one is in detail shown in fig. 4.1, e) aspheric lens, f) outer lens holder tube, g) M4 screws to connect the two copper parts, h) centering rods, i) copper baseplate, j) hole to place a thermistor. What is not shown in the picture is that the grips of the inner lens tubes are knurled.	25
4.4	Aluminum base of the TA design. I) M3 threaded holes to mount the protection circuit, II) M6 clearance holes to put the TA setup on an optical table, III) M4 threaded holes for connection with copper baseplate (cf. fig. 4.3), IV) position of Peltier element, V) tunnels for cables, VI) Sub-D9 sized pockets.	27
4.5	Top view on the whole TA setup.	27
4.6	Special screw with M2 thread at its tip. The cylinder in the middle part is to define the TA chip's position.	28
4.7	Inner (A) and outer (D) lens holder tube together with a combination of Belleville (C) and plain (B) washers to increase the tightness of the fine thread.	29
4.8	Sketch of the slanting output beam. The cone shows the change in position when the aspheric lens is moved.	30

4.9	Components of the cage system. 1) Translation mount, 2) headless M4 plastic set screw for cathode pin guiding, 3) TA chip, 4) M3 plastic set screws for cage rods, 5) adapter for threads of lens and translation mount, 6) cage rods, 7) counterbored holes for plastic screws, 8) M4 countersunk screws, 9) copper baseplate, 10) mounting copper block, 11) aspheric lens.	32
4.10	Aluminum socket to mount the cage system. I) Four M6 counterbored holes to screw the aluminum block to an optical table, II) four M4 threaded holes to connect with the cage system via plastic screws, III) two M3 threaded holes to place the protection circuit, IV) three M3 threaded holes to place a metal plate that holds the plugs for the temperature and current controllers.	33
4.11	Front and back side of the copper housing of the TA chip. a) clearance holes for cage rods, b) slot to place the TA chip, c) M2 threaded hole, d) recess, e) guiding tunnel for cathode connection pin, f) M3 threaded holes for set screws, g) opening for translation mount, h) back wall of slot for TA chip, i) M4 threaded hole for set screw, j) M4 threaded hole to connect with anode cable, k) planes that define the TA chip's position, l) hole to place thermistor.	34
4.12	TA setup with cage system. Also shown on the picture are the protection circuit as well as the connections of the current and temperature controller.	36
4.13	Stand-alone fiber-coupled TA unit with A) fiber couplers, B) mirrors, C) mounting aluminum block, D) optical isolator, E) z-axis translation mount that houses the cylindrical lens, F) cage system with TA diode and aspheric lenses, G) electrical protection circuit. The fibers themselves are not shown in the picture.	37
4.14	Configuration of the stand-alone fiber-coupled TA unit with alternative position of the fiber couplers.	38
4.15	Picture of the bare aluminum block to mount all components that are necessary for a fiber coupled TA setup. 1) Three M6 counterbored holes to connect the block with an optical table, 2) recess to place two sub-D9 connectors for current and temperature controller. The cables can be led from the recess through a tunnel to an opening near the cage system (cf. 5)). 3) Four M4 threaded holes to place mirrors, 4) two M4 threaded holes for alternative position of the fiber couplers, 5) exit of cable tunnel for current and temperature control, 6) two M4 threaded holes to place fiber couplers, 7) two M3 threaded holes to place protection circuit, 8) 25 mm×25 mm array of M6 threaded holes to place additional optics if needed, 9) 25 mm×25 mm array of M6 threaded holes to place cylindrical lens and optical isolator, 10) four M4 threaded holes to place cage system.	40

5.1	a) TA output power as a function of TA driving current for different powers of the seed laser. b) Same data as in a), but this time plotted as output power versus seed power at different TA currents. The range in seed power was chosen according to the recommendations by the manufacturer. The measurements in a) and b) are done after the aspheric lens. c) TA output power as a function of seed polarization angle for $I_{TA} = 1.5$ A and $I_{TA} = 2.0$ A, respectively, at a seed beam power of $P_{seed} = 25$ mW. d) TA output power as a function of seed polarization angle for $I_{TA} = 1.5$ A and $I_{TA} = 2.0$ A, respectively, at a seed beam power of $P_{seed} = 10$ mW. The measurements in c) and d) are done after the optical isolator. The angle shown in c) and d) is the actual seed polarization angle, not the angle of the $\frac{\lambda}{2}$ -waveplate. The errorbars arise from the attenuator of the powermeter and slight power fluctuations. The lines are to guide the eye.	43
5.2	Optical path to couple the TA output beam into a fiber and simultaneously watch its mode profile on a CCD-camera. Right before the fiber coupler, another $\frac{\lambda}{2}$ -waveplate can be placed for polarization maintaining fiber coupling. Cf. also sec. 3.4.	44
5.3	Mode profiles at fiber coupler at $I_{TA} = 1000$ mA. a) 54% coupling efficiency with a $f_{cyl} = 40$ mm cylindrical lens. The concentric interference pattern is caused by one of the elements of the analyzing optics. b) 32% coupling efficiency with a $f_{cyl} = 50$ mm cylindrical lens.	45
5.4	Mode profiles of high coupling efficiencies at high TA currents. a) 35% coupling efficiency at $I_{TA} = 2500$ mA. Serial-no. of this chip: EA-06811. b) 50% coupling efficiency at $I_{TA} = 2800$ mA. Serial-no. of this chip: EA-06820. In both a) and b) a cylindrical lens with $f_{cyl} = 40$ mm was used. The concentric interference pattern most likely comes from the aspheric lens.	46
5.5	Top view on the fiber coupling setup (see also fig. 5.2). The optics to analyze the beam profile on a CCD-camera is removed to achieve maximum power after the optical fiber. The $\frac{\lambda}{2}$ -waveplate in front of the fiber coupler is used for polarization maintaining coupling.	48
5.6	Mode profiles for TA chip with serial-no. EA-06811. a) Mode recorded ca. 0.3 m after the cylindrical lens. Seed beam is centered on the input aperture. $I_{TA} = 1400$ mA. b) Mode recorded ca. 0.3 m after the cylindrical lens. Seed beam is centered on the input aperture. $I_{TA} = 2000$ mA. c) Mode recorded ca. 0.3 m after the cylindrical lens. Seed beam is off-center in horizontal direction. $I_{TA} = 1400$ mA. d) Reference picture of the mode at a distance of ca. 7.9 m after the cylindrical lens, same lens configuration as in a), b) and c). $I_{TA} = 1400$ mA. The vertical stripes are caused by interferences at the CCD-camera.	49

5.7	Mode profiles for TA chip with serial-no. EA-06820, $I_{TA} = 1500$ mA a) Mode recorded ca. 0.4 m after the cylindrical lens. b) Mode recorded ca. 0.4 m after the cylindrical lens, seed beam is off-center in horizontal direction. Output power corresponds to 56 % compared to a centered seed beam. c) Mode recorded ca. 0.4 m after the cylindrical lens, seed beam is off-center in horizontal direction. Output power corresponds to 18 % compared to a centered seed beam. d) Reference picture of the mode at a distance of ca. 3.6 m after the cylindrical lens, same lens configuration as in a), b) and c). Even if this mode might suggest that it is very well suited for fiber coupling as it looks nice and Gaussian, it only shows the intensity distribution at one particular plane and contains no information about the wavefront curvature. . .	50
-----	--	----

List of Tables

F.1	Components required to set up a stand-alone TA unit.	88
-----	--	----

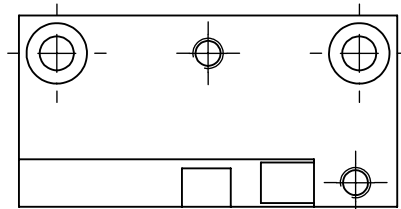
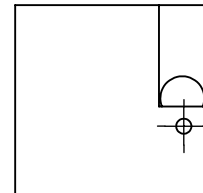
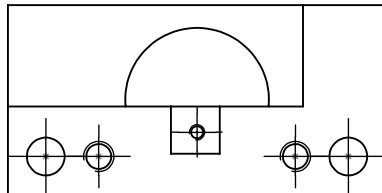
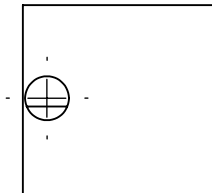
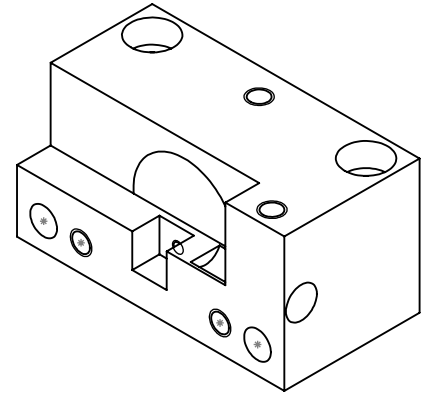
B Components of the protection circuit

Components of the protection circuit described in sec. 3.2:

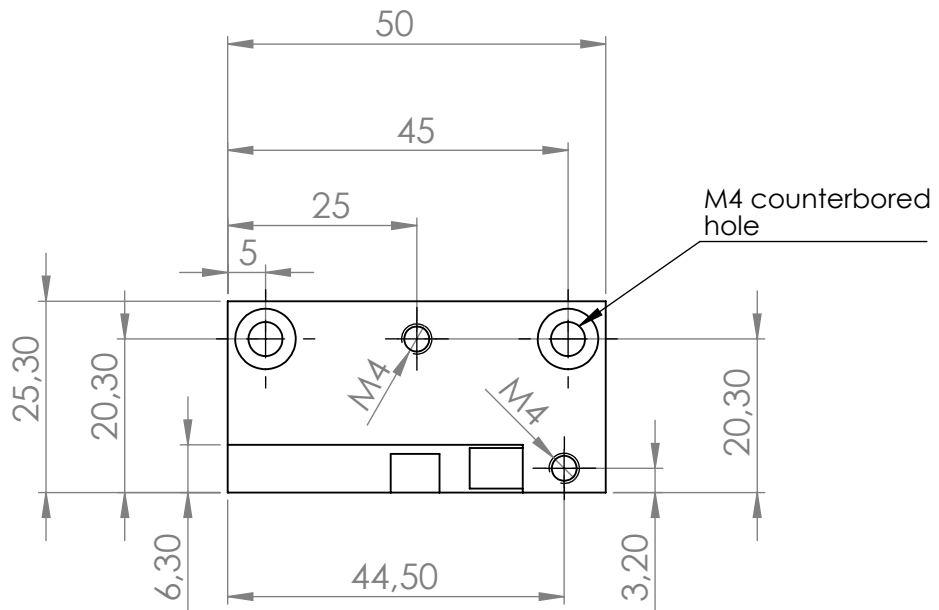
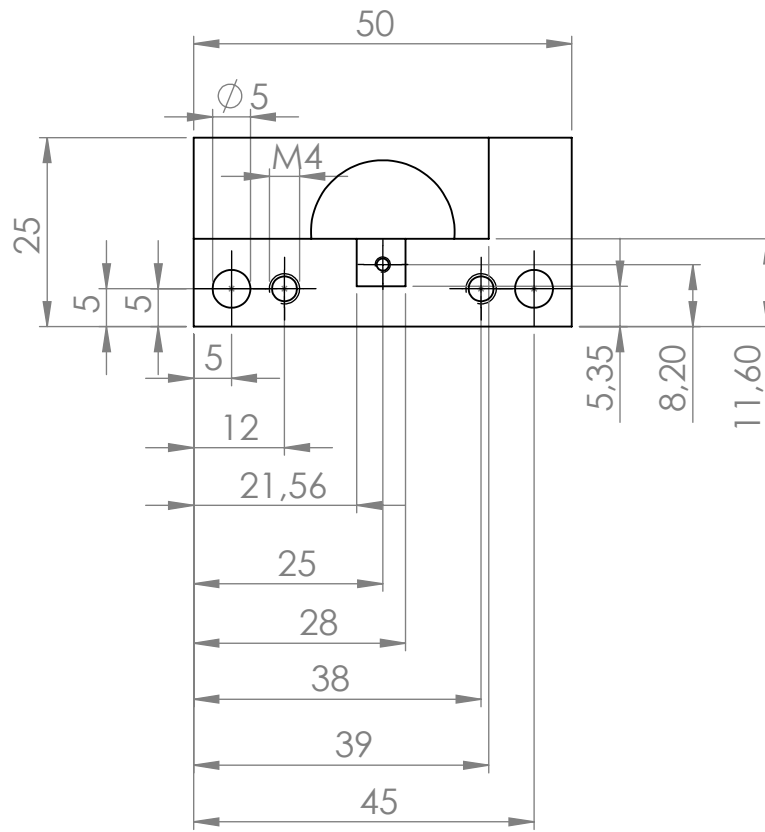
- Rectifier diode: PDU620-13 by DiodesZetex
Available at RS components GmbH, order code: 751-4691
- Ferrite bead: WE-MPSB EMI Multilayer Power Suppression Bead, type 1206
by Würth Elektronik
Available at Würth Elektronik, order code: 74279221100
- 60 m Ω precision resistor: LR2512 2W 0R06 by RALEC
Available at Bürklin Elektronik, order code: 16 E 872
- Bi-directional TVS diode: ESD207-B1-02EL by Infineon
Available at RS components GmbH, order code: 110-7141
- Circuit board: manufactured by Würth Elektronik according to our design
- Plug-in connection terminal: RP02303HBWC by RIA CONNECT
Available at Reichelt Elektronik, order code: AKL 166-03
- 100 nF ceramic capacitor by TDK with dielectric X7R
- 1 μ F ceramic capacitor with dielectric X7R
- 47 μ F tantalum capacitors by AVX

C Drawings of lens holder tube design

The drawings on the following pages are for the lens holder tube design presented in sec. 4.1.1. The drawings are ordered as follows: The two copper blocks, starting with the one that mounts the TA diode, copper baseplate, outer and inner lens holder tube and aluminum base block. All dimensions are in mm.



WENN NICHT ANDERS DEFINIERT: BEMASSUNGEN SIND IN MILLIMETER OBERFLÄCHENBESCHAFFENHEIT: TOLERANZEN: LINEAR: WINKEL:		OBERFLÄCHENGÜTE:		ENTGRATEN UND SCHARFE KANTEN BRECHEN		ZEICHNUNG NICHT SKALIEREN		ÄNDERUNG	
NAME		SIGNATUR		DATUM		BENENNUNG:			
GEZEICHNET		GEPRÜFT		GENEHMIGT		PRODUKTION			
QUALITÄT		WERKSTOFF:		ZEICHNUNGSNR.		<h1>Copper Block 1</h1>		A4	
GEWICHT:		MASSSTAB: 1:1		BLATT 1 VON 3					



WENN NICHT ANDERS DEFINIERT:
BEMASSUNGEN SIND IN MILLIMETER
OBERFLÄCHENBESCHAFFENHEIT:
TOLERANZEN:
LINEAR:
WINKEL:

OBERFLÄCHENGÜTE:

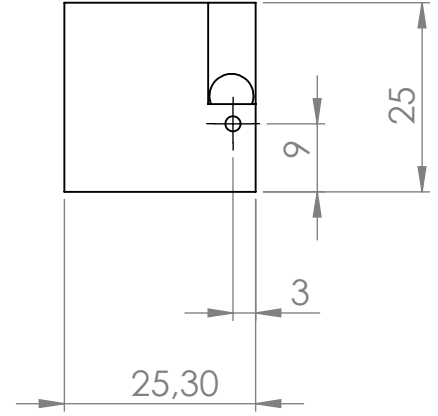
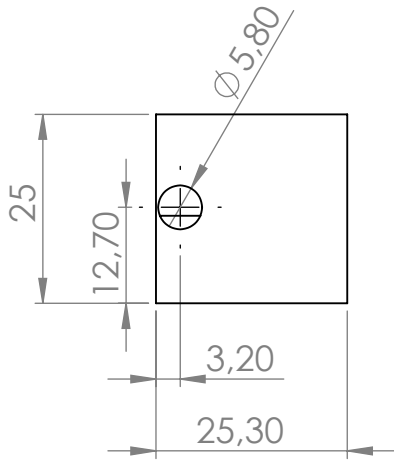
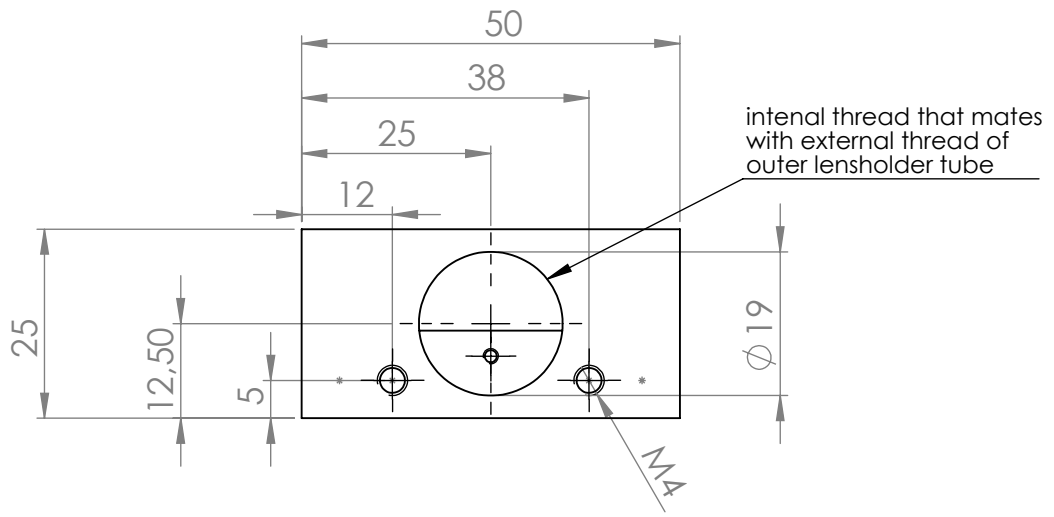
ENTGRATEN
UND SCHARFE
KANTEN
BRECHEN

ZEICHNUNG NICHT SKALIEREN

ÄNDERUNG

	NAME	SIGNATUR	DATUM	
GEZEICHNET				
GEPÜFT				
GENEHMIGT				
PRODUKTION				
QUALITÄT				WERKSTOFF:
				GEWICHT:

BENENNUNG:	
ZEICHNUNGSNR. Copper Block 1	
	A4
MASSTAB: 1:1	BLATT 2 VON 3



WENN NICHT ANDERS DEFINIERT:
BEMASSUNGEN SIND IN MILLIMETER
OBERFLÄCHENBESCHAFFENHEIT:
TOLERANZEN:
LINEAR:
WINKEL:

OBERFLÄCHENGÜTE:

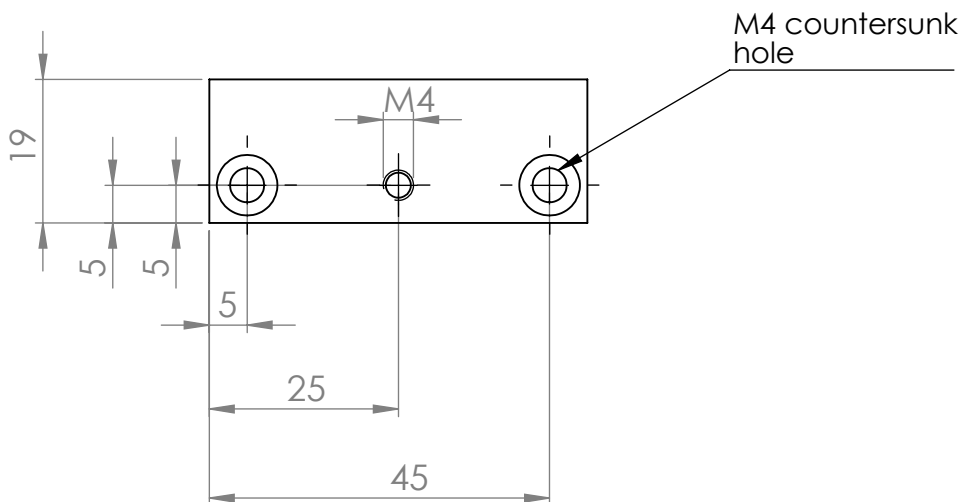
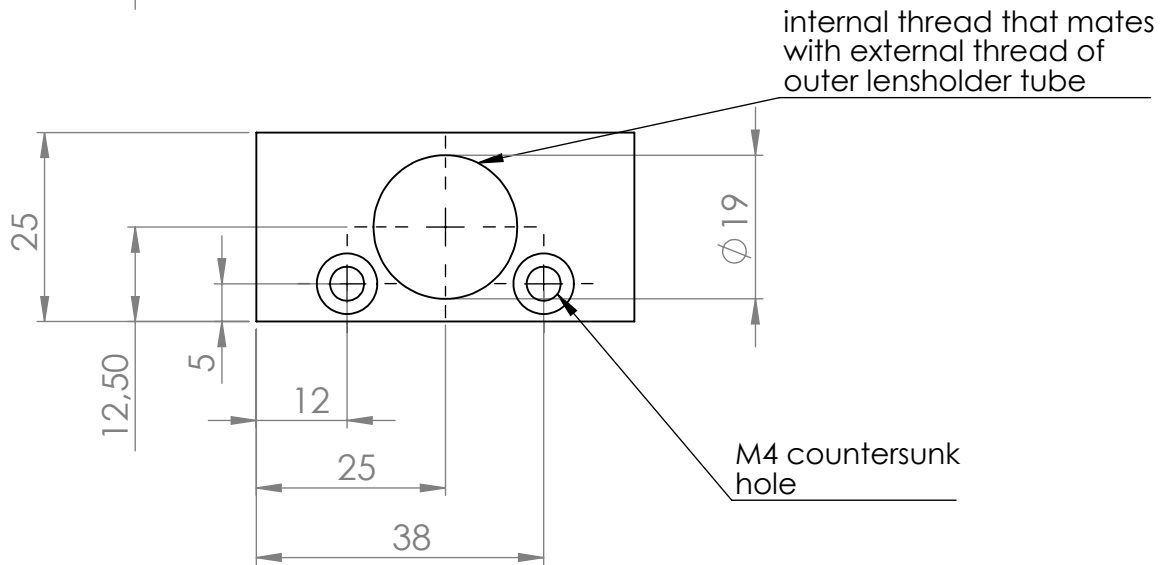
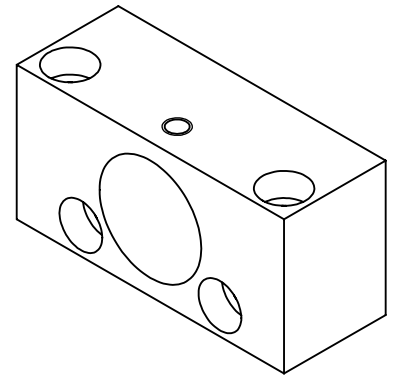
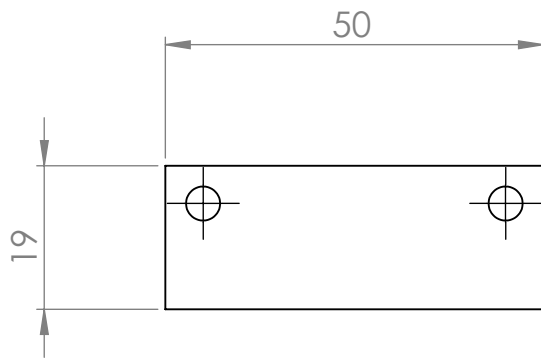
ENTGRATEN
UND SCHARFE
KANTEN
BRECHEN

ZEICHNUNG NICHT SKALIEREN

ÄNDERUNG

	NAME	SIGNATUR	DATUM		
GEZEICHNET					
GEPRÜFT					
GENEHMIGT					
PRODUKTION					
QUALITÄT				WERKSTOFF:	
				GEWICHT:	

BENENNUNG:	
ZEICHNUNGSNR.	Copper Block 1
MASSTAB: 1:1	BLATT 3 VON 3
	A4



WENN NICHT ANDERS DEFINIERT:
BEMASSUNGEN SIND IN MILLIMETER
OBERFLÄCHENBESCHAFFENHEIT:
TOLERANZEN:
LINEAR:
WINKEL:

OBERFLÄCHENGÜTE:

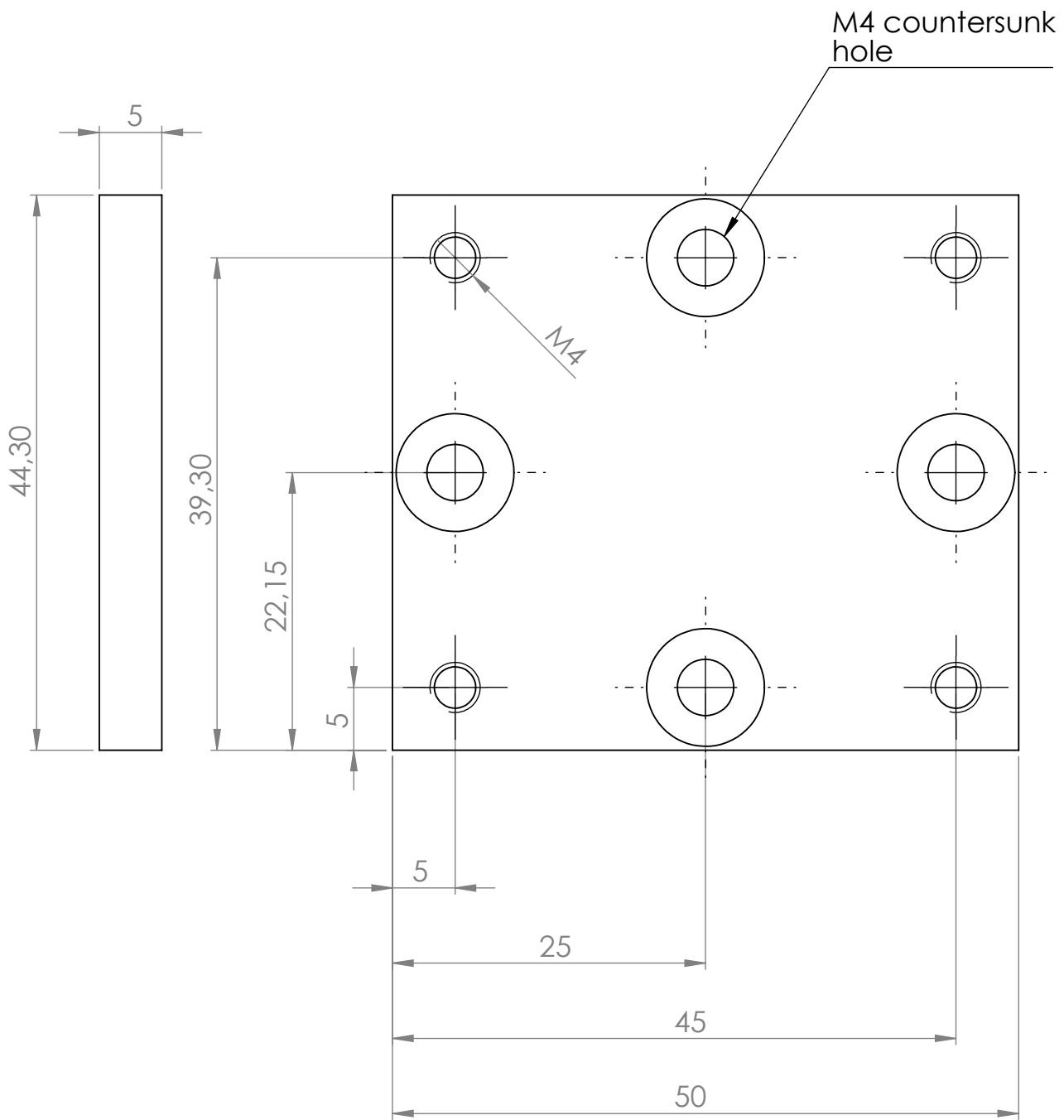
ENTGRATEN
UND SCHARFE
KANTEN
BRECHEN

ZEICHNUNG NICHT SKALIEREN

ÄNDERUNG

	NAME	SIGNATUR	DATUM		
GEZEICHNET					
GEPRÜFT					
GENEHMIGT					
PRODUKTION					
QUALITÄT				WERKSTOFF:	
				GEWICHT:	

BENENNUNG:	
ZEICHNUNGSNR.	Copper Block 2
MASSSTAB: 1:1	BLATT 1 VON 1
	A4



WENN NICHT ANDERS DEFINIERT:
BEMASSUNGEN SIND IN MILLIMETER
OBERFLÄCHENBESCHAFFENHEIT:
TOLERANZEN:
LINEAR:
WINKEL:

OBERFLÄCHENGÜTE:

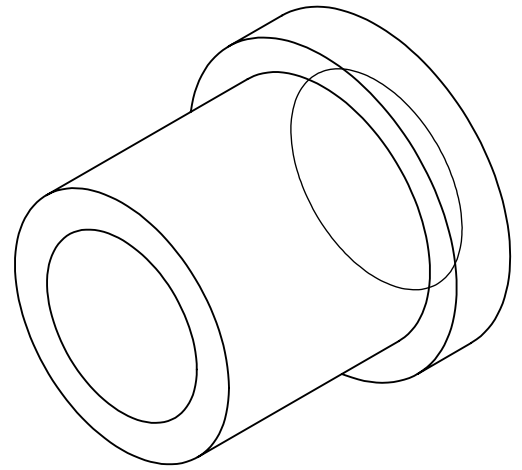
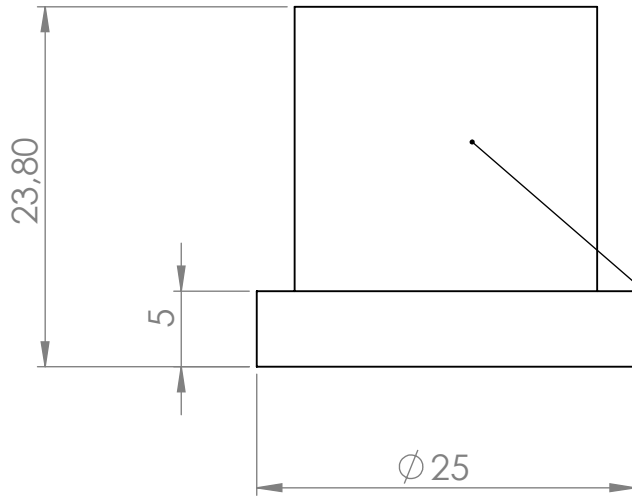
ENTGRATEN
UND SCHARFE
KANTEN
BRECHEN

ZEICHNUNG NICHT SKALIEREN

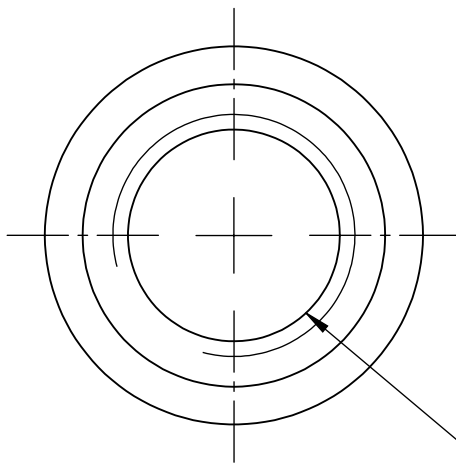
ÄNDERUNG

	NAME	SIGNATUR	DATUM		
GEZEICHNET					
GEPRÜFT					
GENEHMIGT					
PRODUKTION					
QUALITÄT				WERKSTOFF:	
				GEWICHT:	

BENENNUNG:	
ZEICHNUNGSNR.:	Copper baseplate A4
MASSSTAB:2:1	BLATT 1 VON 1



external thread that mates with internal thread of copper blocks



internal fine thread that mates with external fine thread of inner lensholder tube 0.35 mm/turn

WENN NICHT ANDERS DEFINIERT:
BEMASSUNGEN SIND IN MILLIMETER
OBERFLÄCHENBESCHAFFENHEIT:
TOLERANZEN:
LINEAR:
WINKEL:

OBERFLÄCHENGÜTE:

ENTGRATEN
UND SCHARFE
KANTEN
BRECHEN

ZEICHNUNG NICHT SKALIEREN

ÄNDERUNG

	NAME	SIGNATUR	DATUM		
GEZEICHNET					
GEPRÜFT					
GENEHMIGT					
PRODUKTION					
QUALITÄT				WERKSTOFF:	
				GEWICHT:	

BENENNUNG:

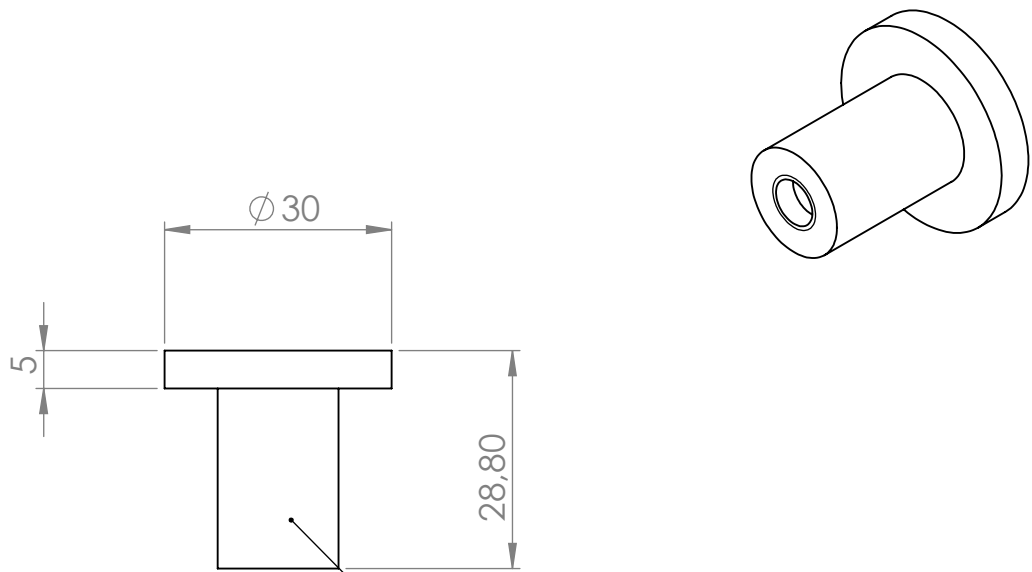
ZEICHNUNGSNR.

Outer lensholder

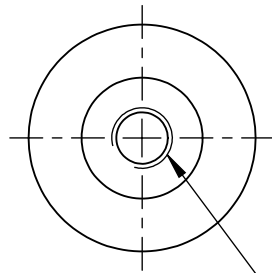
A4

MASSSTAB:2:1

BLATT 1 VON 1



external fine thread that mates with internal fine thread of outer lensholder tube 0.35 mm/turn



internal thread M9-0.5 for aspheric lens

WENN NICHT ANDERS DEFINIERT:
BEMASSUNGEN SIND IN MILLIMETER
OBERFLÄCHENBESCHAFFENHEIT:
TOLERANZEN:
LINEAR:
WINKEL:

OBERFLÄCHENGÜTE:

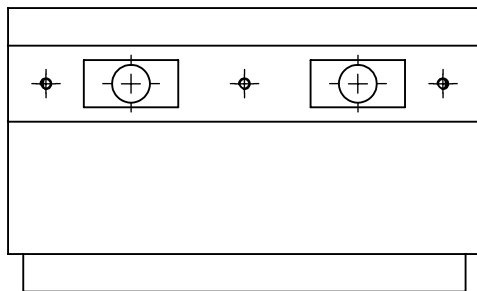
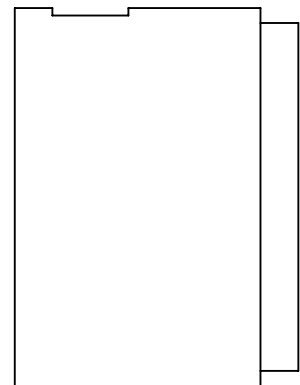
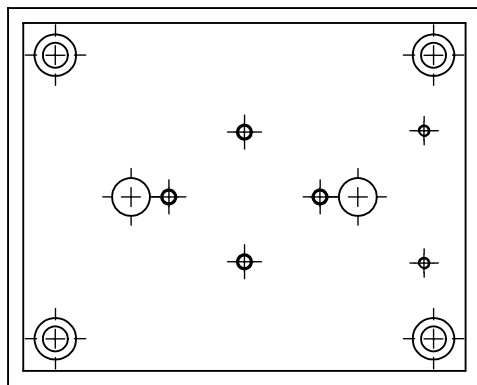
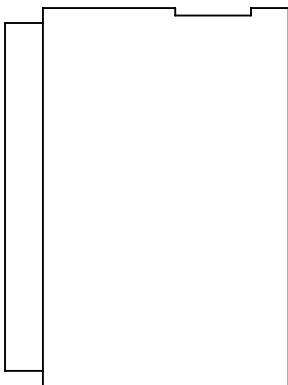
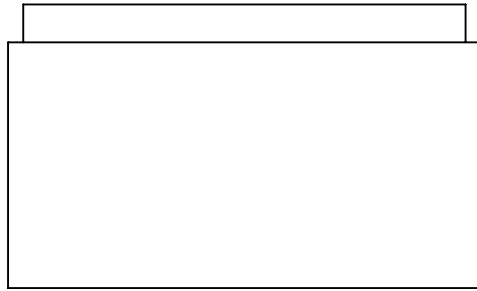
ENTGRATEN
UND SCHARFE
KANTEN
BRECHEN

ZEICHNUNG NICHT SKALIEREN

ÄNDERUNG

	NAME	SIGNATUR	DATUM		
GEZEICHNET					
GEPRÜFT					
GENEHMIGT					
PRODUKTION					
QUALITÄT				WERKSTOFF:	
				GEWICHT:	

BENENNUNG:	
ZEICHNUNGSNR.	Inner lensholder
MASSSTAB: 1:1	BLATT 1 VON 1
	A4



WENN NICHT ANDERS DEFINIERT:
BEMASSUNGEN SIND IN MILLIMETER
OBERFLÄCHENBESCHAFFENHEIT:
TOLERANZEN:
LINEAR:
WINKEL:

OBERFLÄCHENGÜTE:

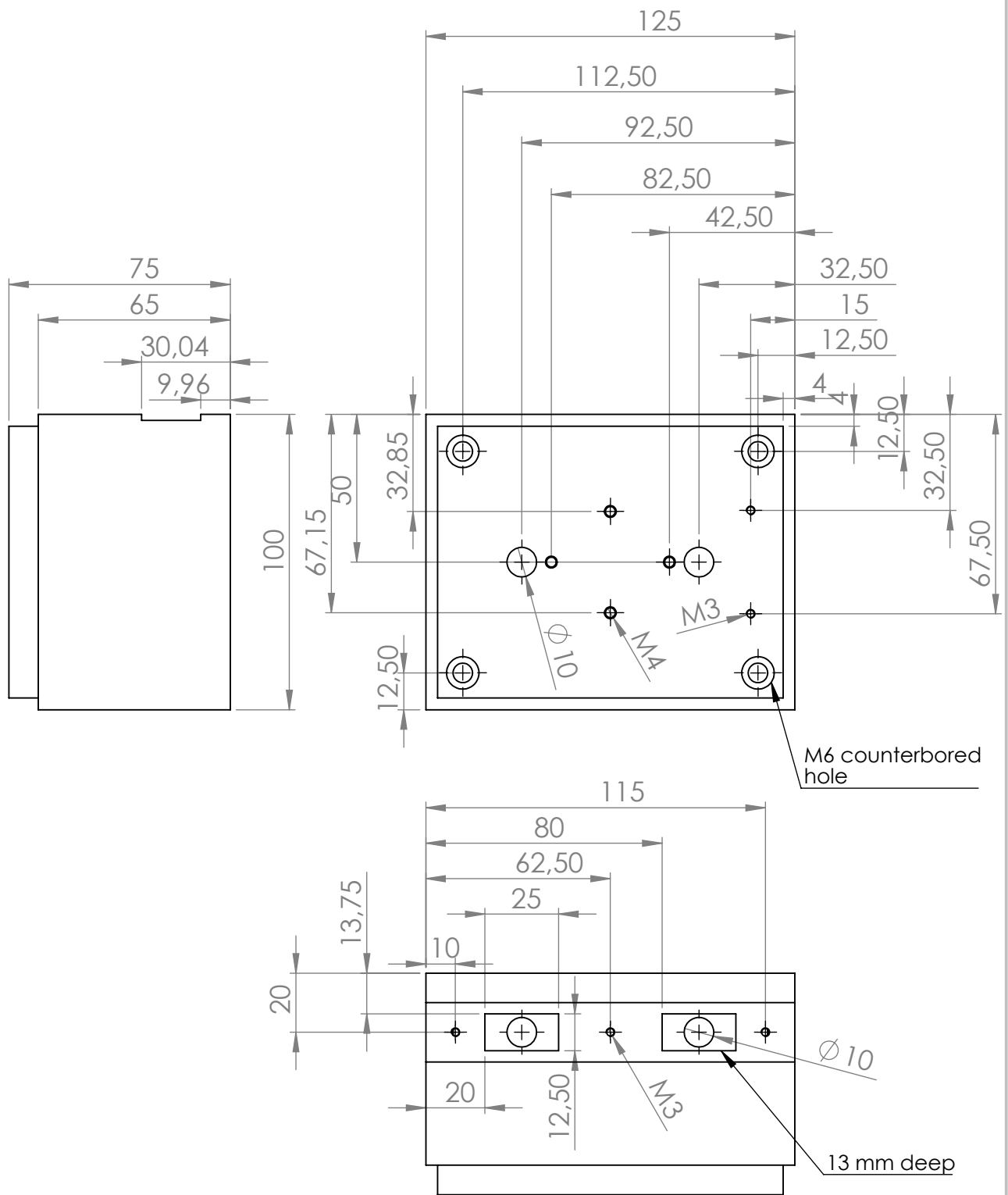
ENTGRATEN
UND SCHARFE
KANTEN
BRECHEN

ZEICHNUNG NICHT SKALIEREN

ÄNDERUNG

	NAME	SIGNATUR	DATUM		
GEZEICHNET					
GEPRÜFT					
GENEHMIGT					
PRODUKTION					
QUALITÄT				WERKSTOFF:	
				GEWICHT:	

BENENNUNG:	
ZEICHNUNGSNR.	Aluminum block
	A4
MASSTAB: 1:2	BLATT 1 VON 2



WENN NICHT ANDERS DEFINIERT:
BEMASSUNGEN SIND IN MILLIMETER
OBERFLÄCHENBESCHAFFENHEIT:
TOLERANZEN:
LINEAR:
WINKEL:

OBERFLÄCHENGÜTE:

ENTGRATEN
UND SCHARFE
KANTEN
BRECHEN

ZEICHNUNG NICHT SKALIEREN

ÄNDERUNG

BENENNUNG:

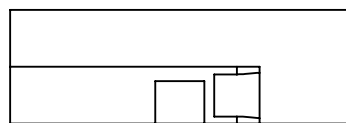
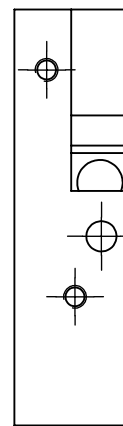
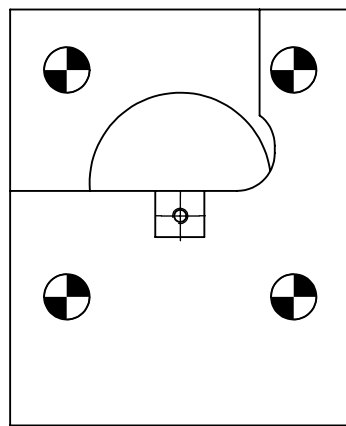
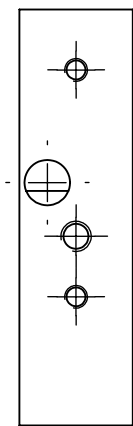
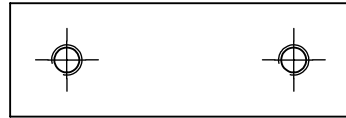
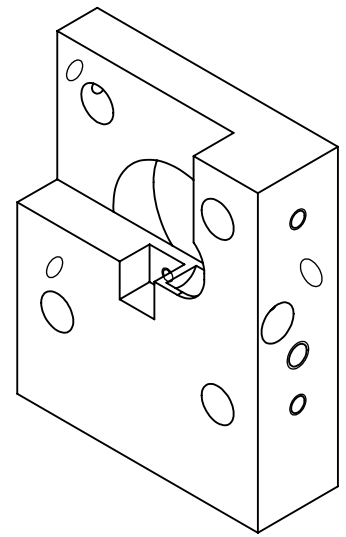
NAME	SIGNATUR	DATUM			
GEZEICHNET					
GEPRÜFT					
GENEHMIGT					
PRODUKTION					
QUALITÄT				WERKSTOFF:	
				GEWICHT:	

ZEICHNUNGSNR.	Aluminum block	A4
MASSTAB: 1:2	BLATT 2 VON 2	

D Drawings of cage system copper parts

The drawings on the following pages are for the TA diode mounting copper block that is presented in sec. 4.2.

On the next page there is an overview of the different projections. The following pages show drawings of the front side, back side, left side, right side, bottom and top side of the mounting block. Then a drawing of the copper baseplate is shown. After that, drawings of the aluminum socket follow. The measures in the drawings are all in mm.



WENN NICHT ANDERS DEFINIERT:
BEMASSUNGEN SIND IN MILLIMETER
OBERFLÄCHENBESCHAFFENHEIT:
TOLERANZEN:
LINEAR:
WINKEL:

OBERFLÄCHENGÜTE:

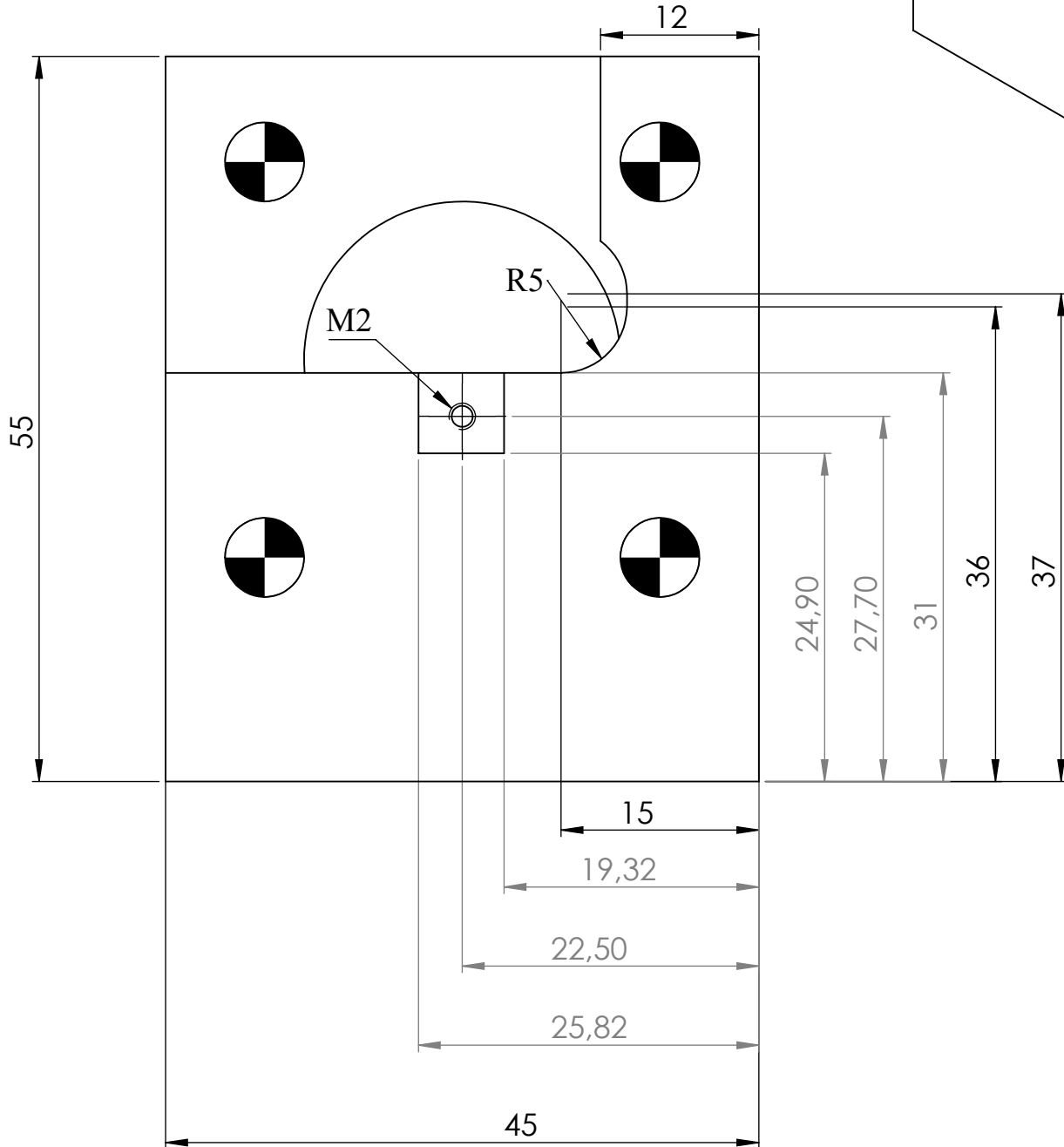
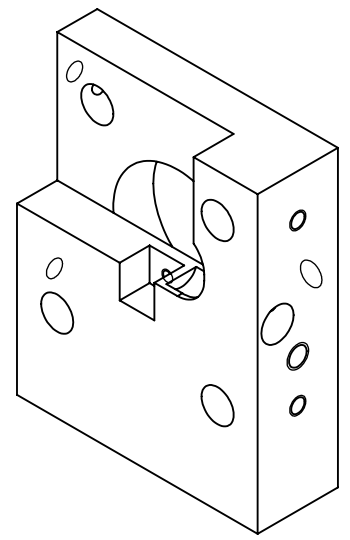
ENTGRATEN
UND SCHARFE
KANTEN
BRECHEN

ZEICHNUNG NICHT SKALIEREN

ÄNDERUNG

	NAME	SIGNATUR	DATUM		
GEZEICHNET					
GEPRÜFT					
GENEHMIGT					
PRODUKTION					
QUALITÄT				WERKSTOFF:	
				GEWICHT:	

BENENNUNG:	
ZEICHNUNGSNR.	Diodehalterung
MASSTAB: 1:1	BLATT 1 VON 6
	A4



WENN NICHT ANDERS DEFINIERT:
BEMASSUNGEN SIND IN MILLIMETER
OBERFLÄCHENBESCHAFFENHEIT:
TOLERANZEN:
LINEAR:
WINKEL:

OBERFLÄCHENGÜTE:

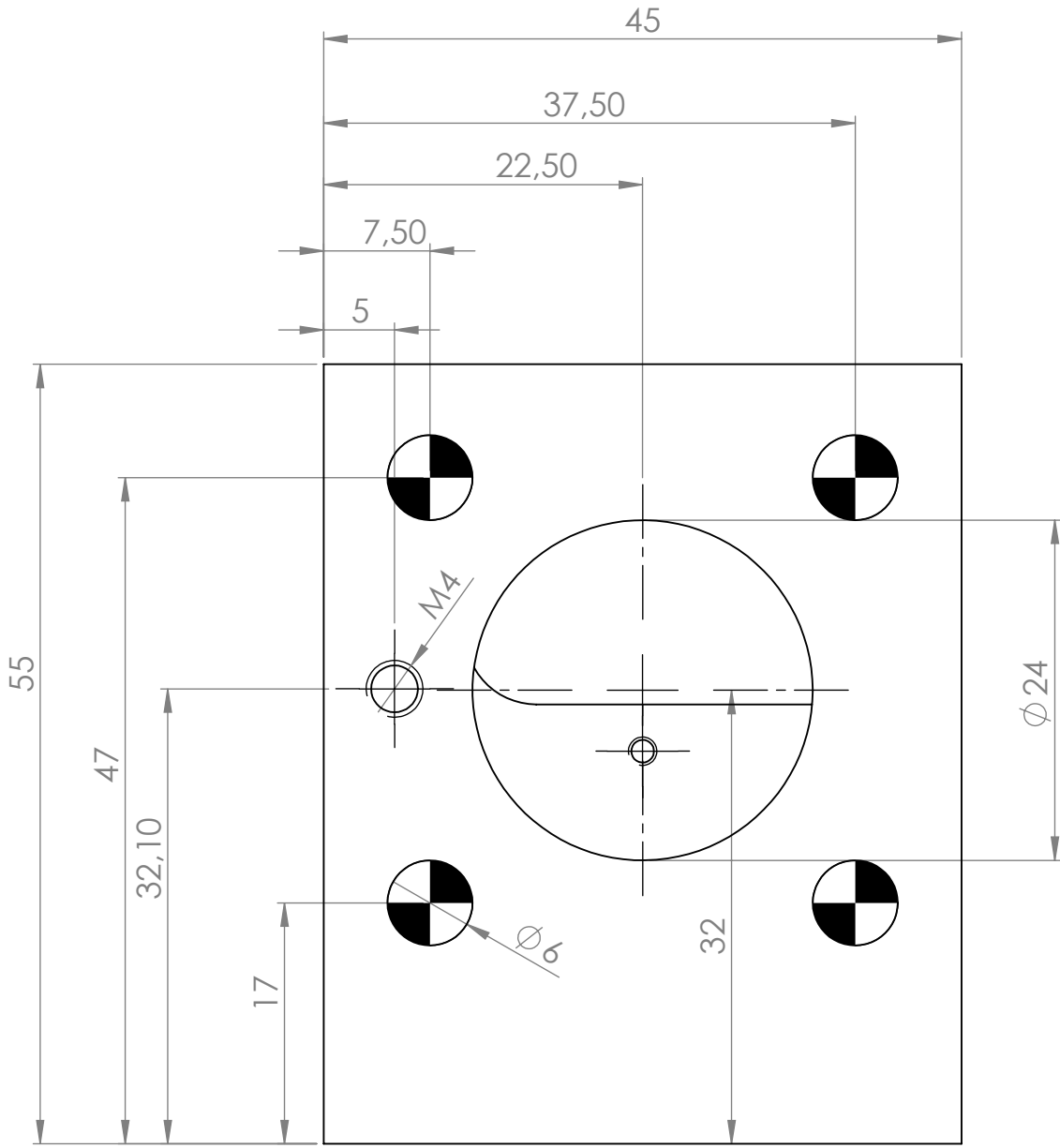
ENTGRATEN
UND SCHARFE
KANTEN
BRECHEN

ZEICHNUNG NICHT SKALIEREN

ÄNDERUNG

	NAME	SIGNATUR	DATUM		
GEZEICHNET					
GEPRÜFT					
GENEHMIGT					
PRODUKTION					
QUALITÄT				WERKSTOFF:	
				GEWICHT:	

BENENNUNG:	
ZEICHNUNGSNR.	Diodehalterung
MASSTAB: 1:1	BLATT 2 VON 6
	A4



WENN NICHT ANDERS DEFINIERT:
BEMASSUNGEN SIND IN MILLIMETER
OBERFLÄCHENBESCHAFFENHEIT:
TOLERANZEN:
LINEAR:
WINKEL:

OBERFLÄCHENGÜTE:

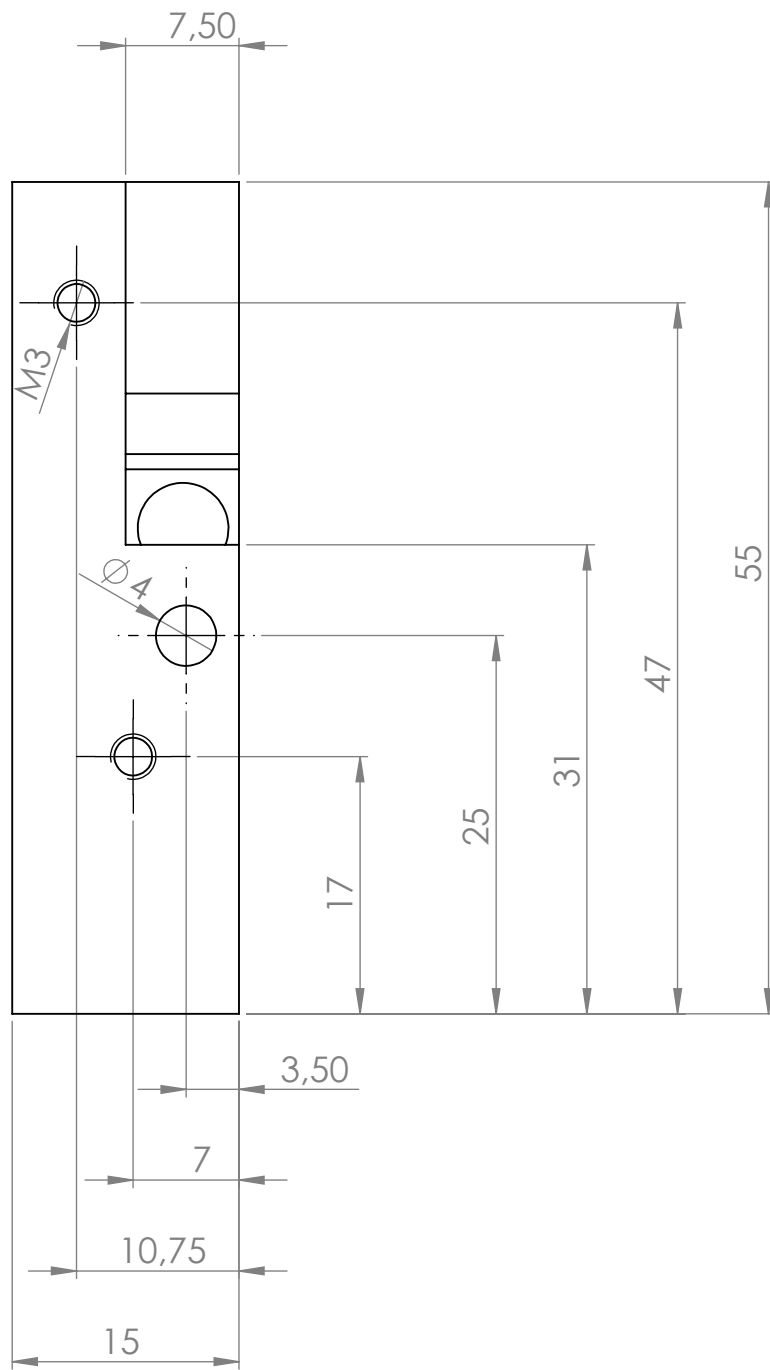
ENTGRATEN
UND SCHARFE
KANTEN
BRECHEN

ZEICHNUNG NICHT SKALIEREN

ÄNDERUNG

	NAME	SIGNATUR	DATUM		
GEZEICHNET					
GEPRÜFT					
GENEHMIGT					
PRODUKTION					
QUALITÄT				WERKSTOFF:	
				GEWICHT:	

BENENNUNG:	
ZEICHNUNGSNR.	Diodehalterung
	A4
MASSSTAB: 1:1	BLATT 3 VON 6



WENN NICHT ANDERS DEFINIERT:
BEMASSUNGEN SIND IN MILLIMETER
OBERFLÄCHENBESCHAFFENHEIT:
TOLERANZEN:
LINEAR:
WINKEL:

OBERFLÄCHENGÜTE:

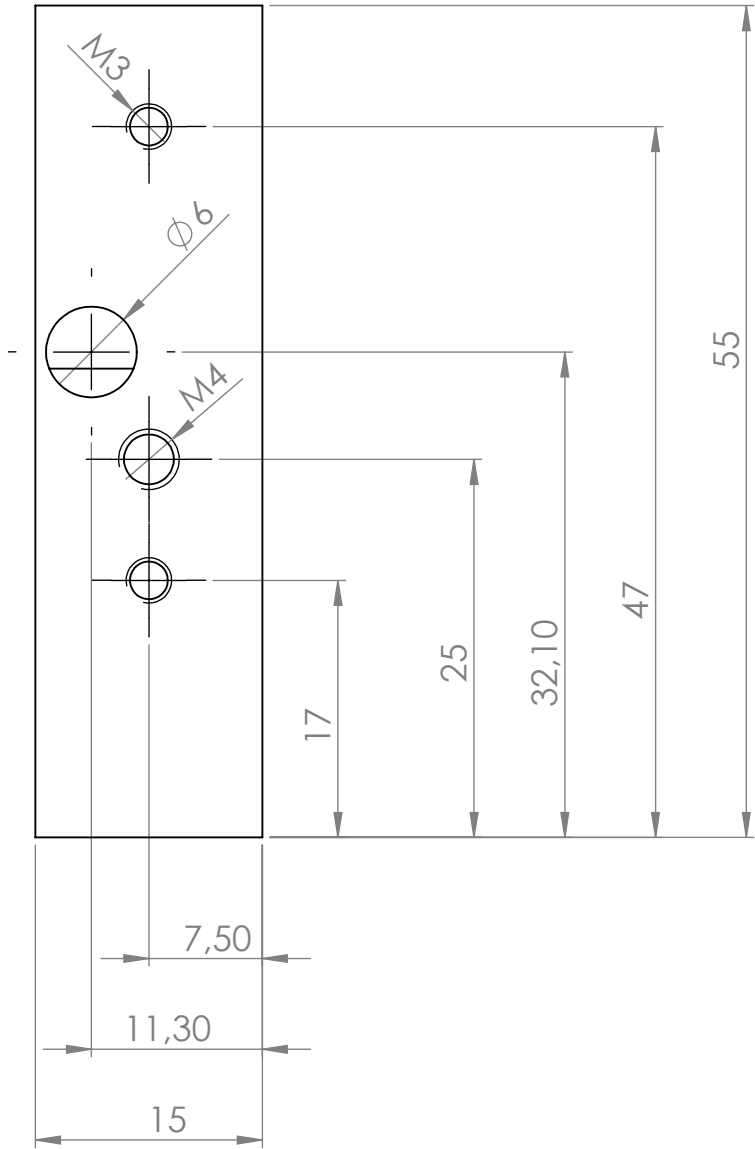
ENTGRATEN
UND SCHARFE
KANTEN
BRECHEN

ZEICHNUNG NICHT SKALIEREN

ÄNDERUNG

	NAME	SIGNATUR	DATUM		
GEZEICHNET					
GEPRÜFT					
GENEHMIGT					
PRODUKTION					
QUALITÄT				WERKSTOFF:	
				GEWICHT:	

BENENNUNG:	
ZEICHNUNGSNR.	Diodehalterung
MASSSTAB: 1:1	BLATT 4 VON 6
	A4



WENN NICHT ANDERS DEFINIERT:
 BEMASSUNGEN SIND IN MILLIMETER
 OBERFLÄCHENBESCHAFFENHEIT:
 TOLERANZEN:
 LINEAR:
 WINKEL:

OBERFLÄCHENGÜTE:

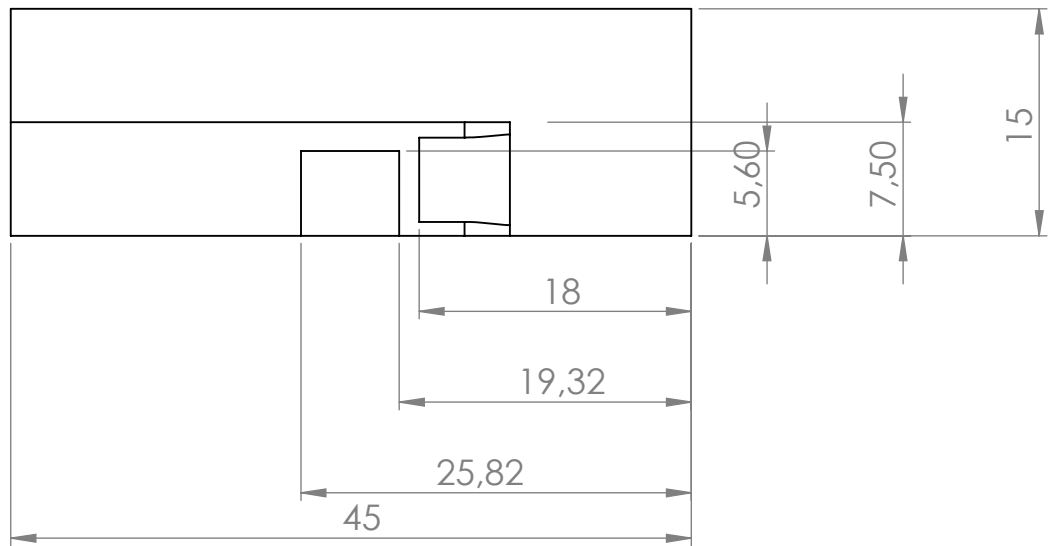
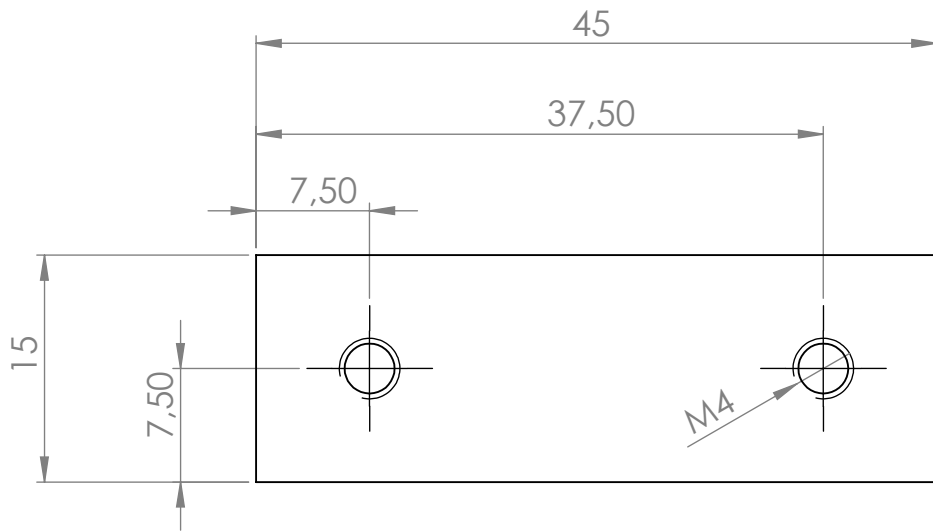
ENTGRATEN
 UND SCHARFE
 KANTEN
 BRECHEN

ZEICHNUNG NICHT SKALIEREN

ÄNDERUNG

	NAME	SIGNATUR	DATUM		
GEZEICHNET					
GEPRÜFT					
GENEHMIGT					
PRODUKTION					
QUALITÄT				WERKSTOFF:	
				GEWICHT:	

BENENNUNG:	
ZEICHNUNGSNR.	Diodehalterung
MASSTAB: 1:1	BLATT 5 VON 6
	A4



WENN NICHT ANDERS DEFINIERT:
BEMASSUNGEN SIND IN MILLIMETER
OBERFLÄCHENBESCHAFFENHEIT:
TOLERANZEN:
LINEAR:
WINKEL:

OBERFLÄCHENGÜTE:

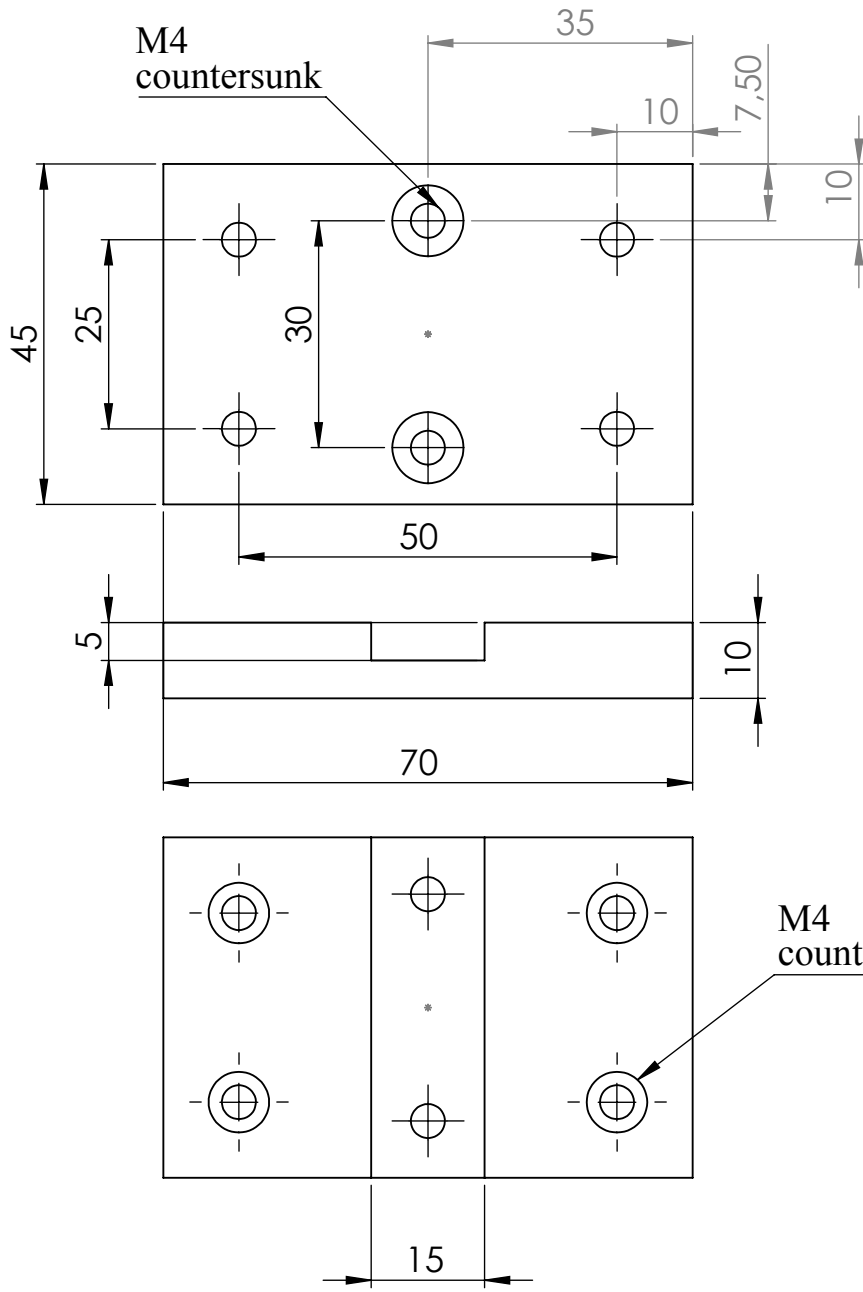
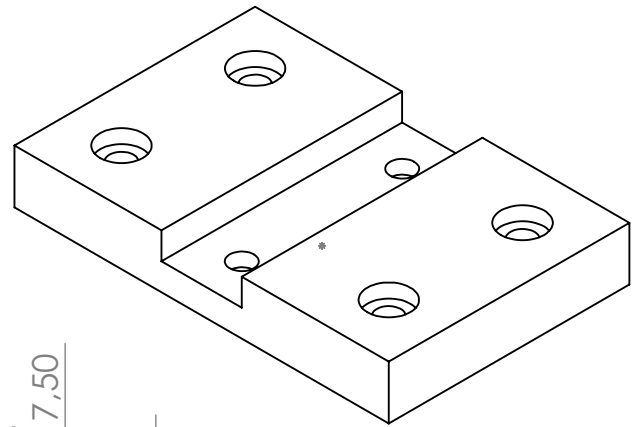
ENTGRATEN
UND SCHARFE
KANTEN
BRECHEN

ZEICHNUNG NICHT SKALIEREN

ÄNDERUNG

	NAME	SIGNATUR	DATUM		
GEZEICHNET					
GEPRÜFT					
GENEHMIGT					
PRODUKTION					
QUALITÄT				WERKSTOFF:	
				GEWICHT:	

BENENNUNG:	
ZEICHNUNGSNR.	Diodehalterung
	A4
MASSSTAB: 1:1	BLATT 6 VON 6



WENN NICHT ANDERS DEFINIERT:
BEMASSUNGEN SIND IN MILLIMETER
OBERFLÄCHENBESCHAFFENHEIT:
TOLERANZEN:
LINEAR:
WINKEL:

OBERFLÄCHENGÜTE:

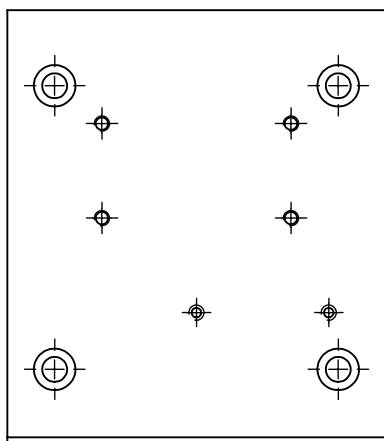
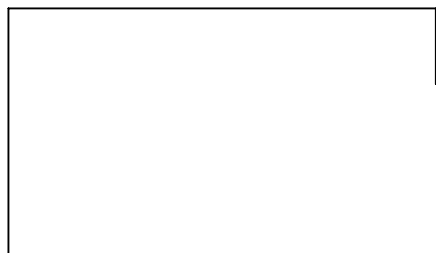
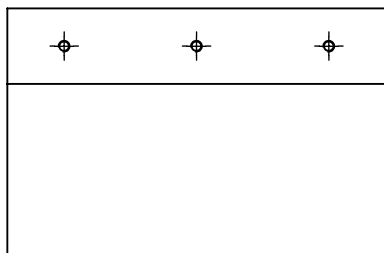
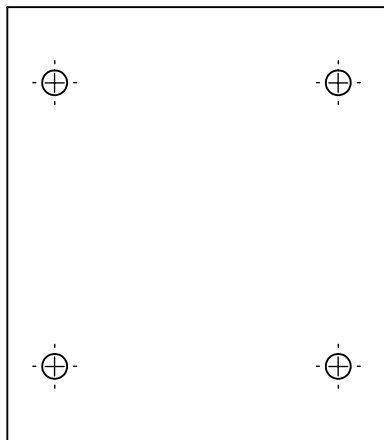
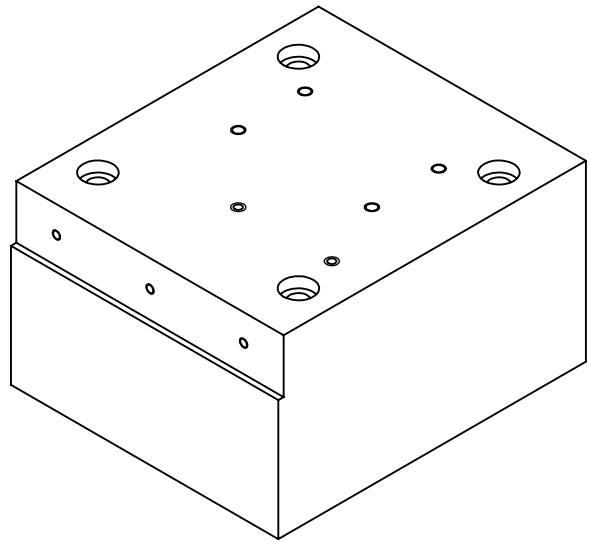
ENTGRATEN
UND SCHARFE
KANTEN
BRECHEN

ZEICHNUNG NICHT SKALIEREN

ÄNDERUNG

	NAME	SIGNATUR	DATUM		
GEZEICHNET					
GEPRÜFT					
GENEHMIGT					
PRODUKTION					
QUALITÄT				WERKSTOFF:	
				GEWICHT:	

BENENNUNG:	
ZEICHNUNGSNR.	Fuß
MASSTAB: 1:1	BLATT 1 VON 1
	A4



WENN NICHT ANDERS DEFINIERT:
 BEMASSUNGEN SIND IN MILLIMETER
 OBERFLÄCHENBESCHAFFENHEIT:
 TOLERANZEN:
 LINEAR:
 WINKEL:

OBERFLÄCHENGÜTE:

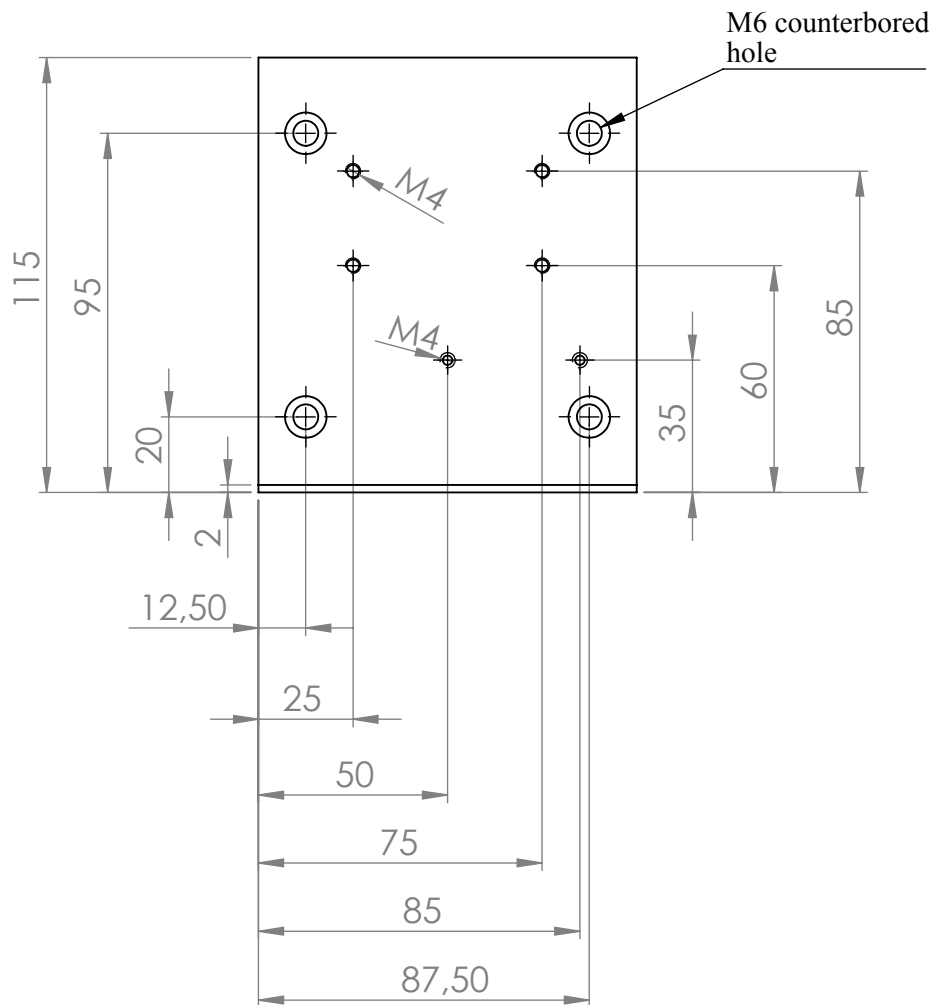
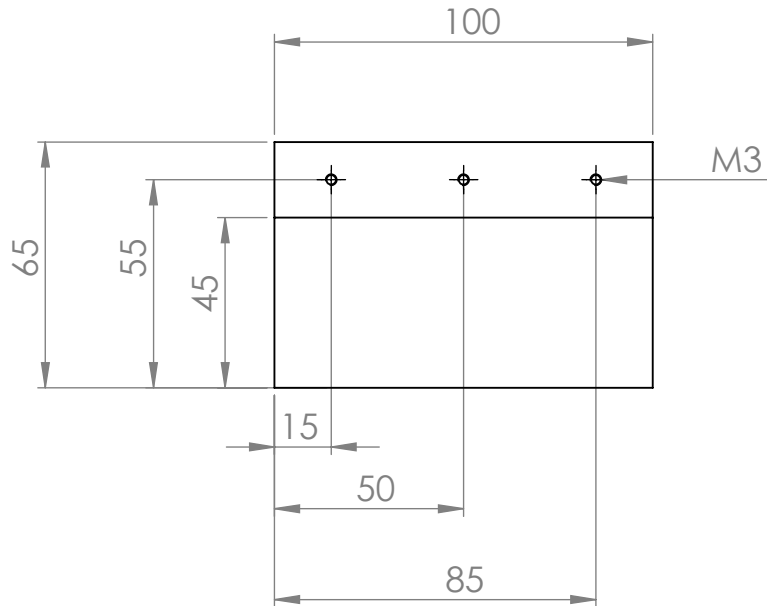
ENTGRATEN
 UND SCHARFE
 KANTEN
 BRECHEN

ZEICHNUNG NICHT SKALIEREN

ÄNDERUNG

	NAME	SIGNATUR	DATUM		
GEZEICHNET					
GEPRÜFT					
GENEHMIGT					
PRODUKTION					
QUALITÄT				WERKSTOFF:	
				GEWICHT:	

BENENNUNG:	
ZEICHNUNGSNR.	Alu Sockel
MASSTAB: 1:2	BLATT 1 VON 2
	A4



WENN NICHT ANDERS DEFINIERT:
BEMASSUNGEN SIND IN MILLIMETER
OBERFLÄCHENBESCHAFFENHEIT:
TOLERANZEN:
LINEAR:
WINKEL:

OBERFLÄCHENGÜTE:

ENTGRATEN
UND SCHARFE
KANTEN
BRECHEN

ZEICHNUNG NICHT SKALIEREN

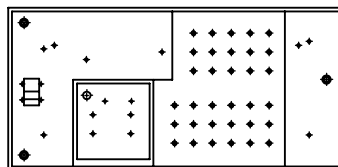
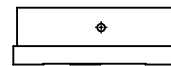
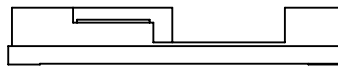
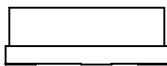
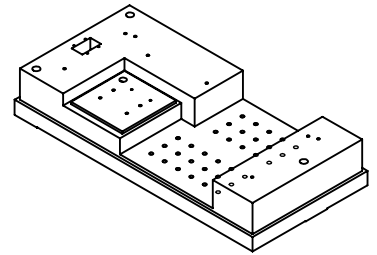
ÄNDERUNG

	NAME	SIGNATUR	DATUM		
GEZEICHNET					
GEPRÜFT					
GENEHMIGT					
PRODUKTION					
QUALITÄT				WERKSTOFF:	
				GEWICHT:	

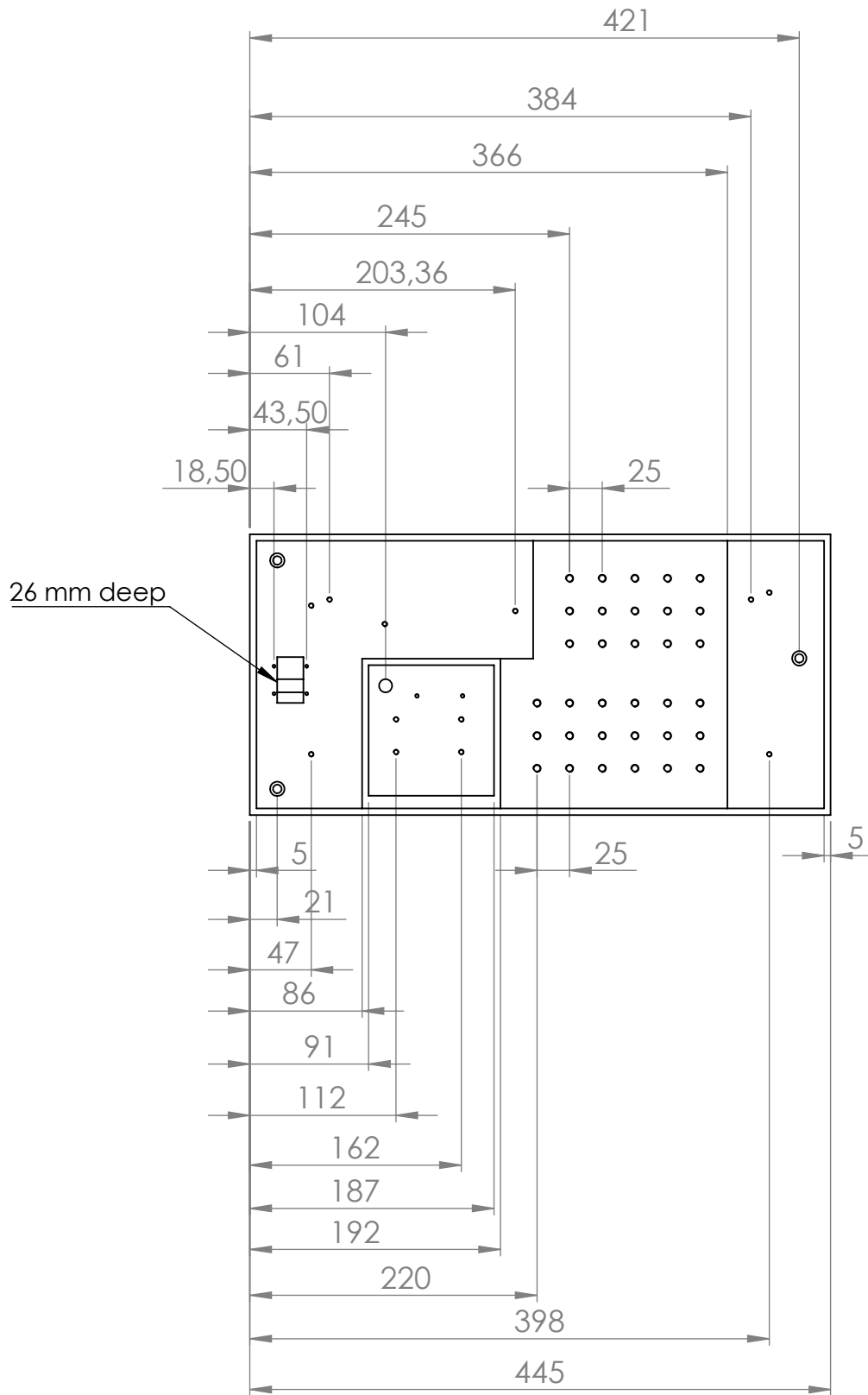
BENENNUNG:	
ZEICHNUNGSNR.	Alu Sockel
	A4
MASSSTAB: 1:2	BLATT 2 VON 2

E Drawings of aluminum block

The drawings on the following pages are for the aluminum block presented in sec. 4.3. The next page shows an overview over the different projections. The pages after show drawings of the top side, bottom side, front side, back side, left side and right side, respectively. The pocket for the sub-D9 plugs is 26 mm deep. The M2,5 threaded holes are 5 mm deep, the M3 threaded holes are 7 mm deep, the M4 threaded holes are 13 mm deep, the M6 threaded holes are 15 mm deep and the 10 mm drilling for the cables is 105 mm deep. Note that the aluminum block stands on three 1 mm high sockets. All measures in the drawing are in mm.



WENN NICHT ANDERS DEFINIERT: BEMASSUNGEN SIND IN MILLIMETER OBERFLÄCHENBESCHAFFENHEIT: TOLERANZEN: LINEAR: WINKEL:		OBERFLÄCHENGÜTE:		ENTGRATEN UND SCHARFE KANTEN BRECHEN		ZEICHNUNG NICHT SKALIEREN		ÄNDERUNG	
NAME		SIGNATUR		DATUM		BENENNUNG:			
GEZEICHNET		GEPRÜFT		GENEHMIGT		PRODUKTION			
QUALITÄT		WERKSTOFF:		ZEICHNUNGSNR.		<h1>Alublock</h1>		A4	
GEWICHT:		MASSSTAB: 1:10		BLATT 1 VON 6					



WENN NICHT ANDERS DEFINIERT:
 BEMASSUNGEN SIND IN MILLIMETER
 OBERFLÄCHENBESCHAFFENHEIT:
 TOLERANZEN:
 LINEAR:
 WINKEL:

OBERFLÄCHENGÜTE:

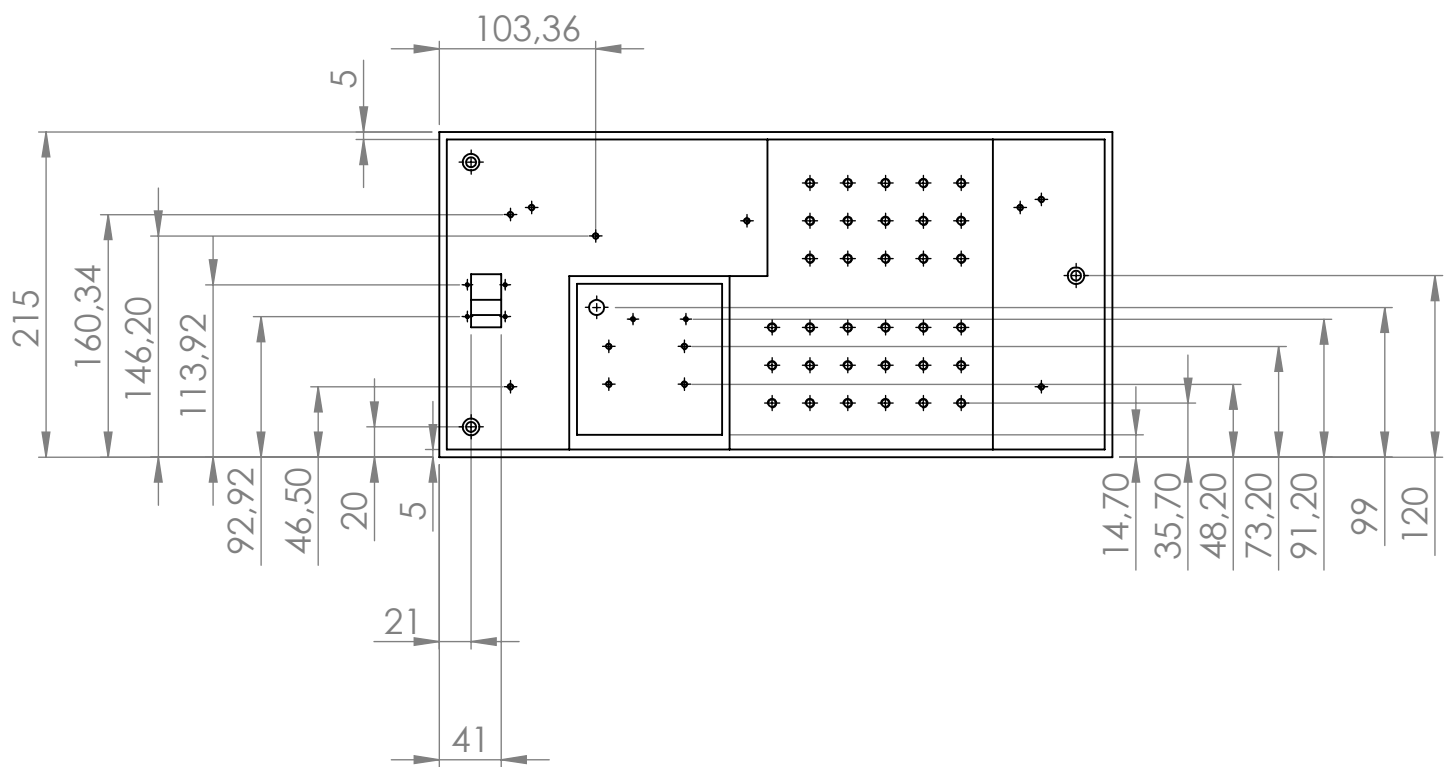
ENTGRATEN
 UND SCHARFE
 KANTEN
 BRECHEN

ZEICHNUNG NICHT SKALIEREN

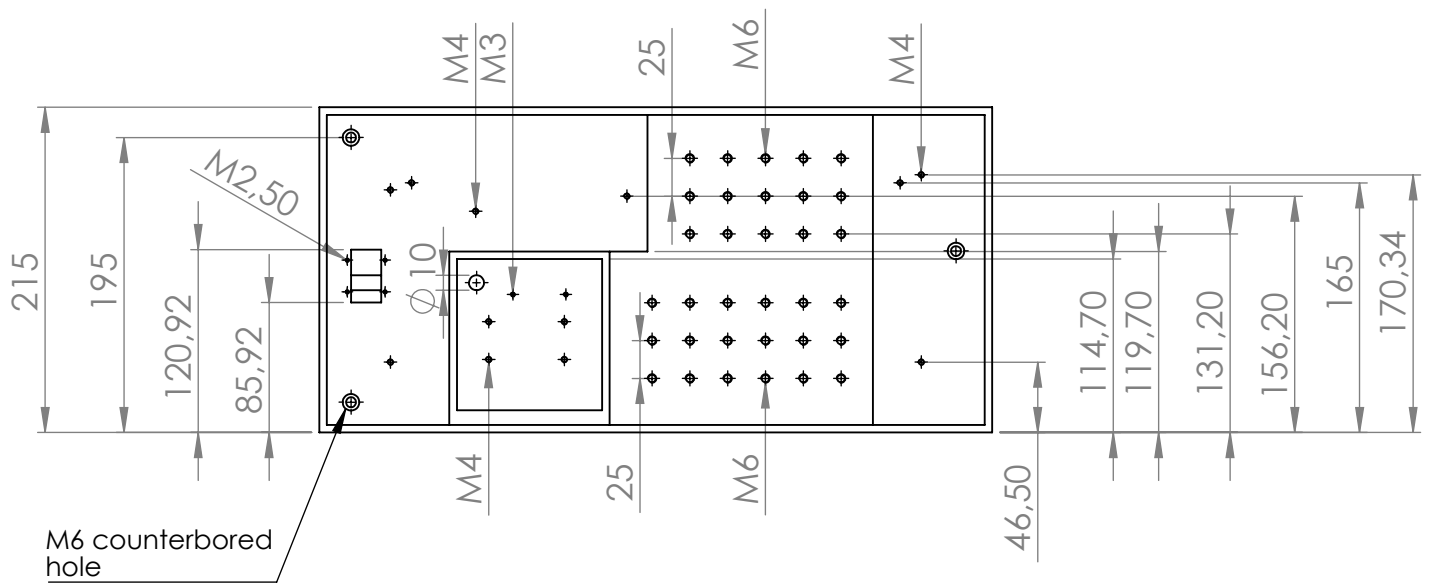
ÄNDERUNG

	NAME	SIGNATUR	DATUM		
GEZEICHNET					
GEPRÜFT					
GENEHMIGT					
PRODUKTION					
QUALITÄT				WERKSTOFF:	
				GEWICHT:	

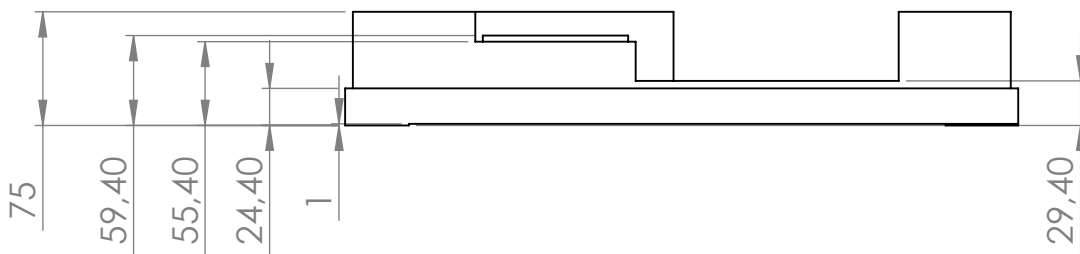
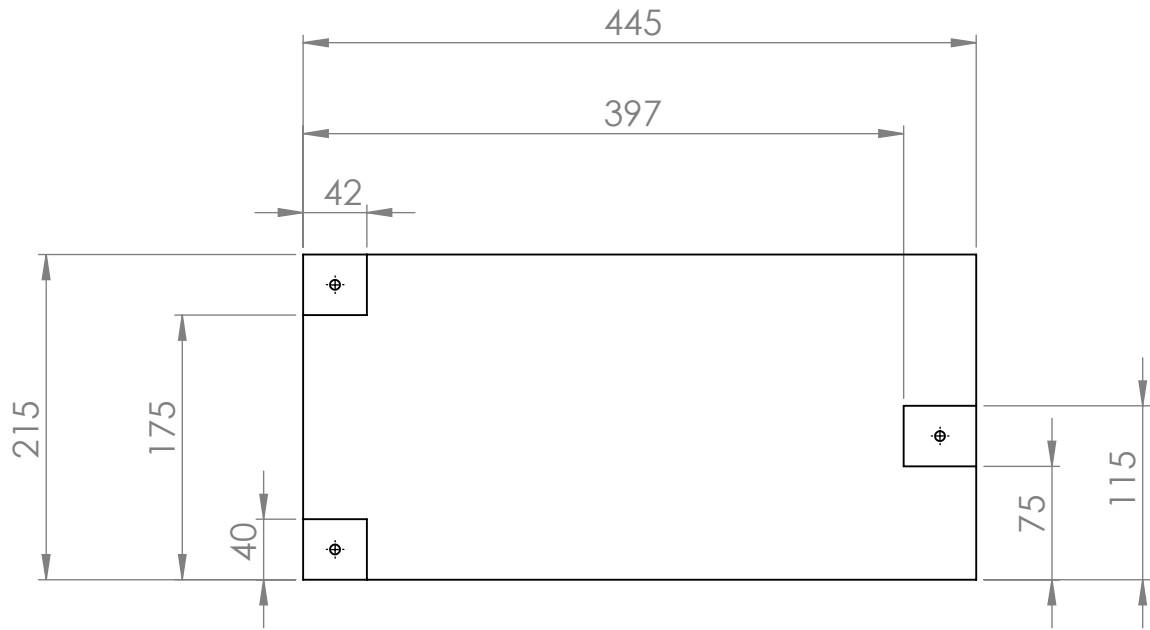
BENENNUNG:	
ZEICHNUNGSNR.	Alublock
MASSSTAB: 1:10	BLATT 2 VON 6
	A4



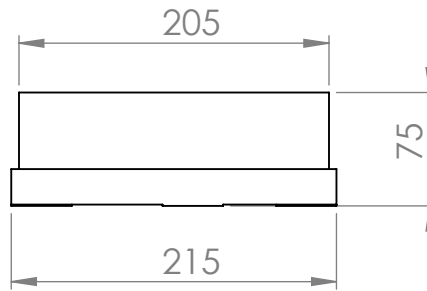
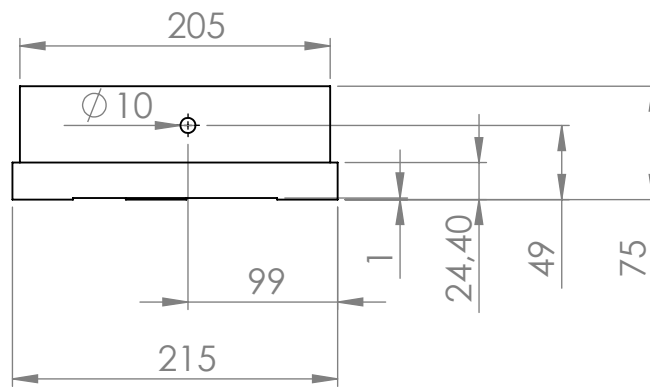
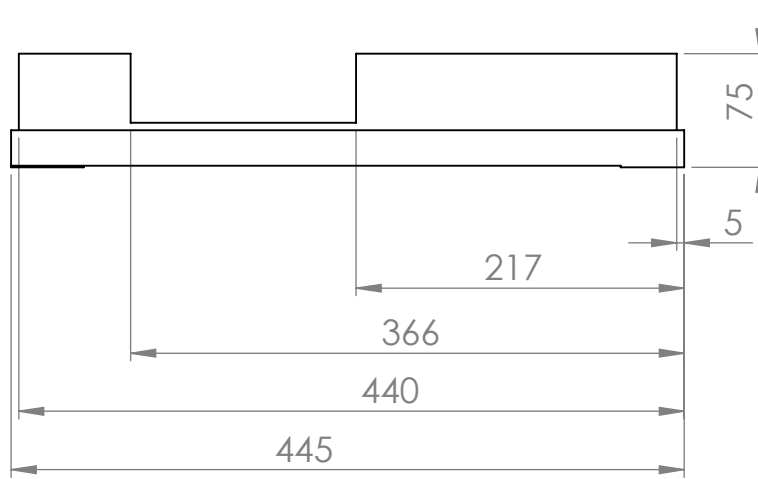
WENN NICHT ANDERS DEFINIERT: BEMASSUNGEN SIND IN MILLIMETER OBERFLÄCHENBESCHAFFENHEIT: TOLERANZEN: LINEAR: WINKEL:		OBERFLÄCHENGÜTE:		ENTGRATEN UND SCHARFE KANTEN BRECHEN		ZEICHNUNG NICHT SKALIEREN		ÄNDERUNG	
NAME		SIGNATUR		DATUM		BENENNUNG:			
GEZEICHNET		GEPÜFT		GENEHMIGT		PRODUKTION			
QUALITÄT		WERKSTOFF:		ZEICHNUNGSNR.		<h1 style="text-align: center;">Alublock</h1>		A4	
GEWICHT:		MASSSTAB: 1:10		BLATT 3 VON 6					



WENN NICHT ANDERS DEFINIERT: BEMASSUNGEN SIND IN MILLIMETER OBERFLÄCHENBESCHAFFENHEIT: TOLERANZEN: LINEAR: WINKEL:		OBERFLÄCHENGÜTE:		ENTGRATEN UND SCHARFE KANTEN BRECHEN		ZEICHNUNG NICHT SKALIEREN		ÄNDERUNG	
NAME		SIGNATUR		DATUM		BENENNUNG:			
GEZEICHNET									
GEPRÜFT									
GENEHMIGT									
PRODUKTION									
QUALITÄT				WERKSTOFF:		ZEICHNUNGSNR.		Alublock	
								A4	
				GEWICHT:		MASSSTAB: 1:10		BLATT 4 VON 6	



WENN NICHT ANDERS DEFINIERT: BEMASSUNGEN SIND IN MILLIMETER OBERFLÄCHENBESCHAFFENHEIT: TOLERANZEN: LINEAR: WINKEL:		OBERFLÄCHENGÜTE:		ENTGRATEN UND SCHARFE KANTEN BRECHEN		ZEICHNUNG NICHT SKALIEREN		ÄNDERUNG	
NAME		SIGNATUR		DATUM		BENENNUNG:			
GEZEICHNET		GEPRÜFT		GENEHMIGT		PRODUKTION			
QUALITÄT		WERKSTOFF:		ZEICHNUNGSNR.		<h1>Alublock</h1>		A4	
GEWICHT:		MASSSTAB: 1:10		BLATT 5 VON 6					



WENN NICHT ANDERS DEFINIERT:
BEMASSUNGEN SIND IN MILLIMETER
OBERFLÄCHENBESCHAFFENHEIT:
TOLERANZEN:
LINEAR:
WINKEL:

OBERFLÄCHENGÜTE:

ENTGRATEN
UND SCHARFE
KANTEN
BRECHEN

ZEICHNUNG NICHT SKALIEREN

ÄNDERUNG

	NAME	SIGNATUR	DATUM		
GEZEICHNET					
GEPRÜFT					
GENEHMIGT					
PRODUKTION					
QUALITÄT				WERKSTOFF:	
				GEWICHT:	

BENENNUNG:	
ZEICHNUNGSNR.	Alublock
MASSSTAB: 1:10	BLATT 6 VON 6
	A4

F Components and prices of a stand-alone TA unit

Table F.1: Components required to set up a stand-alone TA unit.

item	company	item-no.	#	net price per unit [€]	net total [€]
asp. lens $f = 11.0$ mm	Thorlabs	C220TMD-B	2	64,50	129,00
kinematic rotation mount	Thorlabs	KS05RS	2	182,00	364,00
lens cell adapter	Thorlabs	S05TM09	4	17,70	70,80
FC/APC fiber adapter plate	Thorlabs	SM05FCA	2	29,75	59,50
seed beam fiber	Thorlabs	P3-780PM-FC-2	1	166,00	166,00
output beam fiber	Schäfter+Kirchhoff	PMC-E-780-5.1-NA012-3-APC.EC-200-P	1	572,00	572,00

item	company	item-no.	#	net price per unit [€]	net total [€]
mirror mounts	liop-tec	SR100-100R-2- BU	2	53,00	106,00
mirror mounts	liop-tec	SR100-100L-2- BU	2	53,00	106,00
mirrors 1"	lens-optics	M750-860	4	29,00	116,00
current controller	Thorlabs	LDC240C	1	1 153,00	1 153,00
temperature controller	self-built		1	200,00	200,00
Peltier element	reichelt elektronik	TECB 1	1	17,61	17,61
protection circuit	see appendix B		1	20,00	20,00
copper block	institute workshop		1	20,00 ¹	20,00 ¹

¹This is only the value of raw materials, no working hours of the personnel is considered.

item	company	item-no.	#	net price per unit [€]	net total [€]
aluminum block	institute workshop		1	190,00 ²	190,00 ²
TA diode	eagleyard photonics	EYP-TPA-0808- 02000-4006- CMT04-0000	1	2 164,00	2 164,00
XYZ translation mount	Thorlabs	CXYZ05/M	2	297,00	594,00
asp. lens $f = 4.51$ mm	Thorlabs	C230TMD-B ³	2	61,50	123,00
cage rods	Thorlabs	ER3-P4	1	22,80	22,80
NTC thermistor 10 k Ω	reichelt elektronik	NTC-0,2 10K	1	0,28	0,28
cyl. lens $f = 40$ mm	Thorlabs	LJ1402L1-B	1	57,00	57,00

²This is only the value of raw materials, no working hours of the personnel is considered.

³In this work, a C230TME-B lens was used, but during the time this work was written, Thorlabs replaced the C230TME-B lens by the C230TMD-B lens. However, both lenses have the same focal length, the same NA and the same thread of the lens mount.

item	company	item-no.	#	net price per unit [€]	net total [€]
Z translation mount	Thorlabs	SM1ZP/M	1	173,00	173,00
adapter for cyl. lens	Thorlabs	SM1A6	2	17,40	34,80
30 mm post	Thorlabs	TR30/M	2	4,27	8,54
post holder	Thorlabs	PH30/M	2	6,33	12,66
mounting base	Thorlabs	BA1S/M	1	4,68	4,68
mounting base	Thorlabs	BA2/M	1	6,57	6,57
60 dB opt. isolator	Qioptiq Photonics	FI-810-5TVC	1	2 450,00	2 450,00
net total [€]					8 941,24
19% VAT					+1 698,84
Total [€]					10 640,08

G Bibliography

- [1] Wikipedia: Laser medicine. URL https://en.wikipedia.org/wiki/Laser_medicine.
- [2] Marie Freebody. Diode Lasers Break into new Wavelengths, New Applications. *EuroPhotonics, Autumn 2014*, pages 22–25, 2014. URL <https://www.photonics.com/Article.aspx?AID=56645>.
- [3] D. Voigt, E. C. Schilder, R. J. C. Spreeuw, and H. B. Van Linden Van Den Heuvel. Characterization of a high-power tapered semiconductor amplifier system. *arXiv*, 284:6, 2000. ISSN 0946-2171. doi: 10.1007/s003400100513. URL <http://arxiv.org/abs/physics/0004043>.
- [4] Jayampathi C. B. Kangara, Andrew J. Hachtel, Matthew C. Gillette, Jason T. Barkeloo, Ethan R. Clements, Samir Bali, Brett E. Unks, Nicholas A. Proite, Deniz D. Yavuz, Paul J. Martin, Jeremy J. Thorn, and Daniel A. Steck. Design and construction of cost-effective tapered amplifier systems for laser cooling and trapping experiments. *American Journal of Physics*, 82(8):805–817, 2014. ISSN 0002-9505. doi: 10.1119/1.4867376. URL <http://scitation.aip.org/content/aapt/journal/ajp/82/8/10.1119/1.4867376>.
- [5] Joachim Welte. *Atom Trap Trace Analysis of ^{39}Ar* . PhD thesis, Universität Heidelberg, 2011. URL <http://matterwave.de/>.
- [6] Wei Cheng, Ximiao Hou, and Fangmao Ye. Use of tapered amplifier diode laser for biological-friendly high-resolution optical trapping. *Optics letters*, 35(17):2988–2990, 2010. ISSN 0146-9592. doi: 10.1364/OL.35.002988.
- [7] Michael Mikulla. Tapered High-Power, High-Brightness Diode Lasers: Design and Performance. In Roland Diehl, editor, *High-Power Diode Lasers, Fundamentals, Technology, Applications*, pages 265–288. Springer-Verlag, 2000.
- [8] Elhanan Pniel, Benjamin Dalin, Sveta Golod, Shlomo Goldin, and Eyal Shekel. Types of filamentation in tapered diode amplifiers: their causes and features. *Optical and Quantum Electronics*, 47(6):1535–1544, 2015. ISSN 0306-8919. doi: 10.1007/s11082-015-0163-9. URL <http://link.springer.com/10.1007/s11082-015-0163-9>.
- [9] J. N. Walpole. Semiconductor amplifiers and lasers with tapered gain regions. *Optical and Quantum Electronics*, 28(6):623–645, 1996. ISSN 0306-8919. doi: 10.1007/BF00411298. URL <http://link.springer.com/10.1007/BF00411298>.

- [10] E. Gehrig, O. Hess, and R. Wallenstein. Modeling of the Performance of High-Power Diode Amplifier Systems with an Optothermal Microscopic Spatio-Temporal Theory. *IEEE Journal of Quantum Electronics*, 35(3):320–331, 1999. ISSN 00189197. doi: 10.1109/3.748837.
- [11] E. Gehrig, O. Hess, C. Seibert, D. Woll, and R. Wallenstein. Amplification and wave mixing of induced and spontaneous emission in semiconductor laser amplifiers. *Applied Physics B: Lasers and Optics*, 76(3):285–288, 2003. ISSN 09462171. doi: 10.1007/s00340-002-1091-5.
- [12] Edeltraud Gehrig and Ortwin Hess. Semiconductor Laser Theory The Maxwell-Bloch Equations. In *Spatio-Temporal Dynamics and Quantum Fluctuations in Semiconductor Lasers*, pages 13–24. Springer-Verlag, 2003, ISBN 3-540-00741-5.
- [13] Ortwin Hess and Tilmann Kuhn. Maxwell-Bloch equations for spatially inhomogeneous semiconductor lasers. I. Theoretical formulation. *Physical Review A*, 54(4):3347, 1996. ISSN 1050-2947. doi: 10.1103/PhysRevA.54.3347. URL <http://link.aps.org/abstract/PRA/v54/p3347><http://prola.aps.org/abstract/PRA/v54/i4/p3347>.
- [14] Edeltraud Gehrig and Ortwin Hess. Spatio – Temporal Dynamics of Light Amplification and Amplified Spontaneous Emission in High-Power Tapered Semiconductor Laser Amplifiers. *IEEE Journal of Quantum Electronics*, 37(10):1345–1355, 2001.
- [15] Edeltraud Gehrig and Ortwin Hess. Dynamics of High-Power Diode Lasers. In Roland Diehl, editor, *High-Power Diode Lasers, Fundamentals, Technology, Applications*, pages 55–81. Springer-Verlag, 2000.
- [16] Luis Borrueal, Slawomir Sujecki, Pablo Moreno, James Wykes, Michel Krakowski, Bernd Sumpf, Phillip Sewell, Sophie Charlotte Auzanneau, Hans Wenzel, Daniel Rodríguez, Trevor M. Benson, Eric C. Larkins, and Ignacio Esquivias. Quasi-3-D simulation of high-brightness tapered lasers. *IEEE Journal of Quantum Electronics*, 40(5):463–472, 2004. ISSN 00189197. doi: 10.1109/JQE.2004.826424.
- [17] Sujatha Ramanujan and Herbert G Winful. Spontaneous Emission Induced Filamentation in Flared Amplifiers. *IEEE Journal of Quantum Electronics*, 32(5):784–789, 1996.
- [18] Matthias Henrich. Diploma Thesis: Design and Realization of a Laser System for ATTA of Argon 39, Universität Heidelberg, 2010. URL <http://matterwave.de/>.

- [19] Bahaa E. A. Saleh and Malvin Carl Teich. *Fundamentals of photonics*. John Wiley & Sons, Hoboken, New Jersey, 2nd edition, 2007. ISBN 978-0-471-35832-9.
- [20] Yihan Xiong, Sytil Murphy, J. L. Carlsten, and Kevin Repasky. Design and characteristics of a tapered amplifier diode system by seeding with continuous-wave and mode-locked external cavity diode laser. *Optical Engineering*, 45(12): 124205, 2006. ISSN 00913286. doi: 10.1117/1.2404925.

Danksagung

Diese Arbeit wäre ohne die Unterstützung von Kollegen, Freunden und Familie sicherlich nicht in der hier vorliegenden Form entstanden. Für diese Unterstützung möchte ich mich an dieser Stelle ganz herzlich bedanken.

Mein Dank gilt Prof. Dr. Markus K. Oberthaler, der mir diese Arbeit ermöglicht hat und deren Fortschreiten mit Interesse verfolgte. Des Weiteren gab er mir viele nützliche Ratschläge, was die Arbeit als Experimentalphysiker betrifft.

Prof. Dr. Selim Jochim möchte ich für die Zweitkorrektur dieser Arbeit danken.

Zhongyi möchte ich dafür danken, dass er mich unter seine Fittiche genommen hat und mir stets mit Rat und Tat zur Seite stand. Auch die "crazy days" und die sommerlichen Radtouren werden mir in guter Erinnerung bleiben.

Ich danke Helmut, der mir stets all meine vielen Fragen ausführlich und mit großer Geduld beantwortet hat. Auch war auf ihn immer Verlass, wenn man nicht alleine im Botanik zu Abend essen wollte.

Lisa und Sven danke ich für ihre ausführlichen Erklärungen zum ArTTa Experiment und das Korrekturlesen dieser Arbeit.

Philipp danke ich für die motivierenden Worte gerade beim Endspurt dieser Arbeit. Bedanken möchte ich mich bei Andrea und Simon dafür, dass sie durch ihre tief philosophischen Gespräche einen auch mal von der Physik abgelenkt haben.

Anika und Pierre danke ich für die Motivation bei sportlichen Aktivitäten.

Danke an Daniel, Max und Maurus für die gute Büroatmosphäre.

Die komplette Matterwavegruppe ist ein tolles Team und ich weiß die kollegiale Arbeitsatmosphäre sehr zu schätzen! Schließlich sitzen wir ja auch alle zusammen im selben (Drachen)Boot. Auch werden mir diverse Feiern in guter Erinnerung bleiben. Bedanken möchte ich mich auch bei der Werkstatt für das Fertigen der vielen Bauteile und bei Alexander Dobler für das Bestücken der Elektronik boards.

Danke an Anka, Andi und Pirmin für die gemeinsame Zeit seit dem ersten Semester und die vielen gemeinsamen Unternehmungen.

Ein ganz besonderer Dank gilt meinen Eltern und meiner Familie, die mich mein ganzes Leben lang unterstützt und gefördert haben und einfach immer für mich da sind.

Erklärung:

Ich versichere, dass ich diese Arbeit selbstständig verfasst habe und keine anderen als die angegebenen Quellen und Hilfsmittel benutzt habe.

Heidelberg, den 1. März 2017

.....